AN INVESTIGATION OF SOLAR RADIATION IN THAILAND: SATELLITE-BASED APPROACHES AND CLEAR SKY IRRADIANCE MODELING

By
Somjet Pattarapanitchai

A Thesis Submitted in Partial Fulfillment of the Requirements for the Degree
DOCTOR OF PHILOSOPHY
Department of physics
Graduate School
SILPAKORN UNIVERSITY
2011

AN INVESTIGATION OF SOLAR RADIATION IN THAILAND: SATELLITE-BASED APPROACHES AND CLEAR SKY IRRADIANCE MODELING

By
Somjet Pattarapanitchai

A Thesis Submitted in Partial Fulfillment of the Requirements for the Degree
DOCTOR OF PHILOSOPHY
Department of physics
Graduate School
SILPAKORN UNIVERSITY
2011

การศึกษารังสีดวงอาทิตย์ในประเทศไทย: การคำนวณโดยใช้ข้อมูลภาพถ่ายดาวเทียมและการจำลองแบบรังสีดวงอาทิตย์ในสภาพท้องฟ้าปราศจากเมฆ

โดย

นายสมเจตน์ ภัทรพานิชชัย

วิทยานิพนธ์นี้เป็นส่วนหนึ่งของการศึกษาตามหลักสูตรปริญญาปรัชญาดุษฎีบัณฑิต

สาขาวิชาฟิสิกส์

ภาควิชาฟิสิกส์

บัณฑิตวิทยาลัย มหาวิทยาลัยศิลปากร

ปีการศึกษา 2554

The Graduate School, Silpakorn University has approved and accredited the Thesis title of "An investigation of solar radiation in Thailand: Satellite-based approaches and clear sky irradiance modeling" submitted by Mr. Somjet Pattarapanitchai as a partial fulfillment of the requirements for the degree of Doctor of Philosophy in PHYSICS

…….....
(Assistant Professor Panjai Tantatsanawong,Ph.D.)
Dean of Graduate School
...../...../.....

The Thesis Advisor

Associate Professor Serm Janjai, Ph.D.

The Thesis Examination Committee

..... Chairman
(Professor Virulh Sa-yakanit, Ph.D.)
...../...../.....

..... Member
(Dusadee Sukawat, Ph.D.)
...../...../.....

..... Member
(Associate Professor Serm Janjai, Ph.D.)
...../...../.....

52306802 : MAJOR : PHYSICS
KEY WORD : SOLAR RADIATION/SATELLITE DATA/ CLEAR SKY CONDITION / MODEL / THAILAND
SOMJET PATTARAPANITCHAI: AN INVESTIGATION OF SOLAR RADIATION IN THAILAND: SATELLITE-BASED APPROACHES AND CLEAR SKY IRRADIANCE MODELING. THESIS ADVISOR: ASSOC. PROF. SERM JANJAI, Ph.D. 127 pp.

In this work, solar radiation in Thailand was investigated using satellite-based approaches. A satellite-based solar radiation model was developed for calculating monthly average of daily global radiation. Digital data from GMS4, GMS5, GOES9 and MTSAT-1R satellites collected during a 15-year period (1995-2009) were used as the main input of the model. To test its performance, the model was employed to calculate monthly average of daily global solar radiation at 38 solar monitoring stations across the country. The results of the test showed that values of monthly average of daily global radiation calculated from the model and those obtained from the measurements were in good agreement with the root mean square difference of 6.1%. After the validation, the model was used to calculate monthly average of daily global radiation over the country and the results were displayed as solar radiation maps. These maps reveal that the geographical distribution of solar radiation in Thailand is strongly influenced by the northeast and southwest monsoons.

A satellite-based artificial neural network model was also developed to estimate daily global solar radiation. The effect of the cloud on solar radiation was represented by a satellite-derived cloud index. The model was trained by using the back propagation algorithm. To validate the model, it was used to estimate daily global radiation by using independent datasets. The results of the validation showed that the values root mean square difference (RMSD) between the estimated and measured daily global radiation were in the range of 10.1-13.9%.

Finally, semi-empirical models for estimating global, direct and diffuse solar irradiance under clear sky condition in Thailand were developed. The models express global, direct and diffuse irradiances as function of aerosol optical properties, water vapour and total column ozone. The models were validated against independent datasets. It was found that values of global, direct and diffuse solar irradiances calculated from the models and those obtained from the measurements were in good agreement.

Department of physics Graduate School, Silpakorn University
Student's signature ..... Academic Year 2011
Thesis Advisor's signature .....

52306802 : สาขาวิชาฟิสิกส์
คำสำคัญ : รังสีดวงอาทิตย์/ ภาพถ่ายดาวเทียม/ แบบจำลอง/ประเทศไทย

สมเจตน์ ภัทรพานิชชัย : การศึกษารังสีดวงอาทิตย์ในประเทศไทย: การคำนวณโดยใช้ข้อมูลภาพถ่ายดาวเทียมและการจำลองแบบรังสีดวงอาทิตย์ในสภาพท้องฟ้าปราศจากเมฆ. อาจารย์ที่ปรึกษาวิทยานิพนธ์ : รศ.ดร.เสริม จันทร์ฉาย. 127 หน้า.

ในงานวิจัยนี้ ผู้วิจัยได้ทำการศึกษาความเข้มรังสีดวงอาทิตย์โดยการใช้ข้อมูลภาพถ่ายดาวเทียม โดยได้ทำการพัฒนาแบบจำลองสำหรับคำนวณความเข้มรังสีรวมรายวันเฉลี่ยต่อเดือนจากข้อมูลภาพถ่ายดาวเทียม แบบจำลองดังกล่าวจะใช้ข้อมูลจากดาวเทียม GMS4 GMS5 GOES9 และ MTSAT-1R เป็นเวลา 15 ปี (ค.ศ. 1995-2009) เป็นข้อมูลอินพุท ในการทดสอบสมรรถนะของแบบจำลอง ผู้วิจัยได้ใช้แบบจำลองคำนวณความเข้มรังสีรวมรายวันเฉลี่ยต่อเดือนที่สถานีวัดรังสีดวงอาทิตย์ 38 แห่ง ซึ่งตั้งกระจายอยู่ทั่วประเทศ ผลการทดสอบพบว่าความเข้มรังสีรวมรายวันเฉลี่ยต่อเดือนที่ได้จากแบบจำลองและที่ได้จากการวัดที่สถานีดังกล่าวมีความสอดคล้องกันในเกณฑ์ที่ดี โดยมีความแตกต่างในรูปของ root mean square difference (RMSD) เท่ากับ 6.1% หลังจากนั้นผู้วิจัยได้ใช้แบบจำลองดังกล่าวคำนวณค่าความเข้มรังสีรวมรายวันเฉลี่ยต่อเดือนทั่วประเทศ และนำผลที่ได้มาจัดแสดงในรูปของแผนที่รังสีดวงอาทิตย์ จากแผนที่ที่ได้พบว่า การกระจายตามพื้นที่ของรังสีดวงอาทิตย์ในประเทศได้รับอิทธิพลอย่างมากจากมรสุมตะวันออกเฉียงเหนือและตะวันตกเฉียงใต้

นอกจากนี้ ผู้วิจัยได้ทำการพัฒนาแบบจำลองสำหรับคำนวณค่าความเข้มรังสีรวมรายวันโดยใช้โครงข่ายประสาทเทียม (artificial neural network, ANN) ในแบบจำลองดังกล่าวจะแสดงผลของเมฆโดยใช้ดัชนีเมฆซึ่งคำนวณจากข้อมูลภาพถ่ายดาวเทียม ผู้วิจัยได้ทำการฝึกสอนโครงข่ายประสาทเทียมด้วยวิธีการแพร่กลับ (back propagation algorithm) จากนั้นได้ทำการทดสอบสมรรถนะของโครงข่ายประสาทเทียมที่ได้โดยนำโครงข่ายประสาทเทียมไปทำการคำนวณความเข้มรังสีดวงอาทิตย์จากชุดข้อมูลอิสระ ผลการทดสอบแสดงให้เห็นว่าความแตกต่างในรูปของ RMSD ระหว่างค่าความเข้มรังสีรวมรายวันที่ได้จากโครงข่ายประสาทเทียมและจากการวัดมีค่าอยู่ในช่วง 10.1%-13.9%

สุดท้าย ผู้วิจัยได้ทำการพัฒนาแบบจำลองสำหรับคำนวณค่าความเข้มรังสีรวม รังสีตรงและรังสีกระจายขณะใดๆ (irradiance) ภายใต้สภาพท้องฟ้าปราศจากเมฆ แบบจำลองดังกล่าวจะแสดงค่าความเข้มรังสีรวม รังสีตรง และรังสีกระจาย ในรูปของฟังก์ชั่นของสมบัติเชิงแสงของฝุ่นละออง ปริมาณไอน้ำและโอโซน ผู้วิจัยได้ทำการทดสอบสมรรถนะของแบบจำลองโดยใช้แบบจำลองดังกล่าวคำนวณค่ารังสีดวงอาทิตย์จากชุดข้อมูลอิสระ ผลที่ได้พบว่าค่าความเข้มรังสีรวม รังสีตรงและรังสีกระจาย ที่ได้จากแบบจำลองและที่ได้จากการวัดมีความสอดคล้องกันในเกณฑ์ที่ดี

ภาควิชาฟิสิกส์ บัณฑิตวิทยาลัย มหาวิทยาลัยศิลปากร

ลายมือชื่อนักศึกษา..... ปีการศึกษา 2554

ลายมือชื่ออาจารย์ที่ปรึกษาวิทยานิพนธ์ .....

Acknowledgments

A thesis entitled “An investigation of solar radiation in Thailand: Satellite-based approaches and clear sky irradiance modeling” is submitted in partial fulfillment of the requirements for the degree of Doctor of Philosophy (Physics), Graduate School, Silpakorn University.

I would like to express my sincere thanks to Assoc. Prof. Dr. Serm Janjai, my supervisor for his helpful guidance and support throughout this study.

I am grateful to Assist. Prof. Poolsak Intawee, Head of Department of Physics, for the administrative support during the study. Prof. Dr. Virulh Sa-yakanit and Dr. Dusadee Sukawat are gratefully acknowledged for examining this thesis.

I would like to thank all researchers in Solar Energy Research Laboratory of Silpakorn University for their helps and friendship during the study.

Finally, I would like to specially express my gratitude and deepest appreciation to my parents and relatives for their love and support throughout my life.

Table of Contents

List of Tables

List of Figures

Figures Page

Chapter 1
Introduction

1.1 Rationale of the study

The sun is the main energy source of all living organisms on the earth. It also provides energy to drive the air circulation in the earth atmospheric system and water circulation in the oceans. The energy generated by the sun travels to the earth in the form of electromagnetic wave called solar radiation. The solar radiation consists of several wavelength bands, namely gamma rays, x-rays, ultraviolet radiation, visible radiation, infrared radiation, microwave and radio wave. Solar radiation in these wavelength bands arrived at the top of the earth atmosphere. While traveled through the earth atmosphere, gamma rays and x-rays are completely absorbed by the upper atmosphere and most parts of visible and infrared radiation arrive at the earth surface. In addition, small part of ultraviolet radiation, microwave and radio wave also reach the earth surface.

The amount of solar radiation incident on the earth surface varies with the incident angle and atmospheric conditions. For example, under clear sky condition, more solar radiation is received on a horizontal plane at noon time than that received at 8:00 am, due to the difference in the incident angle. The incident angle depends on the positions of the sun which varies with the latitude of the location of interest, the time in a day and the season. The atmospheric condition also has strongly influences on the incident radiation. For example, solar radiation at noon time of a clear day is higher than that of a cloudy day at the same time and location.

In contrast to the amount of solar radiation at the top of the atmosphere which can be accurately calculated by using theoretical approach, the amount of solar radiation at the earth surface is difficult to estimate due to the temporal and spatial variation of the earth atmosphere.

However, information on the amount of solar radiation at the earth surface is still required for research and applications in many fields, such as solar energy, meteorology, climatology, agriculture, etc. Although solar radiation data can be obtained by using a measurement approach, however, for the case of Thailand, the

number of solar measuring stations is too sparse to provide sufficient data for users in these fields. Therefore, in this work we propose to obtain solar radiation data in Thailand by using modeling approaches. Consequently, we propose to estimate solar radiation by using satellite-based solar radiation model and artificial neural network method. As solar radiation under a clear sky condition is also essential information for a number of solar energy applications, we also propose semi-empirical models to estimate global, direct and diffuse solar radiation under this condition.

1.2 Objectives

This study has the following specific objectives.

1) To calculate monthly average daily global solar radiation from satellite data over Thailand.
2) To propose an artificial neural network (ANN) model for the estimation of daily global solar radiation using satellite-derived cloud index as the main input.
3) To develop semi-empirical models for determining global, direct and diffuse solar radiation under a clear sky condition.

1.3 Organization of the thesis

This thesis is composed of 6 Chapters. The first chapter describes the rationale, objective and organization of the thesis. The second chapter presents the estimation of monthly average daily global radiation employing satellite data. The estimation of daily global radiation by using ANN is presented in chapter 3. Chapter 4 and 5 describe the semi-empirical models for calculating global, direct and diffuse radiation under a clear sky condition. Finally, Chapter 6 presents the conclusion of the work.

Chapter 2

Calculation of monthly average daily global solar radiation over Thailand using satellite data*

2.1 Introduction

As cloud is the main factor affecting solar radiation on the earth's surface and meteorological satellites can detect the cloud, it is possible to use satellite data to derive solar radiation and display it as solar radiation maps. In the past 30 years, a number of models have been proposed to derive solar radiation from satellite data. (e.g. Gautier et al., 1980; Tarpley, 1979; Cano et al., 1986). The use of satellite data to derive surface solar radiation has an advantage that the radiation is obtained for all areas corresponding to satellite pixels including in mountainous areas where solar radiation measurement is difficult to conduct. Therefore, in this work we propose to calculate monthly average daily global radiation by using long-term satellite data.

2.2 Methodology

The methodology of this work consists of processing of satellite data, formulation of the model, calculation of model parameters and model validation. The schematic of the procedure is shown in Fig 2.1.

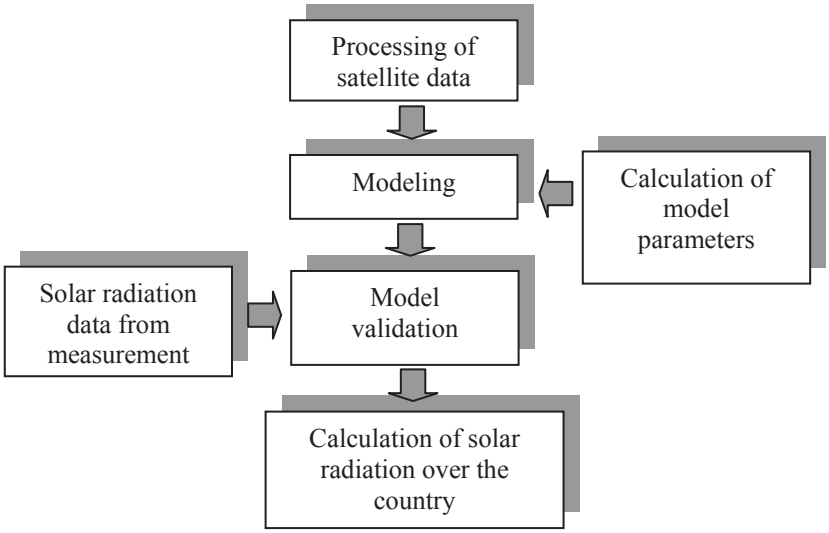

Fig. 2.1 Schematic diagram of the process for the retrieval of the solar radiation data from satellites for Thailand.

*This chapter has been published in Journal of the Institute of Engineering 8 (3), 130–139 (2012)

2.2.1 Processing of satellite data

In this study, satellite data obtained from four geostationary meteorological satellites including GMS4, GMS5, GOES9 and MTSAT-1R were used as the main input of a satellite-based model for calculating solar radiation. These satellites provide information on clouds which play an important role to solar radiation at the earth's surface. Details of each satellites are as following.

1) GMS4 satellite

The GMS4 satellite started operating in December, 1989 (Fig. 2.2). Its orbital altitude is 35,800 km above the ground. The satellite was located at the latitude 140 °E above the equator. This satellite was equipped with the Visible Infrared Spin Scan Radiometer (VISSR), which is used to record the earth's atmosphere in several wavelength bands ranging from the visible to infrared. GMS4 rotated 100 rounds per minute which allowed the VISSR to complete a scan of the earth's full-dish image within 30 minutes. Image signals obtained from the satellite were sent to a receiver at the Japanese Meteorological Agency (JMA) in Tokyo. After the signal processing, the image signals were sent back to the satellite and then broadcasted to Asia-pacific countries.

GMS4 provides the image signals in two different formats, namely digital stretched VISSR (S-VISSR) and weather facsimile format (WEFAX). The S-VISSR signal requires a large receiver and high capacity of computer to produce the images. As a result, the images obtained from the VISSR have high spatial resolution. On the other hand, the WEFAX signal needs a smaller receiver dish but the resolutions of the images are relatively poor. For solar radiation mapping purpose, the S-VISSR signals are normally used, because they provide better resolution compared to those from the WEFAX. An example image from S-VISSR signal is shown in Fig. 2.3.

Fig. 2.2 Geostationary meteorological satellite GMS4.

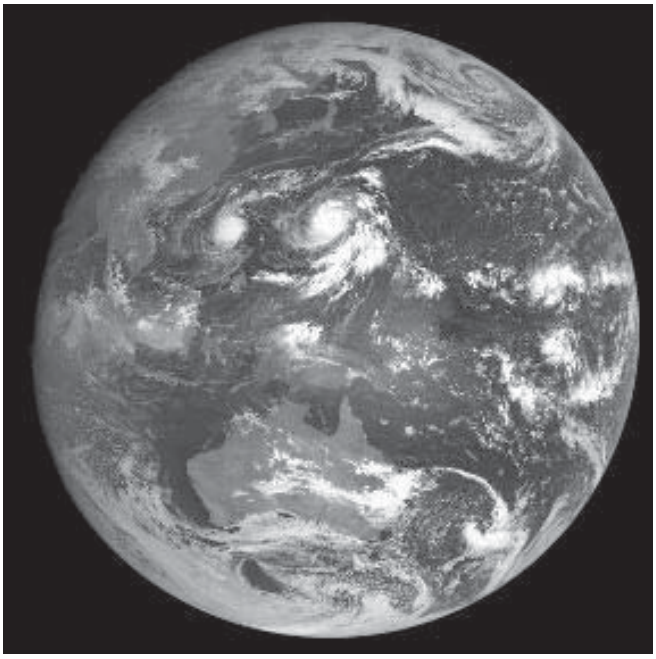

Fig. 2.3 Example of an image from GMS4.

In this study, hourly S-VISSR data from 8 am to 4 pm from January 1990 to May 1995 were used. The data have a spectral response covering the visible region (0.55-0.90 μm), which is presented in an 8-bit binary format with a resolution of 3x3 km^2 at the position of Thailand.

2) GMS 5 satellite

In June 1995, GMS4 satellite was replaced by GMS5 satellite. GMS5 has a similar specification as that of GMS4, expect for the number of signal channels. GMS5 has two infrared channels and one water vapour channel. The satellite was functioned until May, 2003.

3) GOES9 satellite

Due to a system failure of the GMS5, the GOES9 (Geostationary Operational Environmental Satellite 9) was temporally moved to replace the GMS5 during June 2003 to July 2005. GOES9 is a meteorological satellite of USA. It is located at 30,000 km above the Pacific Ocean near the west coast of USA. The instrument includes a new generation imager which operates on visible and infrared channels. This instrument is programmed to capture images of the earth for every hour.

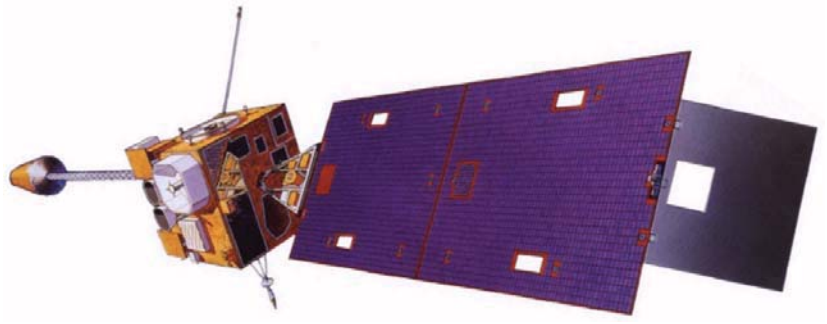

Fig. 2.4 Geostationary Operational Environmental Satellite 9 (GOES9).

The process of the GOES9 imaging system is shown in Fig. 2.4. The optical recording system comprises of mirrors, lens, filters and sensors which detect the reflected radiance in visible and infrared wavelength bands. The raw signals from the instrument are converted into the digital signals and sent to the ground station in USA. Afterwards, the signals are transformed into the 8-bit digital images which then are sent back to the satellite for distribution. An example image obtained from GOES9 satellite is shown in Fig. 2.5.

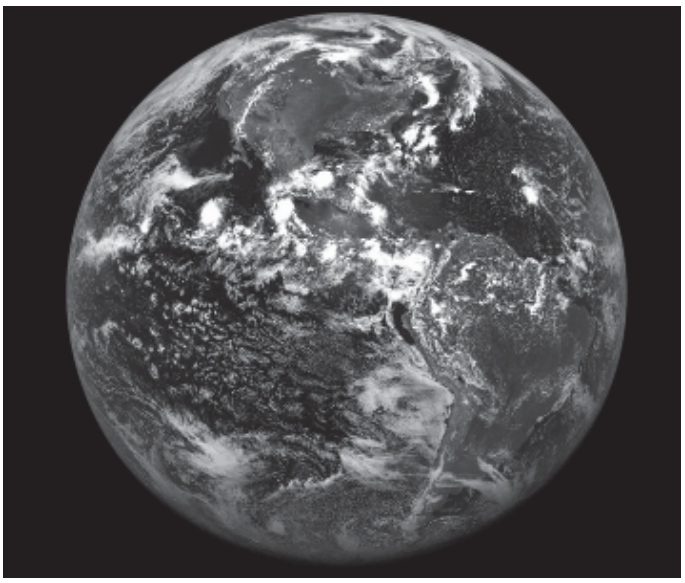

Fig. 2.5 An image from GOES9.

4) MTSAT-1R satellite

MTSAT-1R is one of the newest satellites used for weather forecast and aviation controls (Fig. 2.6). The satellite is owned by Japanese Meteorological Agency (JMA) and Japanese Ministry of Land, Infrastructure and Transport. The satellite was launched in February 2005 to replace GMS5. The MTSAT-1R comprises of a 5-channel spectroradiometer: one operating in the visible channel (0.55-0.80 μm) and the others in the infrared channels. The MTSAT-1R satellite is located at 140 °E above the equator at an altitude of 35,800 km. It records the images of the earth every half-hour with a resolution of 1x1 km^2.

Fig. 2.6 Multifunctional Transport Satellite-1R (MTSAT-1R).

On-board instrument of the MTSAT-1R satellite comprises optical system including lens, filters and mirrors which reflect the earth-reflected radiance into the sensors. The sensors convert the radiance into digital signals, which are then sent back to the JMA ground-based station in Japan. The signals are processed at the JMA station in Japan and then sent back to MTSAT-1R for distribution. The spectral response of MTSAT-1R is nearly the same wavelength range of GMS5. An example of the image from MTSAT-1R is shown in Fig. 2.7.

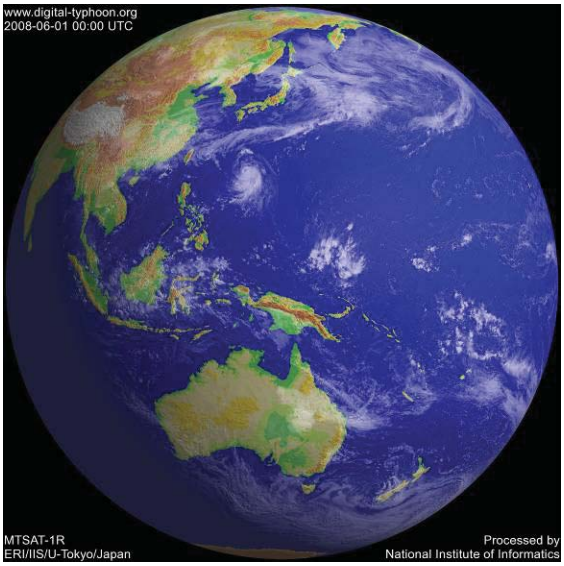

Fig. 2.7 Example image from MTSAT-1R.

The satellite images used in this work were presented in an 8-bit digital format. The visible data were obtained from 4 geostationary satellites namely GMS4, GMS5, GOES9 and MTSAT-1R. The periods of the satellite data used in this study are shown in Table 2.1.

Table 2.1 Period of the satellite data used in this study.

Satellite	Periods
GMS4	January, 1995 - May, 1995
GMS5	June, 1995 - May, 2003
GOES9	June, 2003 - July, 2005
MTSAT-1R	August, 2005 - December, 2009

Nine hourly images per day (8:30 am - 4.30 pm) collected for a total period of 15-year (1995-2009) and approximately 35,600 images were used in this work. When displayed as images, the digital data covered the entire area of Thailand with a spatial resolution of 3 x 3 km^2. These images were projected in satellite projection which are the globe was seen by the satellite. To use in this work the images were transformed into a cylindrical projection, being linear in latitude and longitude. After that, they were navigated by using features of the coastline as a reference. An example of the rectified image is shown in Fig. 2.8. Each image consists of a matrix of 500 x 800 pixels representing the reflected of solar radiation from the earth-atmosphere system in type of gray levels (digital count, 0-255). The values of the gray level were conversed to the pseudo-reflectivity (ρ'_{SAT}) by using calibration tables provided by the satellite agencies. In the final step, the pseudo-reflectivity was divided by cosine of the zenith angle of each pixel to obtain earth-atmospheric albedo (ρ'_{EA}). The values of ρ'_{EA} are used in the satellite-based radiation model.

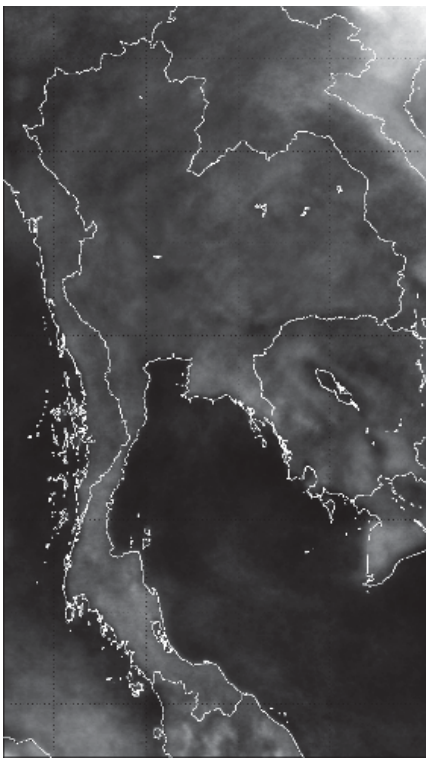

Fig. 2.8 Satellite data in cylindrical projection.

2.2.2 Satellite-based solar radiation model

A satellite-based solar radiation model proposed by Janjai et al. (2005) was modified for the calculation of surface global solar radiation from satellite data. The modified model considers absorption and scattering processes due to clouds, ozone, aerosols, water vapour and trace gases in the atmosphere both for the upwelling and downwelling path of solar radiation. The multiple reflection between the atmosphere and the ground is also taken into account in this model. The absorption and scattering of solar radiation in the earth-atmosphere system of this model are schematically shown in Fig. 2.9.

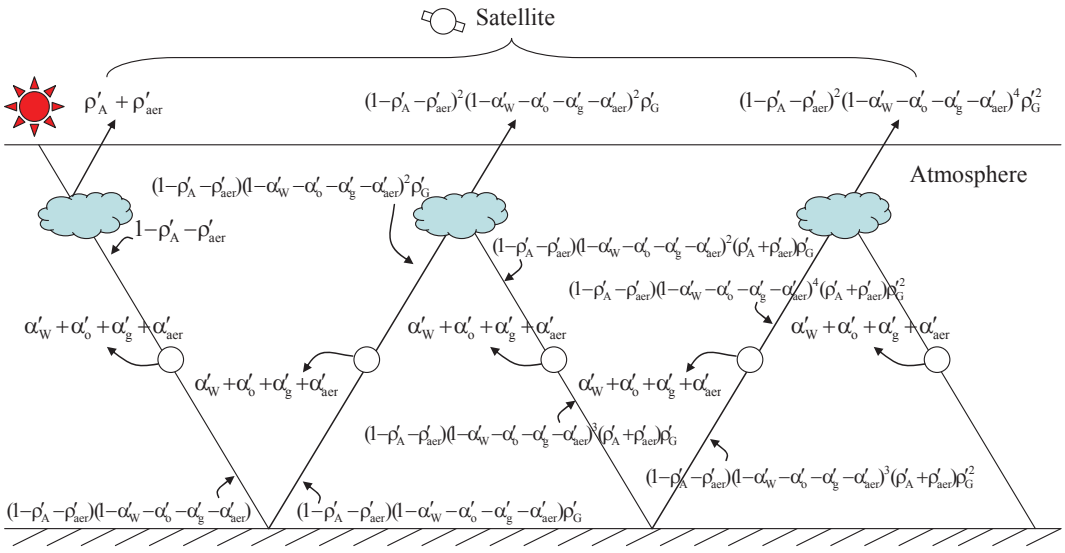

Fig. 2.9 Schematic diagram of the radiation budget as seen by the satellite (ρ'_A = scattering by gases and cloud, ρ'_{aer} = scattering by aerosols, α'_w = absorption by water vapour, α'_o = absorption by ozone, α'_g = absorption by gas, α'_{aer} = absorption by aerosols, ρ'_G = surface albedo).

Consider a unit of the downwelling solar radiation entering the earth's atmosphere, part of it is scattered to the outer space by air molecules and aerosols. The scattering due to air molecules and aerosols in the atmosphere can be represented in terms of reflectivity coefficients ($\rho'_A + \rho'_{aer}$), hence the remaining portion of radiation in its path is $1-\rho'_A-\rho'_{aer}$. From this point, the rest of the downwelling

radiation is absorbed by ozone, gases, water vapour and aerosols with the absorption coefficients of α'_o, α'_g, α'_w and α'_{aer}, respectively. The remaining solar radiation arriving at the ground is $(1-\rho'_A-\rho'_{aer})(1-\alpha'_w-\alpha'_o-\alpha'_{aer}-\alpha'_g)$. This term of solar radiation is then reflected back to the atmosphere by the ground with the surface albedo of ρ'_G. Part of the reflected solar radiation is again absorbed by aerosols and scattered by air molecules, aerosols and clouds. Hence, the solar radiation leaving the atmosphere to the outer space is written as $(1-\rho'_A-\rho'_{aer})^2 \times (1-\alpha'_w-\alpha'_o-\alpha'_{aer}-\alpha'_g)^2\rho'_G$. A combination of this reflected terms and the reflected terms in the downwelling path $(\rho'_A+\rho'_{aer})$ is called earth-atmospheric albedo (ρ'_{EA}) and it is captured by the satellite. With multiple reflection process of this the absorption and scattering terms continues, the earth atmospheric albedo (ρ'_{EA}), accounted for the multiple reflection, can be written as:

$$\rho'_{EA} = \rho'_A + \rho'_{aer} + \frac{(1-\rho'_A-\rho'_{aer})^2(1-\alpha'_w-\alpha'_o-\alpha'_{aer}-\alpha'_g)^2\rho'_G}{1-(\rho'_A+\rho'_{aer})(1-\alpha'_w-\alpha'_o-\alpha'_{aer}-\alpha'_g)^2\rho'_G} \qquad (2.1)$$

where ρ'_{EA} = earth-atmospheric albedo in the satellite wavelength band or narrow-band wavelength

ρ'_A = atmospheric albedo due to the scattering of cloud and air molecule in satellite band

ρ'_{aer} = scattering coefficient of aerosols in satellite band

α'_{aer} = absorption coefficient of aerosols in satellite band

α'_w = absorption coefficient of water vapour in satellite band

α'_o = absorption coefficient of ozone in satellite band

α'_g = absorption coefficient of gases in satellite band

ρ'_G = surface albedo in satellite band

Rearranging Eq. (2.1) yields:

$$\rho'_A = \frac{A - AC + ABC + BC^2}{C - 1 + BC + AC} \qquad (2.2)$$

where

$$A = \rho_{aer} - \rho_{EA}$$

$$B = 1 - \rho_{aer}$$

$$C = (1 - \alpha_w - \alpha_o - \alpha_{aer} - \alpha_g)^2 \rho_G$$

From Eq. (2.2), ρ'_{EA} is obtained from satellite data, ρ'_{aer}, α'_o, α'_w and α'_g can be derived from ground-based measurements. The surface albedo ρ'_G is also derived from satellite data. The method for deriving these coefficients is explained in the next section. Therefore, values of ρ'_A can be calculated from Eq. (2.2). In the next step ρ'_A, which is in satellite band (e.g. 0.55-0.90 μm for GMS5), is converted into broadband atmospheric albedo (ρ_A: 0.3-3.0 μm) using empirical formula explained in the next section. Then broadband atmospheric albedo (ρ_A) is used to calculate broadband atmospheric transmittance, which is expressed as:

$$\tau = \frac{(1 - \rho_A - \rho_{aer})(1 - \alpha_w - \alpha_o - \alpha_{aer} - \alpha_g)}{1 - (\rho_A + \rho_{aer})(1 - \alpha_w - \alpha_o - \alpha_{aer} - \alpha_g)^2 \rho_G} \qquad (2.3)$$

where τ = broadband transmittance of the atmosphere

ρ_A = atmospheric albedo due to the scattering of cloud and air molecule in broadband

ρ_{aer} = scattering coefficient of aerosols in broadband

α_{aer} = absorption coefficient of aerosols in broadband

α_w = absorption coefficient of water vapour in broadband

α_o = absorption coefficient of ozone in broadband

α_g = absorption coefficient of gases in broadband

ρ_G = surface albedo in broadband

The denominator term represents the multiple reflections between the ground and the atmosphere. The values of ρ_G, ρ_{aer}, α_{aer}, α_o and α_w can be calculated using ground-based data as explained in the next section. Therefore, values of τ are obtained from Eq. (2.3). These values are finally employed to compute solar radiation incident on the ground using the following equation.

$$H = \tau H_0 \tag{2.4}$$

where τ = solar radiation transmittance coefficient of the atmosphere

H = daily irradiation on the earth's surface

H_0 = extraterrestrial daily irradiation

The values of H_0 are calculated from

$$H_0 = \frac{24}{\pi} I_{sc} E_0 [(\pi/180)\omega_s \sin\delta \sin\phi + \cos\delta \cos\phi \sin\omega_s] \tag{2.5}$$

where I_{sc} = solar constant

E_0 = eccentricity correction factor of the earth's orbital

ω_s = sunset hour angle

δ = declination angle of the sun

ϕ = latitude of a position where solar radiation is calculated

2.2.3 Calculation of model parameters

2.2.3.1 Surface albedo (ρ_G)

Surface albedo represents the ratio of the incident solar radiation to the reflected solar radiation from the earth's surface. It depends on types of the earth's surface. Generally, surface albedo ranges from 20% for vegetative area to 90% for snow surface. Because surface albedo has an effect on radiative balance of the earth's

atmosphere, the values of surface albedo are usually required from satellite-based solar radiation models.

Surface albedo can be measured using an albedo meter. The instrument is made of two pyranometers: one is placed upward on a horizontal plane and the other is placed on the opposite direction. The albedo meter can be practically used to measure the surface albedo in a small area. For a large area, the measurements of surface albedo by using albedo meter are difficult and costly. However, the values of surface albedo for a large area can be obtained from the satellite-derived earth-atmosphere reflectivity. In this work, a technique for deriving surface albedo from the satellite data developed by Janjai et al. (2006) was used. This method is schematically shown in Fig. 2.10. Detail of each step is described as follows.

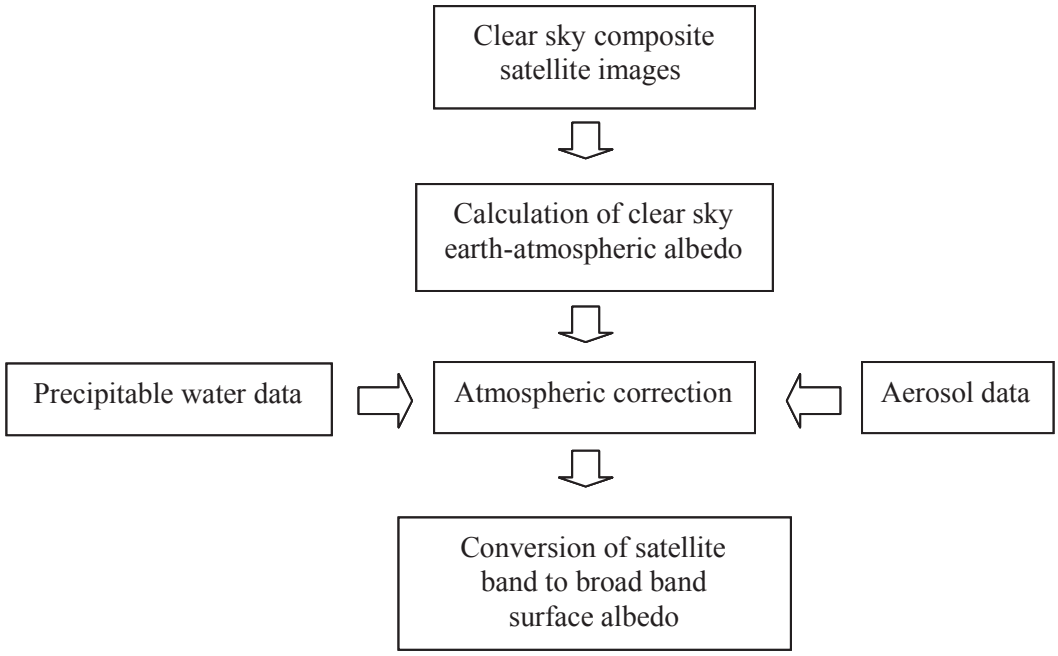

Fig. 2.10 Schematic diagram of the method for determining surface albedo.

In general, a satellite image features clouds, ocean and the earth's surface. However, in order to derive the surface albedo, only cloud free images are used. To obtain a cloud free image, a composite image was constructed for each month. The satellite images taken at 12:30 local time of each month were used for constructing the composite image. For a given month, the values of the gray level of pixel (1,1) of

all images taken at 12:30 in that month were compared and the lowest gray level was selected to be the gray level of pixel (1,1) of the composite image (Fig. 2.11). The process was repeated for all pixels to complete the composite image. Finally, this composite image was assumed to be a cloud-free image.

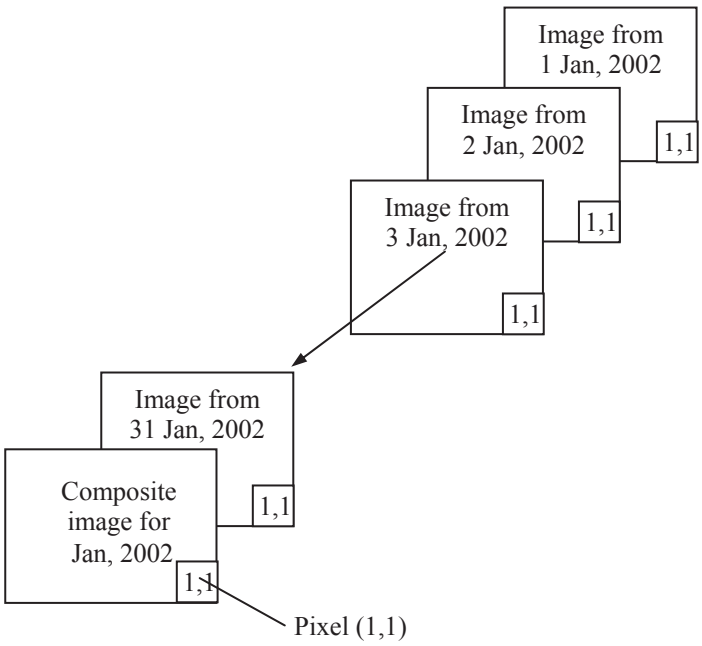

Fig. 2.11 Diagram of the process for constructing a composite image.

The gray level values of the composite image were converted into earth-atmospheric albedo by using a calibration curves given by the satellite agencies. As the earth-atmospheric albedo is the combination of the effect of the reflectivity from the ground and the reflectivity of the atmosphere, the effect of the reflectivity of the atmosphere needs to be eliminated by using an empirical formula (Eq. (2.6)) obtained from the 5S radiative transfer model (Tanre′ et al., 1986) as follows:

$$\rho'_G = c_0 + c_1\rho'_{EA} + c_2 w + c_3 VIS + c_4\theta_z \qquad (2.6)$$

where ρ'_G = surface albedo (-)

ρ'_{EA} = earth-atmospheric albedo of the cloud-free composite image (-)

w = precipitable water (cm)

VIS = visibility (km)

θ_z = solar zenith angle (degree)

c_0, c_1, c_2, c_3 and c_4 are constants. The values of these constants for January, April, July and October are shown in Table 2.2. For the other months, they are obtained from interpolation.

Table 2.2 Value of the constants c_0, c_1, c_2, c_3 and c_4 in Eq. (3.6)

Month	c_0	c_1	c_2	c_3	c_4
January	-0.064209	1.743128	0.002325	-0.000132	-0.000321
April	-0.056316	1.603282	0.000630	-0.000488	0.000330
July	-0.049643	1.529811	0.001134	-0.000296	0.000064
October	-0.055334	1.622538	0.001224	-0.000218	-0.000143

Eq. (2.6) was employed to convert earth-atmospheric albedo into the satellite band surface albedo over the country.

The surface albedo data calculated from the above process are in the satellite bands: 0.55-0.75 μm for GMS 4, 0.55-0.90 μm for GMS 5, 0.55-0.72 μm for GOES 9 and 0.55-0.80 μm for MTSAT-1R. The 5S radiative transfer code was used to convert these satellite bands into broadband surface albedo. In this study, the surface of Thailand is assumed to be vegetation type for the whole country.

The surface albedo in satellite band can be obtained from the following equation:

$$\rho'_G = \frac{\int_{\lambda_1}^{\lambda_2} I_\lambda \rho_{g\lambda} d\lambda}{\int_{\lambda_1}^{\lambda_2} I_\lambda d\lambda} \qquad (2.7)$$

where ρ'_G = satellite-band surface albedo

$\rho_{g\lambda}$ = spectral reflectance of vegetation

I_λ = solar spectral irradiance (W/m^2-μm)

λ_1 and λ_2 are wavelength intervals of the satellites.

The broadband surface albedo was calculated from:

$$\rho_G = \frac{\int_{0.3\mu m}^{3.0\mu m} I_\lambda \rho_{g\lambda} d\lambda}{\int_{0.3\mu m}^{3.0\mu m} I_\lambda d\lambda} \qquad (2.8)$$

where ρ_G = broadband surface albedo (-)

Applying the 5S code to equation (2.6)-(2.8), the relation between ρ_G and ρ'_G was obtained. This relation was applied to compute broad-band surface albedo of Thailand. An example of surface albedo for the year 2008 is shown in Fig. 2.12.

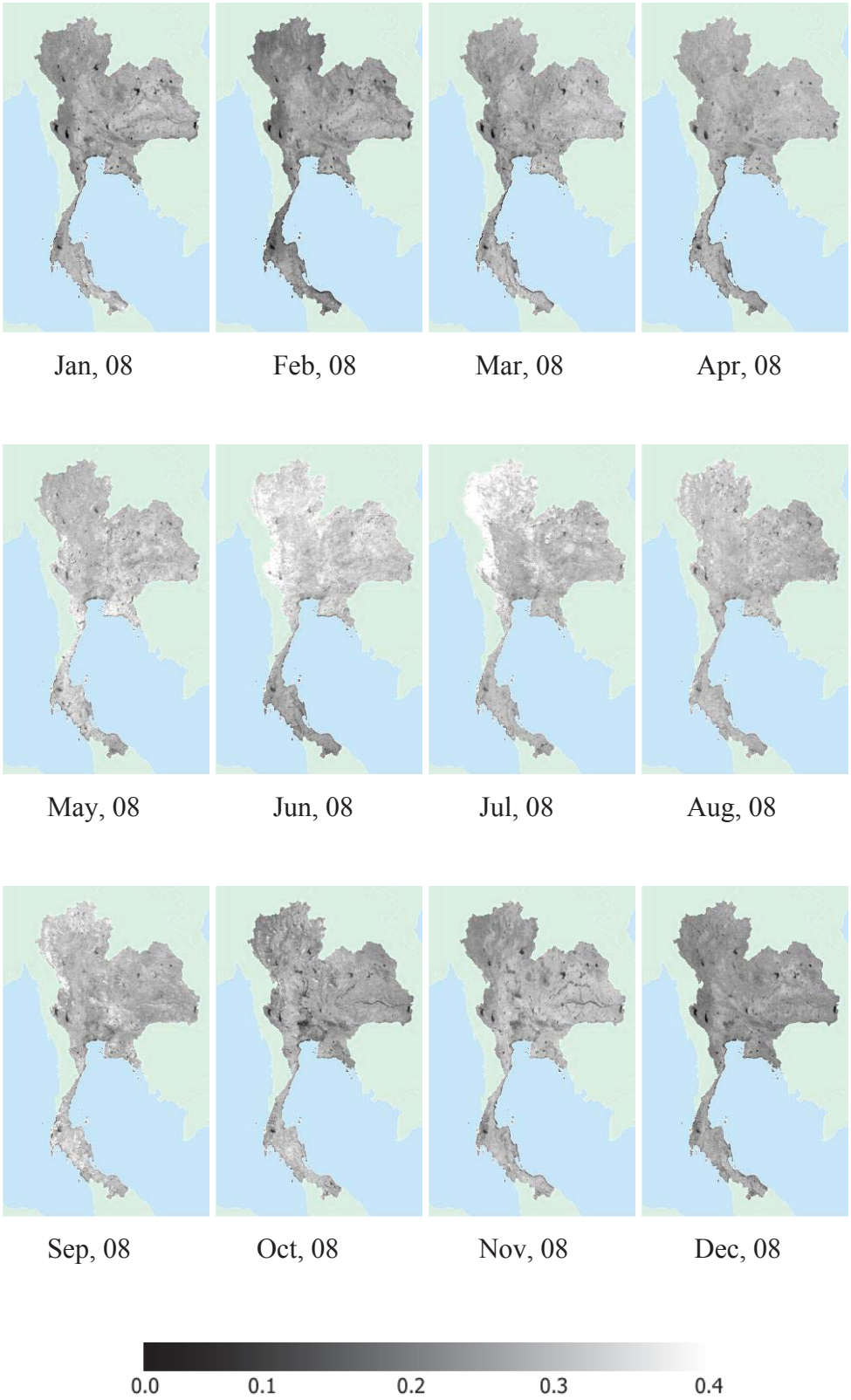

Fig. 2.12 An example of surface albedo for the year 2008.

2.2.3.2 Absorption coefficient of atmospheric gases

The relationship described by Iqbal (1983) for spectral transmission after absorption by carbon dioxide, oxygen and other trace gases was used. It can be expressed as:

$$\tau_{g\lambda} = \exp[-1.41 k_{g\lambda} m_a / (1 + 118.93 k_{g\lambda} m_a)^{0.45}] \quad (2.9)$$

where $\tau_{g\lambda}$ = spectral transmittance of gases

$k_{g\lambda}$ = extinction coefficient of gases

m_a = air mass for local conditions

The absorption coefficient of gases is calculated from:

- in satellite band

$$\alpha_g' = 1 - \frac{\int_{\lambda_1}^{\lambda_2} I_{0\lambda} \tau_{g\lambda} d\lambda}{\int_{\lambda_1}^{\lambda_2} I_{0\lambda} d\lambda} \quad (2.10)$$

- in broadband

$$\alpha_g = 1 - \frac{\int_{0.3}^{3.0} I_{0\lambda} \tau_{g\lambda} d\lambda}{\int_{0.3}^{3.0} I_{0\lambda} d\lambda} \quad (2.11)$$

where α_g' = absorption coefficient of gases in satellite band

α_g = absorption coefficient of gases in broadband

$I_{0\lambda}$ = extraterrestrial spectral irradiance (W/m^2-μm)

$\tau_{g\lambda}$ = spectral transmittance of gases

λ_1, λ_2 = wavelength band of the satellites (μm)

The air mass for the local condition (m_a) is calculated from (Iqbal, 1983):

$$m_a = m_r (p / 1013.25) \quad (2.12)$$

where m_r = air mass

p = local atmospheric pressure (mbar)

The air mass (m_a) is computed from the following formula (Iqbal, 1983):

$$m_r = [\cos\theta_z + 0.15(93.885 - \theta_z)^{-1.253}]^{-1} \quad (2.13)$$

where θ_z = zenith angle (degree)

The local atmospheric pressure (p) is obtained from (Iqbal, 1983):

$$p = p_0 \exp(-0.0001184z) \quad (2.14)$$

where p_0 = standard pressure (mbar)

z = altitude of the location above the mean sea level (m)

2.2.3.3 Absorption coefficient of ozone

Ozone absorbs solar radiation in the wavelengths of ultraviolet and a small part of the visible region. The ozone in the atmosphere is quantified in Dobson unit. In general, the total column ozone is measured using a Dobson spectroradiometer. Since 1979, the space-borne ozone monitoring radiometers such as Total Ozone Mapping Spectroradiometer (TOMS) and Ozone Monitoring Instrument (OMI) have also provided the total column ozone data.

In this study, the absorption coefficients due to ozone are calculated from the following equations.

- for satellite band

$$\alpha_o' = 1 - \frac{\int_{\lambda_1}^{\lambda_2} I_{0\lambda}\tau_{o\lambda}d\lambda}{\int_{\lambda_1}^{\lambda_2} I_{0\lambda}d\lambda} \quad (2.15)$$

- for broadband

$$\alpha_o = 1 - \frac{\int_{0.3}^{3.0} I_{0\lambda}\tau_{o\lambda}d\lambda}{\int_{0.3}^{3.0} I_{0\lambda}d\lambda} \quad (2.16)$$

where α'_o = absorption coefficient of ozone in satellite band

α_o = absorption coefficient of ozone in broadband

$I_{0\lambda}$ = extraterrestrial spectral irradiance (W/m^2-μm)

$\tau_{o\lambda}$ = spectral transmittance of ozone

λ_1, λ_2 = wavelength band of the satellites (μm)

Spectral transmittance coefficient of ozone was calculated from Eq. (2.17) (Iqbal, 1983):

$$\tau_{o\lambda} = \exp(-k_{o\lambda} l m_a) \quad (2.17)$$

where $\tau_{o\lambda}$ = ozone spectral transmittance

$k_{o\lambda}$ = extinction coefficient of ozone

l = total column ozone (cm)

m_a = air mass

The total column ozone from TOMS and OMI were used for the calculation of the spectral transmittance coefficient. Daily total column ozone from these satellites was averaged over individual months to arrive at monthly total column ozone map. These available data at a resolution of 1.0° (latitude) x 1.25° (longitude) were subdivided into pixels of 3x3 km^2 to match the GMS4, GMS5, GOES9 and MTSAT-1R pixels. By using Eq. (2.17), the absorption coefficient of ozone over Thailand was determined. An example of the map of total column ozone for the year 2008 is shown in Fig. 2.13.

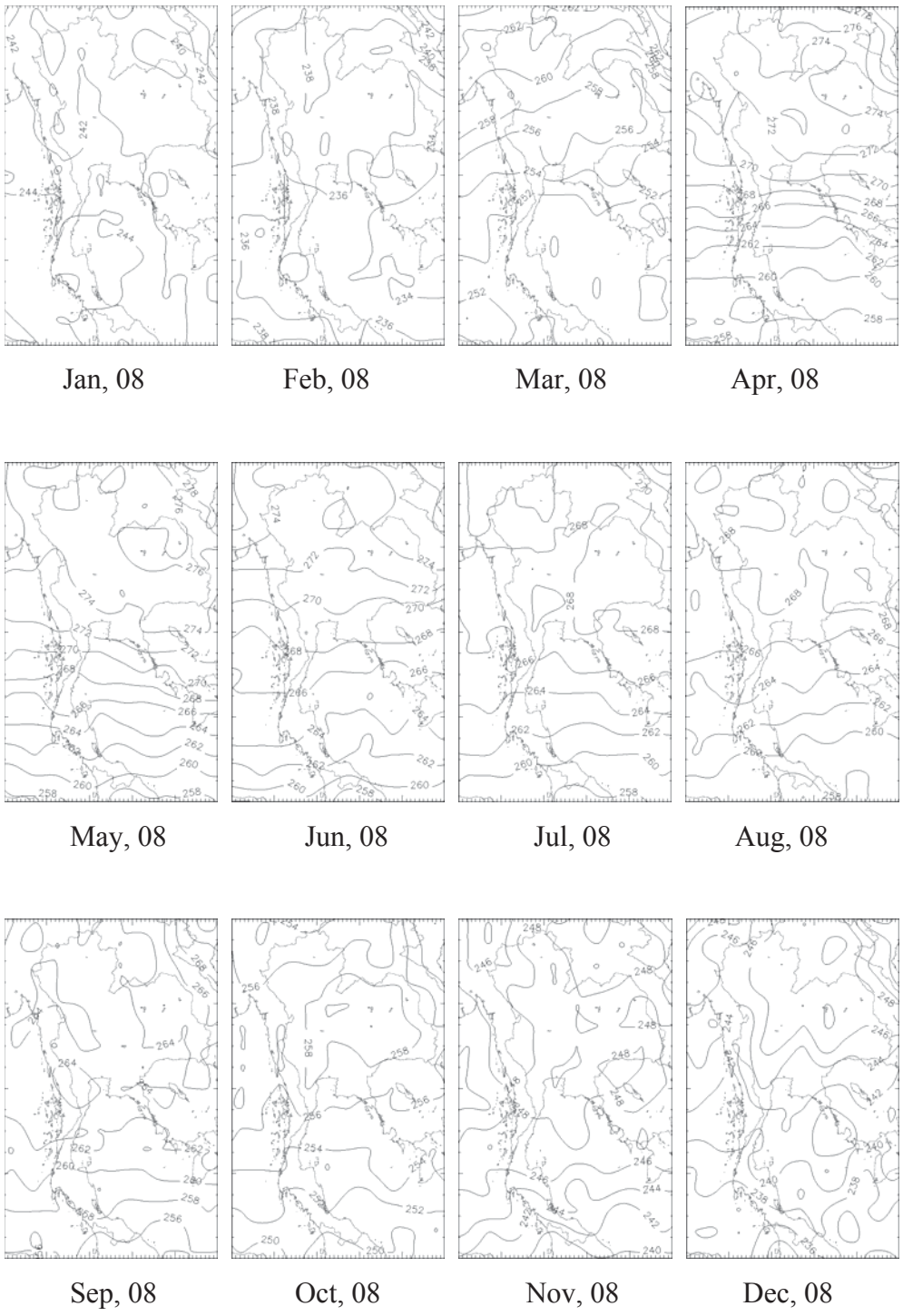

Fig. 2.13 An example of the map of total column ozone (Dobson) for the year 2008.

2.2.3.4 Absorption coefficient of water vapour

Atmospheric water vapour is the gas phase of water in the atmosphere. Under normal condition, water vapour is produced from evapouration processes. Water vapour in the atmosphere of the tropical regions absorbs solar radiation 10-14% (Janjai et al., 2005). Therefore, the atmospheric water vapour is very important to the solar radiation estimates. The amount of the atmospheric water vapour depends on the environment and climate. Water vapour is high in the tropics where most of the areas are covered with forest and wet-land. In contrast, water vapour is low in winter as dry weather condition brought from the mid-latitude reduces rainfall and the photosynthesis activities in the tropics.

The amount of atmospheric water vapour is usually quantified as a thickness (in cm) of precipitable water vapour. The absorption coefficient of water vapour can be determined by the followings Eqs.

- in satellite band

$$\alpha'_w = 1 - \frac{\int_{\lambda_1}^{\lambda_2} I_{0\lambda}\tau_{w\lambda}d\lambda}{\int_{\lambda_1}^{\lambda_2} I_{0\lambda}d\lambda} \qquad (2.18)$$

- in broadband

$$\alpha_w = 1 - \frac{\int_{0.3}^{3.0} I_{0\lambda}\tau_{w\lambda}d\lambda}{\int_{0.3}^{3.0} I_{0\lambda}d\lambda} \qquad (2.19)$$

where $I_{0\lambda}$ = extraterrestrial spectral irradiance (W/m^2-μm)

$\tau_{w\lambda}$ = spectral transmittance of water vapour (-)

α'_w = absorption coefficient of water vapour in satellite band (-)

α_w = absorption coefficient of water vapour in broadband (-)

λ_1, λ_2 = wavelength bands of the satellite (μm)

Transmittance of water vapour) $\tau_{w\lambda}$ (is determined by Eq. (2.20) (Iqbal, 1983).

$$\tau_{w\lambda} = \exp[-0.2385k_{w\lambda}wm_r/(1+20.07k_{w\lambda}wm_r)^{0.45}] \qquad (2.20)$$

where $k_{w\lambda}$ = extinction coefficient of water vapour

m_r = air mass (-)

w = precipitable water (cm)

In general, monthly averages of the precipitable water have statistical relation with monthly averages of ambient temperature and relative humidity. The relationship is written as Eq. (2.21) (Janjai et al., 2005):

$$w = 0.8933 \exp(0.1715\, rh\, p_s / T) \tag{2.21}$$

where w = precipitable water (cm)

rh = relative humidity (decimal)

T = temperature (K)

p_s = saturated water pressure (mbar)

By using Eq. (2.18), monthly average values of precipitable water were calculated from temperature and relative humidity data collected at 85 meteorological stations over Thailand. The positions of meteorological stations are shown in Fig. 2.14. The values of precipitable water were then mapped for the entire country by using an interpolation technique. Example of the precipitable water map for the year 2008 is shown in Fig. 2.15.

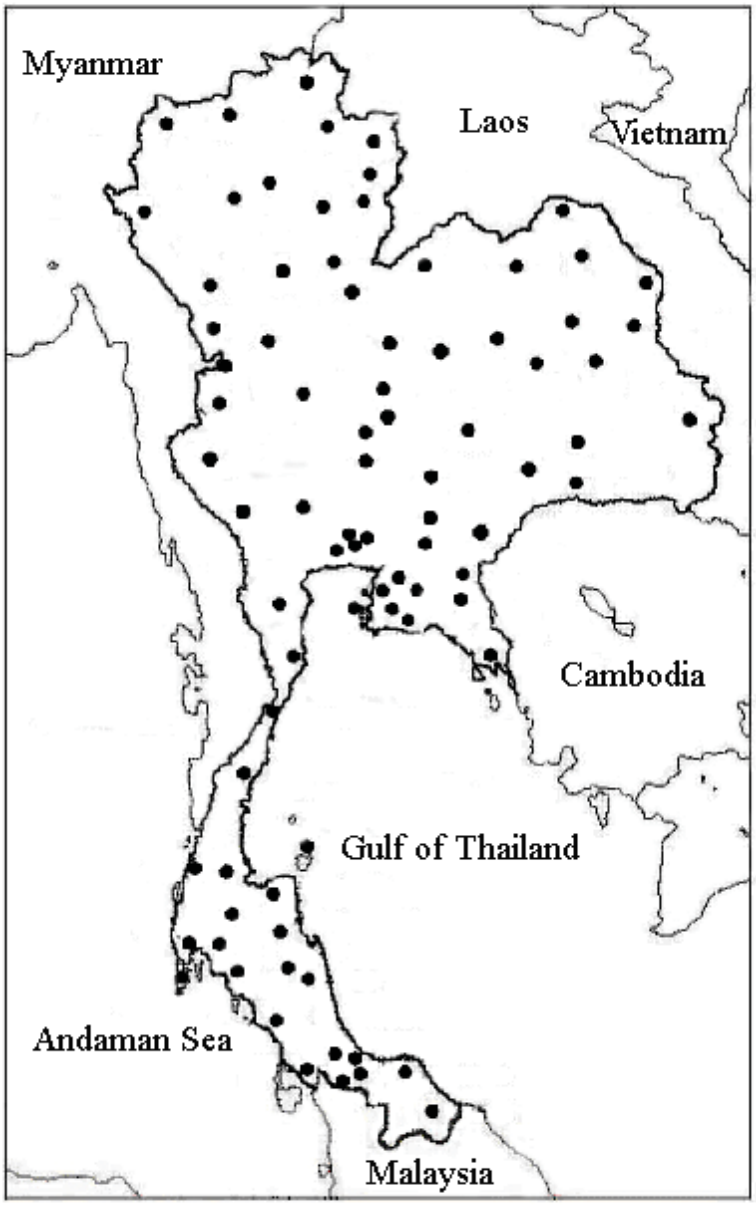

Fig. 2.14 Positions of the meteorological stations where ambient air temperature and relative humidity were used to calculate precipitable water.

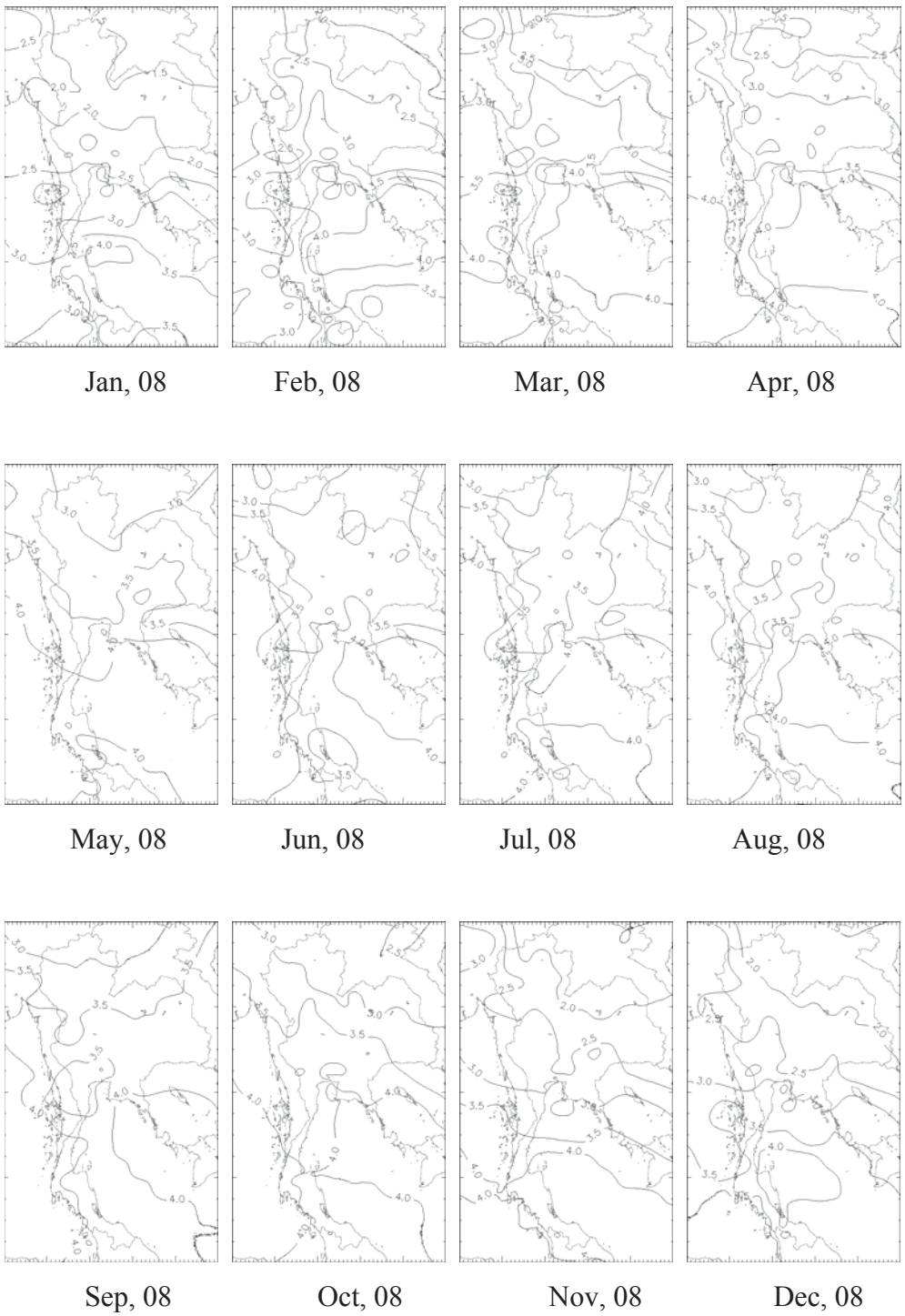

Fig. 2.15 Map of precipitable water (cm) for the year 2008.

2.2.3.5 Solar radiation depletion by aerosols

Aerosols are fine solid and liquid particles which suspend in the atmosphere. These are produced from human activities or natural processes such as volcanic eruptions, bush fires, oceanic haze and sands from deserts. Size of the aerosols ranges from a few nm to 100 μm. In general, the aerosols produced over land areas are called "continental aerosols". In cities and industrial areas, most aerosols are produced from combustion processes or burning of fossil fuels and these are called "urban aerosols". Small sea salt particles from the oceans are called "maritime aerosols".

In high polluted areas, aerosols can diminish solar radiation by 20-40% (Nunez, 1993). Furthermore, the lifetime of these aerosols ranges from several days to a few weeks. Thus, aerosols play an important role in depleting solar radiation within the atmosphere. Aerosol properties in the atmosphere can be measured by using ground-based instruments such as sunphotometers. However, it is costly to deploy such instruments over a large area. The amount of aerosols has an inverse relationship to values of visibility. The more aerosols exist in the atmosphere, the lower visibility is observed. Therefore, visibility was used to quantify the effect of aerosols on solar radiation in this study.

In Thailand, visibility observations were obtained from the meteorological stations. In addition, the visibility observations from the neighboring countries including China and cargo ships in the Gulf of Bengal were also used in this work. An interpolation technique was applied to determine visibility over Thailand.

The depletion of solar radiation due to aerosols can be estimated from the visibility data. A relationship between the visibility data and the depletion due to aerosols, which was developed by Janjai et al. (2005) was used in this work. This relationship is written as:

$$D_{aer} = 0.3631 - 0.0222(VIS) + 0.0003(VIS)^2 \qquad (2.22)$$

where D_{aer} = solar radiation depletion coefficient due to aerosols

VIS = visibility (km)

The visibility data obtained from 85 meteorological stations (Fig. 2.16) across the country were used in this work. The data from these stations were interpolated to obtain the visibility data covering the entire areas of the country.

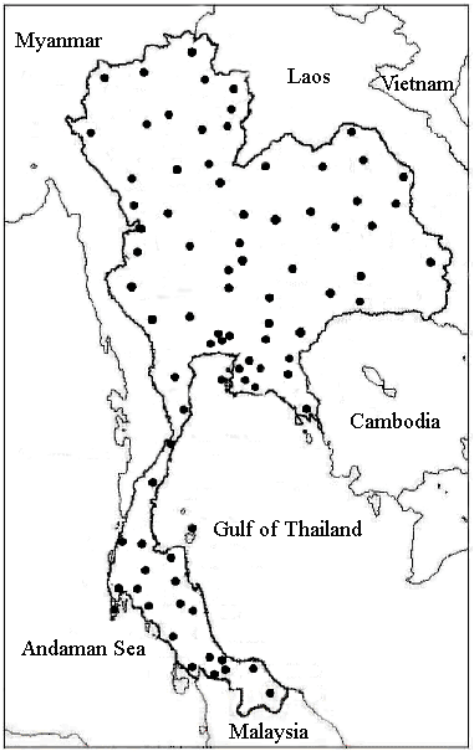

Fig. 2.16 Positions of the meteorological stations where visibility data were used in this work.

The depletion of solar radiation caused by aerosols (D_{aer}) is a result of absorption and scattering processes. Hence, Eq. (2.22) can be written:

$$D_{aer} = D_{ab} + D_{sc} \tag{2.23}$$

where D_{aer} = solar radiation depletion coefficient due to aerosols

D_{ab} = fraction of solar radiation absorbed by aerosols

D_{sc} = fraction of solar radiation scattered by aerosols

To determine the scattering and absorption effects, single scattering albedo data (SSA) provided by AERONET (Aerosol Robotic Network of NASA) were collected from eighty-two sites located across East Asia. The data were used to determine the proportion between the scattering and absorption caused by aerosols over Thailand. The data were arranged into three groups by seasons: February to June, July to September and October to January, then the absorption and scattering fractions were mapped for the entire areas of Thailand using an interpolation technique. Using these fractions, the scattering and absorption coefficients were determined using Eq. (2.24) and (2.25), respectively.

$$\rho_{aer} = D_{sc} D_{aer} \tag{2.24}$$

$$\alpha_{aer} = D_{ab} D_{aer} \tag{2.25}$$

where ρ_{aer} = solar radiation scattering coefficient of aerosols

α_{aer} = solar radiation absorption coefficient of aerosols

2.2.3.6 Broadband atmospheric reflectivity (ρ_A)

The broadband atmospheric reflectivity (ρ_A) is required for the calculation of the surface solar radiation (Eq. 2.3 and 2.4). However, the satellite gives only the satellite band reflectivity (ρ'_A in Eq. (2.2)). We proposed to convert ρ'_A into ρ_A by using statistical relations derived from solar radiation data collected from four solar radiation monitoring stations of Silpakorn University. Details of these stations are given in Table 2.3 and the procedure for deriving the relations are explained as follows.

Table 2.3 Details of the stations and their data.

Stations	Latitude	Longitude	Period of data
Chiang Mai	18.78 ºN	98.98 ºE	Jan, 1995-Dec, 2008
Ubon Ratchathani	15.25 ºN	104.87 ºE	Jan, 1995-Dec, 2008
Nakhon Pathom	13.82 ºN	100.04 ºE	Jan, 1990-Dec, 2008
Songkhla	7.20 ºN	100.60 ºE	Jan, 1995-Dec, 2008

Firstly, the equation for calculating the broadband atmospheric transmittance (Eq. (2.3)) was rearranged to obtain the broadband atmospheric reflectivity as:

$$\rho_A = \frac{(1-\rho_{aer})(1-\alpha_o-\alpha_w-\alpha_{aer})-\tau(1-\rho_G)(1-\alpha_o-\alpha_w-\alpha_{aer})^2}{1-\alpha_o-\alpha_w-\alpha_{aer}-\tau\rho_G(1-\alpha_o-\alpha_w-\alpha_{aer})^2} \quad (2.26)$$

In Eq. (2.20), the atmospheric transmittance τ was calculated by

$$\tau = \frac{H}{H_0} \quad (2.27)$$

where τ = atmospheric transmittance

H = monthly average daily global radiation

H_0 = monthly average daily extraterrestrial radiation

The values of H were obtained from the measurements at all four stations. The other parameters of Eq. (2.26) were estimated using the method described in the previous sections with the input data measured at all four stations.

Secondly, the values of the satellite band atmospheric albedo (ρ'_A) were computed from Eq. (2.2) employing the satellite-derived earth-atmospheric albedo (ρ'_{EA}) and the other parameters at the four stations.

Thirdly, the values of the broadband atmospheric reflectivity (ρ_A) were plotted against those of the satellite band reflectivity. The results are shown in Fig. 2.17-2.20.

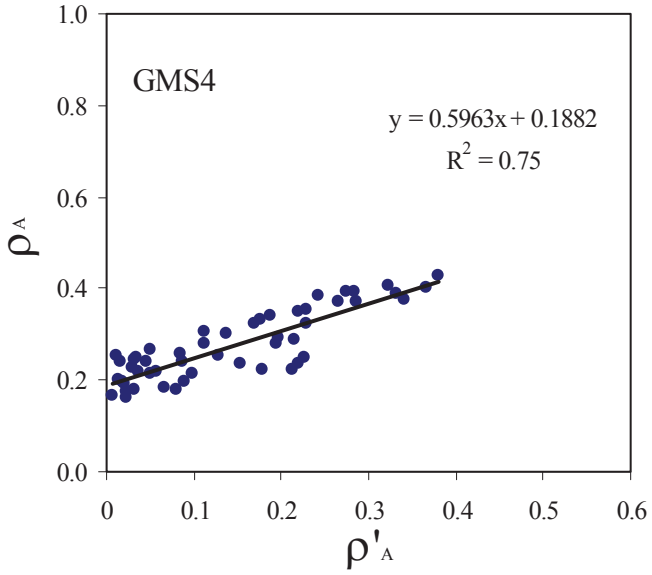

Fig. 2.17 Relation between the broadband atmospheric reflectivity (ρ_A) and satellite band atmospheric reflectivity (ρ'_A) for GMS4.

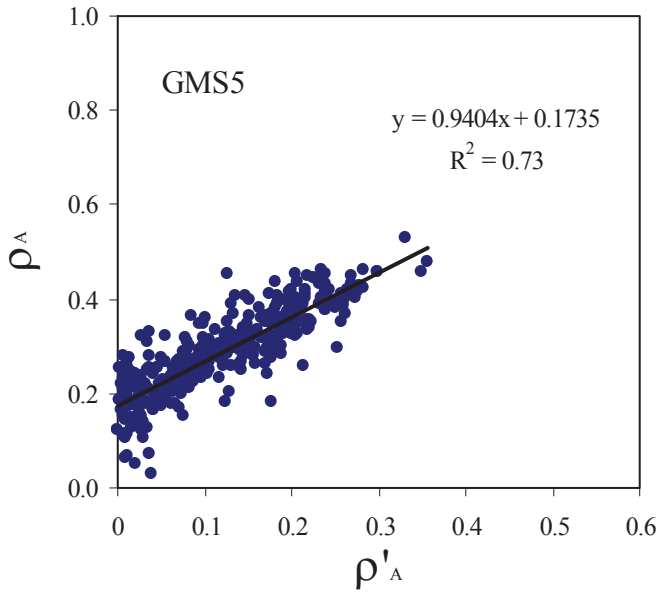

Fig. 2.18 Relation between the broadband atmospheric reflectivity (ρ_A) and satellite band atmospheric reflectivity (ρ'_A) for GMS5.

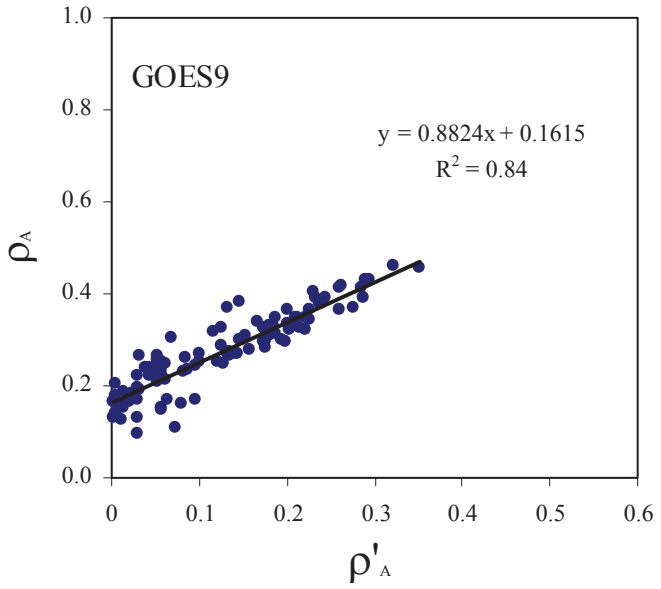

Fig. 2.19 Relation between the broadband atmospheric reflectivity (ρ_A) and satellite band atmospheric reflectivity (ρ'_A) for GOES9.

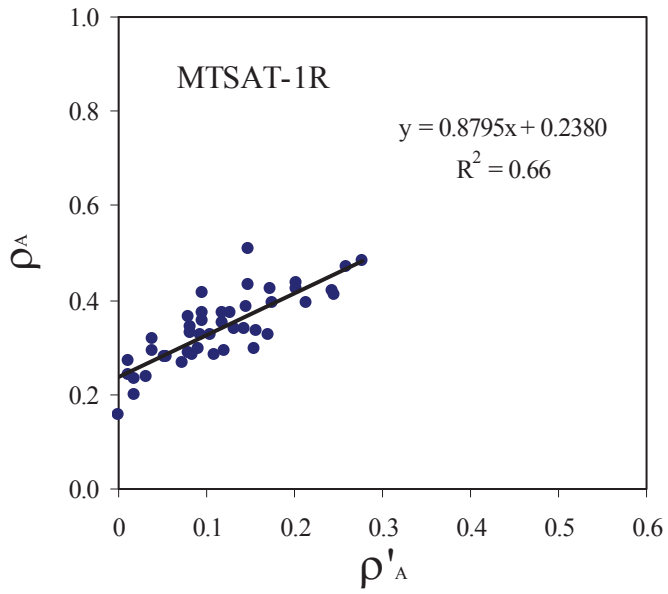

Fig. 2.20 Relation between the broadband atmospheric reflectivity (ρ_A) and satellite band atmospheric reflectivity (ρ'_A) for MTSAT-1R.

Finally, the graphs in Fig. 2.17-2.20 were fitted with empirical equation written as follows:

For GMS4 $\rho_A = 0.5963\,\rho'_A + 0.1882$ $R^2 = 0.75$ (2.28)

For GMS5 $\rho_A = 0.9404\,\rho'_A + 0.1735$ $R^2 = 0.73$ (2.29)

For GOES9 $\rho_A = 0.8824\,\rho'_A + 0.1615$ $R^2 = 0.84$ (2.30)

For MTSAT-1R $\rho_A = 0.8795\,\rho'_A + 0.2380$ $R^2 = 0.66$ (2.31)

These empirical relations were used to convert ρ'_A into ρ_A in the model validation and radiation mapping processes.

2.2.4 Model validation

The technique used in this study relies on the satellite data and ground based observations. A validation scheme which compares the satellite-derived solar radiation to the ground measurements was still needed prior to the generation of solar radiation maps. To accomplish this step, the models written in Eqs. (2.1)-(2.4) were used to calculate solar radiation at positions of 38 solar monitoring stations of Thailand. The values of solar radiation obtained form the models were then compared with the measurements of each station. The positions of these stations are shown in Fig. 2.24, and their name and latitude and longitude are given in Table 2.4.

Table 2.4 Name, latitude, longitude of measurement stations and period of data.

No.	Stations	Latitude	Longitude	Period of data
1	Chiang Rai	20.08	99.88	Jan, 2002 – Dec, 2009
2	Mae Hong Son	19.43	97.96	Jan, 2002 – Dec, 2009
3	Doi Intanon (Mae Klang)	18.40	98.67	Mar, 2005 – Dec, 2009
4	Doi Intanon (Tourist center)	18.54	98.52	Apr, 2005 – Dec, 2009
5	Doi Intanon (Radar)	18.50	98.40	Jan, 2006 – Dec, 2009
6	Nan	18.72	100.75	Jan, 2002 – Dec, 2009
7	Chiang Mai (Sansai)	18.83	98.88	Jan, 2002 – Dec, 2009
8	Mae Sa Riang	18.17	97.93	Jan, 2005 – Dec, 2009
9	Phrae	18.06	100.06	Jan, 2005 – Dec, 2009
10	Tak	16.80	98.90	Jan, 2002 – Dec, 2009
11	Loei	17.40	101.00	Apr, 2005 – Dec, 2009
12	Nong Khai	17.87	102.72	Jan, 2002 – Dec, 2009
13	Khon Kaen	16.45	102.78	Feb, 2002 – Dec, 2009
14	Nakhon Panom	16.97	104.73	Jan, 2002 – Dec, 2009
15	Surin	14.88	103.50	Jan, 2002 – Dec, 2009
16	Ubon Ratchathani	15.28	105.14	Jan, 2002 – Dec, 2009
17	Nakhon Ratchasima	14.97	102.08	Jan, 2002 – Dec, 2009
18	Roi Et	16.07	103.00	Mar, 2006 – Dec, 2009
19	Phitsanulok	16.78	100.27	Jan, 2002 – Dec, 2009
20	Phetchabun	16.43	101.15	Jan, 2002 – Dec, 2009
21	Nakhon Sawan	15.67	100.12	Jan, 2002 – Dec, 2009
22	Lop Buri	14.83	100.62	Jan, 2002 – Dec, 2009
23	Bangkok	13.75	100.52	Apr, 2002 – Dec, 2009
24	Kanchanaburi (Muang)	14.02	99.53	Jan, 2005 – Dec, 2009
25	Kanchanaburi (Thong Pha Phum)	14.73	98.63	Jan, 2002 – Dec, 2009
26	Sa Kaeo (Aranyaprathet)	13.70	102.00	Jan, 2007 – Dec, 2009
27	Trat	11.77	102.88	Mar, 2006 – Dec, 2009

No.	Stations	Latitude	Longitude	Period of data
28	Prachin Buri	13.97	101.70	Jan, 2002 – Dec, 2009
29	Chon Buri	13.37	100.97	Mar, 2005 – Dec, 2009
30	Prachuap Khiri Khan	11.83	99.83	Feb, 2002 – Dec, 2009
31	Chumphon	10.40	99.18	Mar, 2005 – Dec, 2009
32	Ranong	9.98	98.62	Jan, 2002 – Dec, 2009
33	Surat Thani (Samui)	9.47	100.05	Jan, 2002 – Dec, 2009
34	Surat Thani (Punpin)	9.13	99.15	Apr, 2005 – Dec, 2009
35	Phuket	8.13	98.30	Jan, 2002 – Dec, 2009
36	Trang	7.52	99.62	Mar, 2005 – Dec, 2009
37	Songkhla (Hadyai)	6.92	100.43	Jan, 2002 – Dec, 2009
38	Narathiwat	6.40	101.82	Feb, 2002 – Dec, 2009

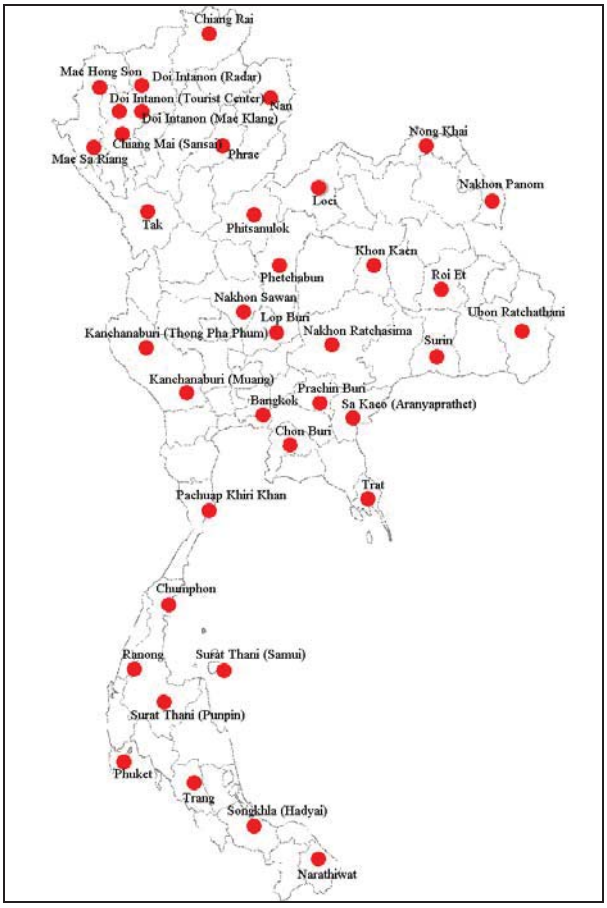

Fig. 2.21 Positions of solar radiation monitoring stations where solar radiation data were used for the model validation.

Monthly average of the earth atmospheric albedo (ρ'_{EA}) was determined from satellite data. The data were selected over sub-arrays of 3×3 pixels, centered at the stations. The values of ρ'_{EA} obtained from all pixels in each sub-array were then averaged to obtain the average earth atmospheric albedo of the stations. Using the measurement data, the scattering and absorption coefficients α'_w, α'_o, ρ'_G, α'_{aer} and ρ'_{aer} were also computed for each stations. All coefficients were then substituted into Eq. (2.2), and the values of ρ'_A were obtained for each station. Using Eq. (2.28), (2.29), (2.30) or (2.31), the values of ρ'_A were converted into the broadband atmospheric reflectivity (ρ_A). All variables estimated for the broadband wavelength including $\rho_A, \rho_G, \rho_{aer}, \alpha_{aer}, \alpha_o$ and α_w were used to compute the broadband atmospheric transmittance (τ) from Eq. (2.3). Finally, broadband surface solar radiation (H) was estimated for all stations by using Eq. (2.4).

Comparisons of monthly averages of satellite-derived daily solar radiation and the measurement data collected from 38 stations were carried out. Results of the comparison are shown in Fig. 2.22 – 2.60.

The performance of the model is expressed in terms of root mean square difference (RMSD) and mean bias difference (MBD) defined as follows (Iqbal, 1983):

$$\text{RMSD} = \frac{\sqrt{\dfrac{\sum_{i=1}^{N}(H_{model,i} - H_{meas,i})^2}{N}}}{\overline{H}_{meas}} \times 100\% \qquad (2.32)$$

$$\text{MBD} = \frac{\dfrac{H_{model,i} - H_{meas,i}}{N}}{\overline{H}_{meas}} \times 100\% \qquad (2.33)$$

where RMSD = root mean square difference (%)

MBD = mean bias difference (%)

$H_{model,i}$ = monthly average daily radiation calculated from the model for the month i (i = 1,2,….,12)

$H_{meas,i}$ = monthly average daily radiation obtained from the measurements for the month i

$\overline{H}_{meas}$ = monthly average daily radiation obtained from the measurements for the whole data

From Fig. 2.22– 2.59, it is observed that the discrepancies between the measured and calculated solar radiation in terms of root mean square difference (RMSD) and mean bias difference (MBD) are relatively low. The value of calculated radiation were also plotted against the measured radiation for all stations. The result is shown in Fig. 2.60. RMSD and MBD for all stations are 6.1% and 0.3%, respectively.

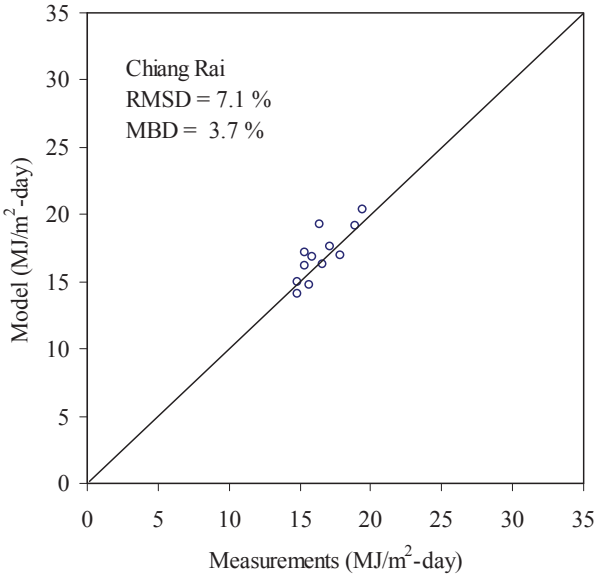

Fig. 2.22 Comparison between the monthly average daily global radiation from the model and from the measurements in Chiang Rai.

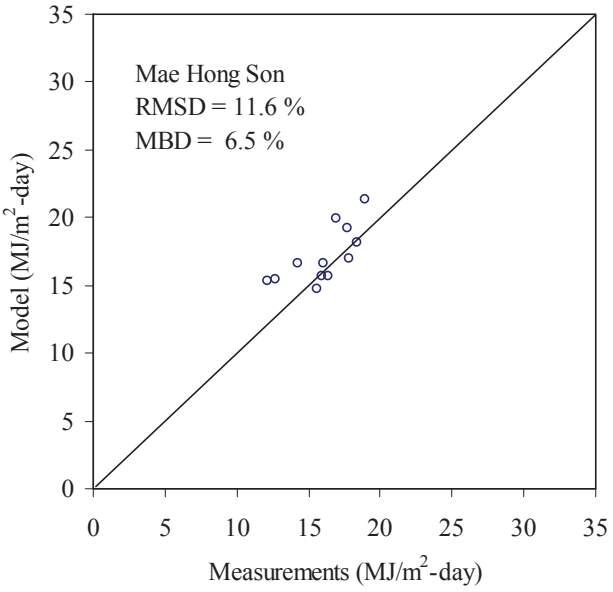

Fig. 2.23 Comparison between the monthly average daily global radiation from the model and from the measurements in Mae Hong Son.

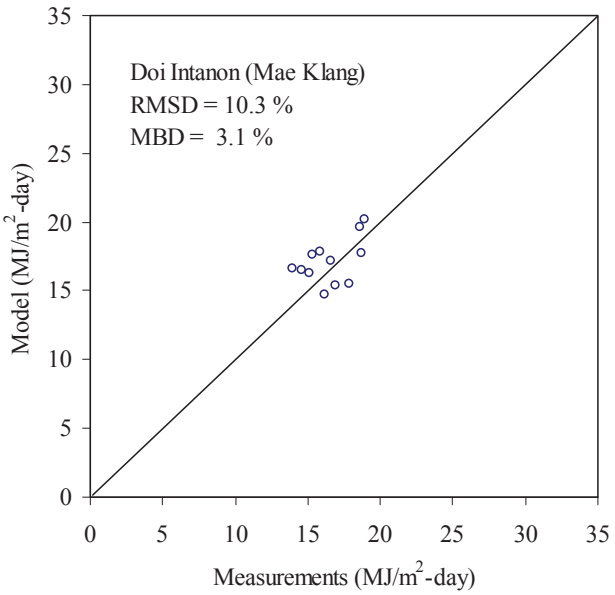

Fig. 2.24 Comparison between the monthly average daily global radiation from the model and from the measurements at Doi Intanon (Mae Klang).

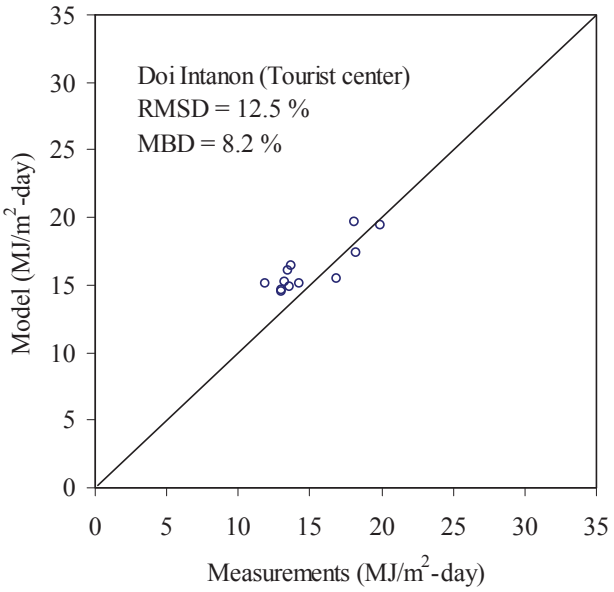

Fig. 2.25 Comparison between the monthly average daily global radiation from the model and from the measurements at Doi Intanon (Tourist center).

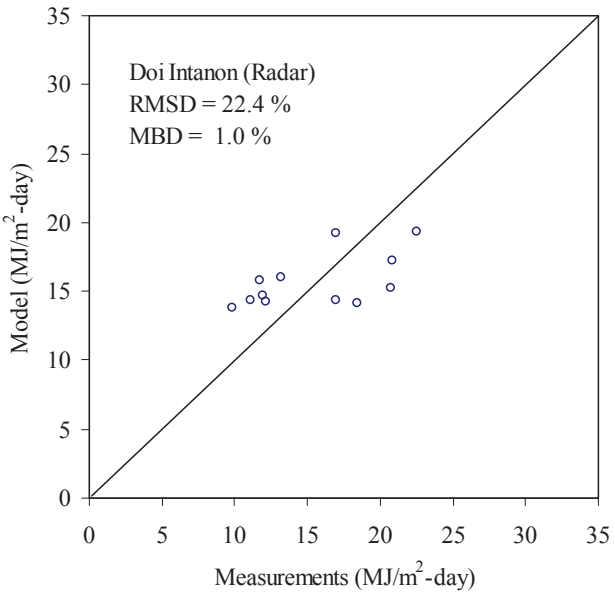

Fig. 2.26 Comparison between the monthly average daily global radiation from the model and from the measurements at Doi Intanon (Radar).

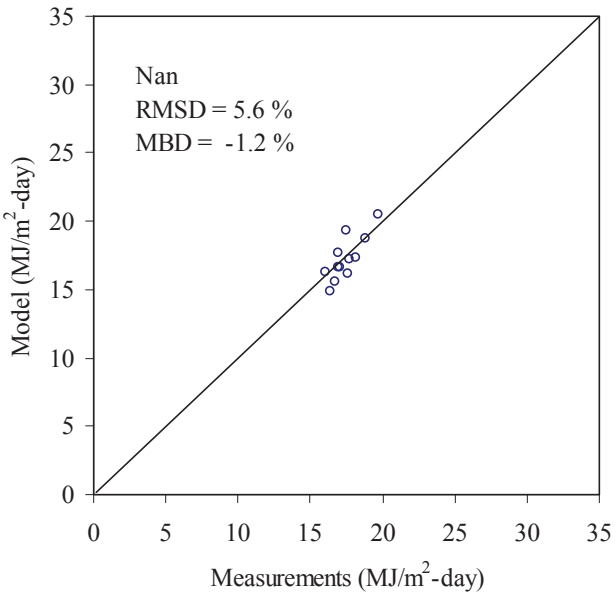

Fig. 2.27 Comparison between the monthly average daily global radiation from the model and from the measurements in Nan.

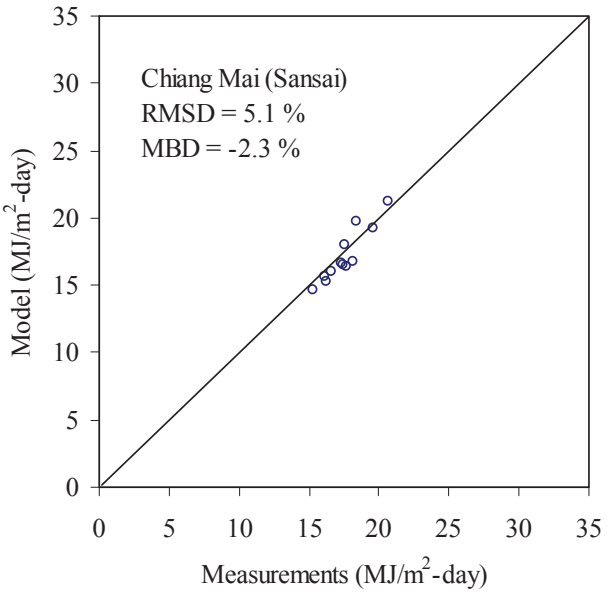

Fig. 2.28 Comparison between the monthly average daily global radiation from the model and from the measurements in Chiang Mai (Sansai)

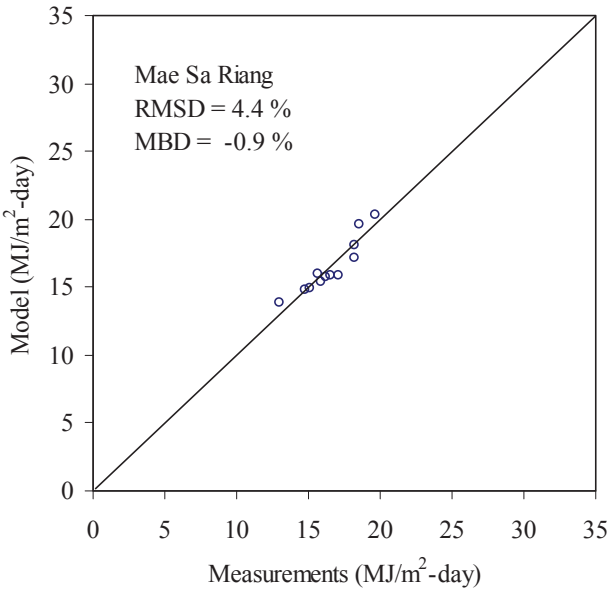

Fig. 2.29 Comparison between the monthly average daily global radiation from the model and from the measurements in Mae Sa Riang.

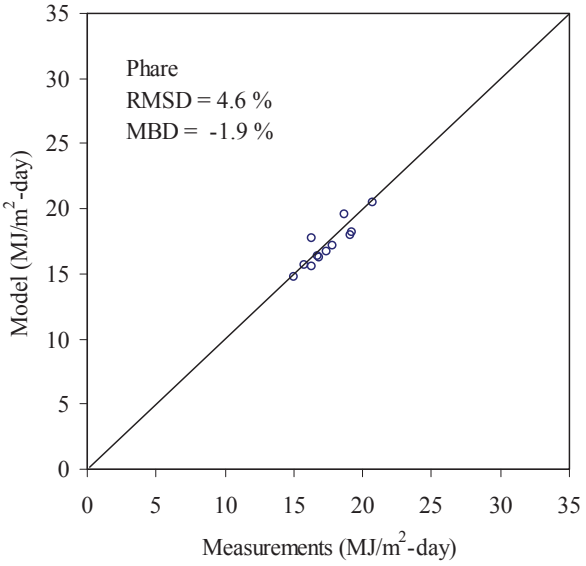

Fig. 2.30 Comparison between the monthly average daily global radiation from the model and from the measurements in Phare.

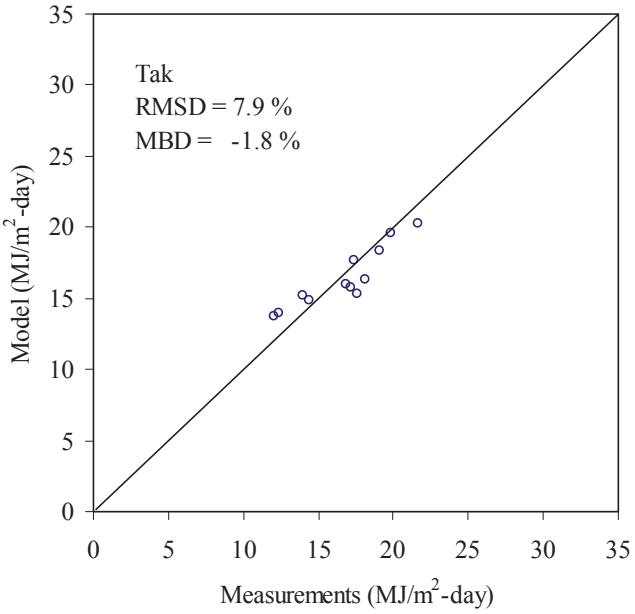

Fig. 2.31 Comparison between the monthly average daily global radiation from the model and from the measurements in Tak.

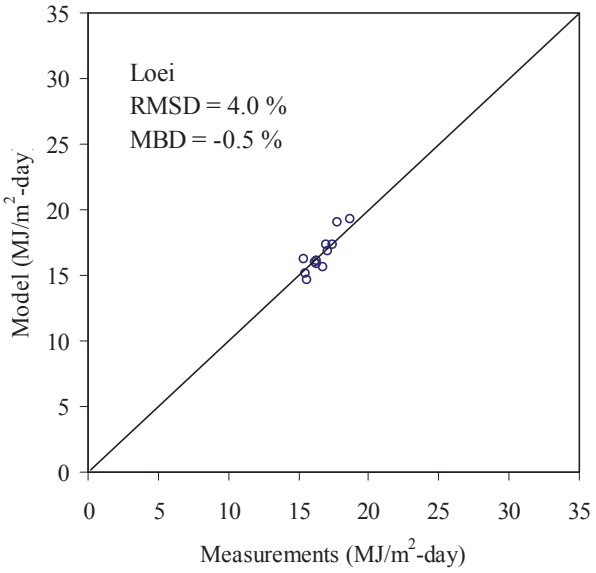

Fig. 2.32 Comparison between the monthly average daily global radiation from the model and from the measurements in Loei.

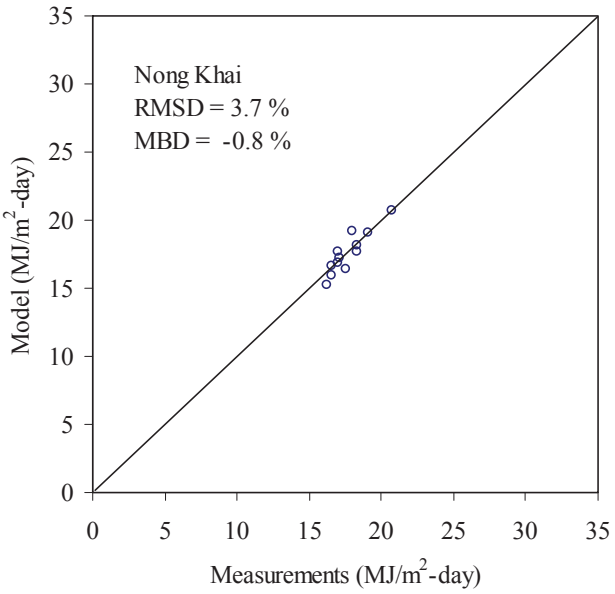

Fig. 2.33 Comparison between the monthly average daily global radiation from the model and from the measurements in Nong Khai.

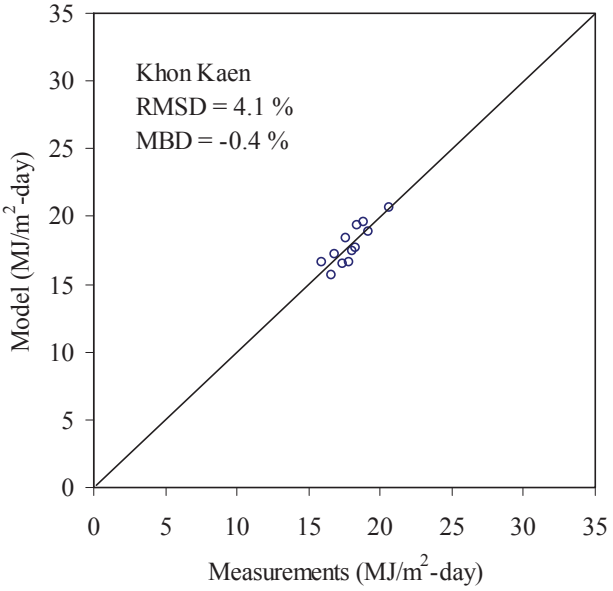

Fig. 2.34 Comparison between the monthly average daily global radiation from the model and from the measurements in Khon Kaen.

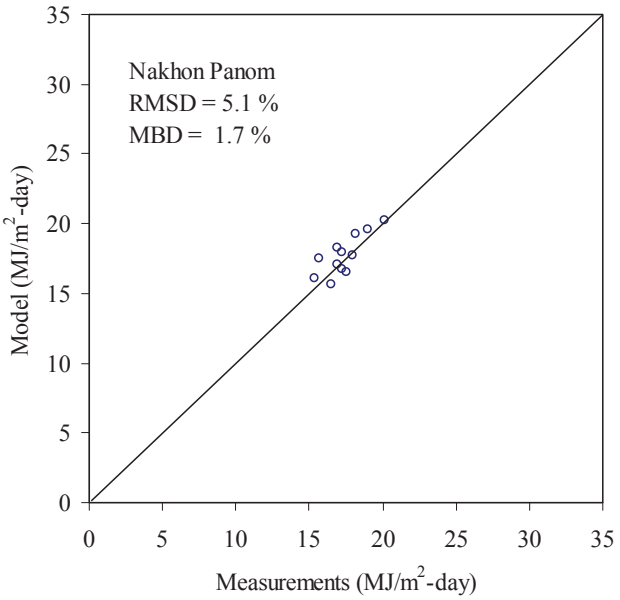

Fig. 2.35 Comparison between the monthly average daily global radiation from the model and from the measurements in Nakhon Panom.

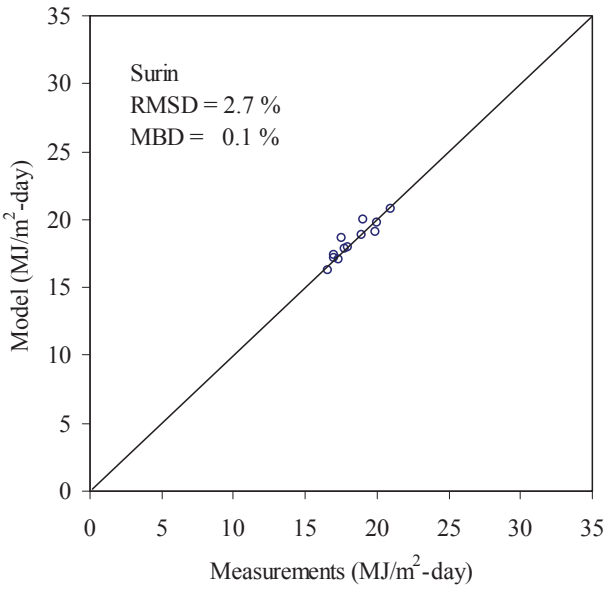

Fig. 2.36 Comparison between the monthly average daily global radiation from the model and from the measurements in Surin.

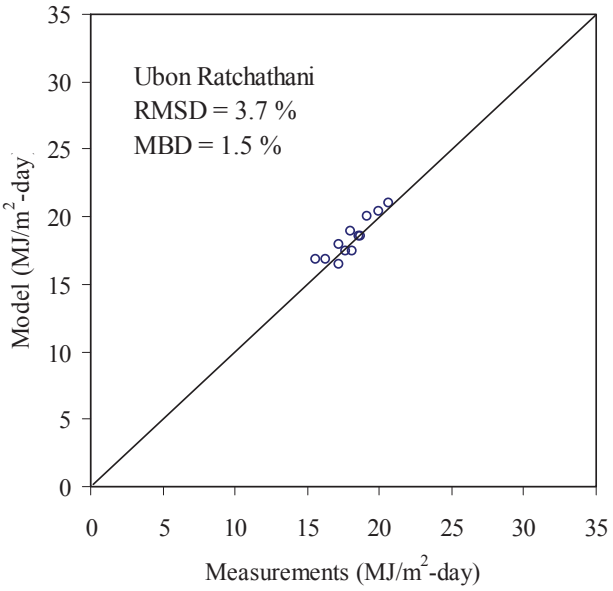

Fig. 2.37 Comparison between the monthly average daily global radiation from the model and from the measurements in Ubon Ratchathani.

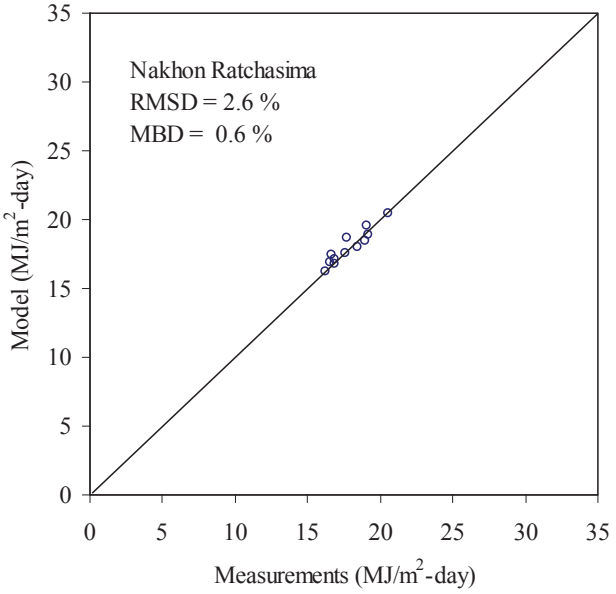

Fig. 2.38 Comparison between the monthly average daily global radiation from the model and from the measurements in Nakhon Ratchasima.

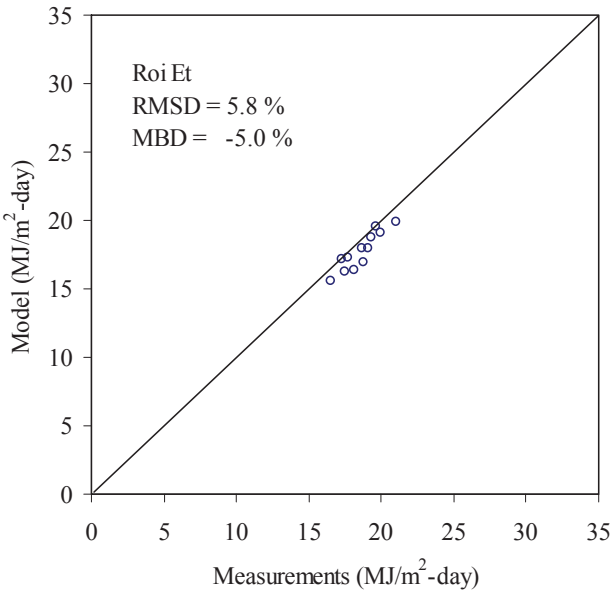

Fig. 2.39 Comparison between the monthly average daily global radiation from the model and from the measurements in Roi Et.

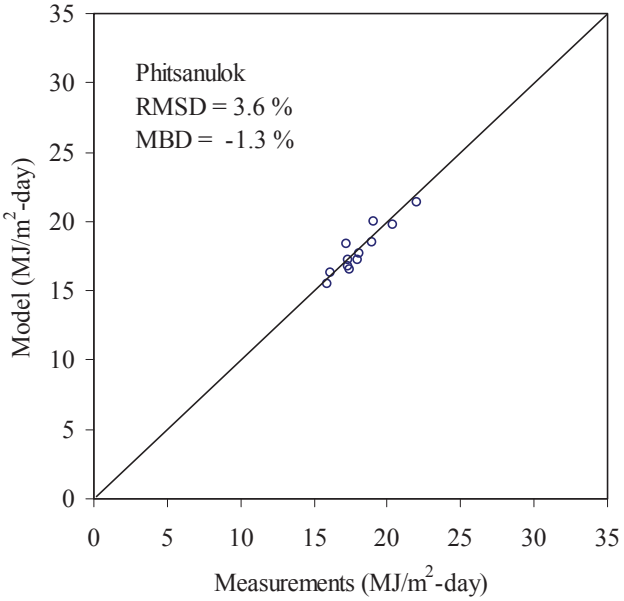

Fig. 2.40 Comparison between the monthly average daily global radiation from the model and from the measurements in Phitsanulok.

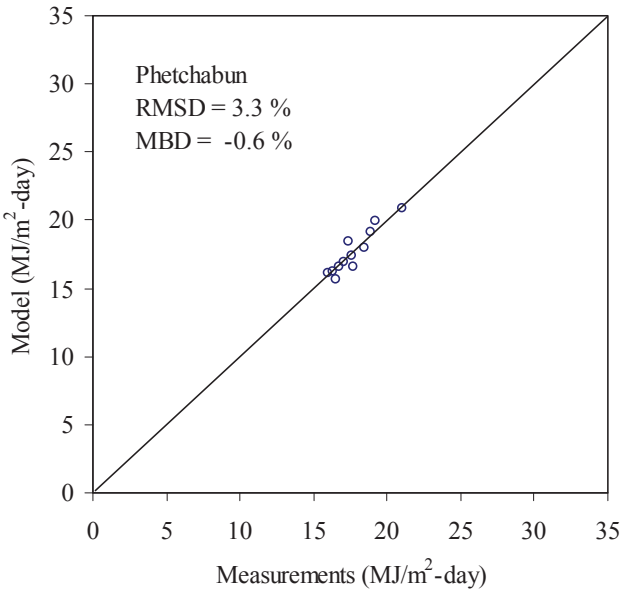

Fig. 2.41 Comparison between the monthly average daily global radiation from the model and from the measurements in Phetchabun.

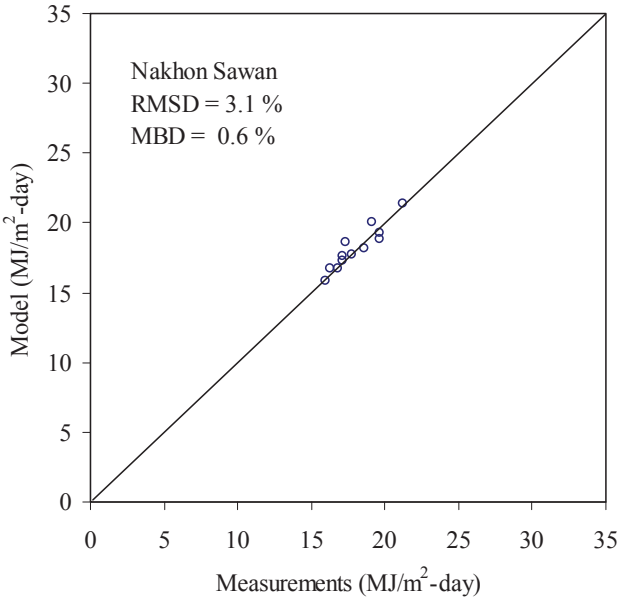

Fig. 2.42 Comparison between the monthly average daily global radiation from the model and from the measurements in Nakhon Sawan.

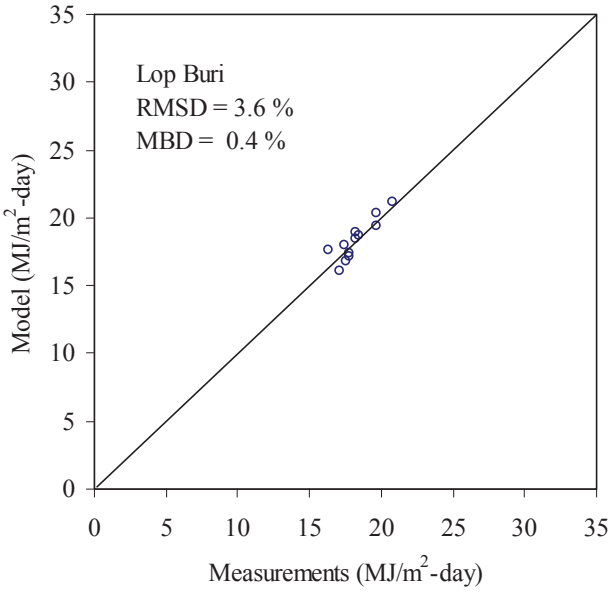

Fig. 2.43 Comparison between the monthly average daily global radiation from the model and from the measurements in Lop Buri.

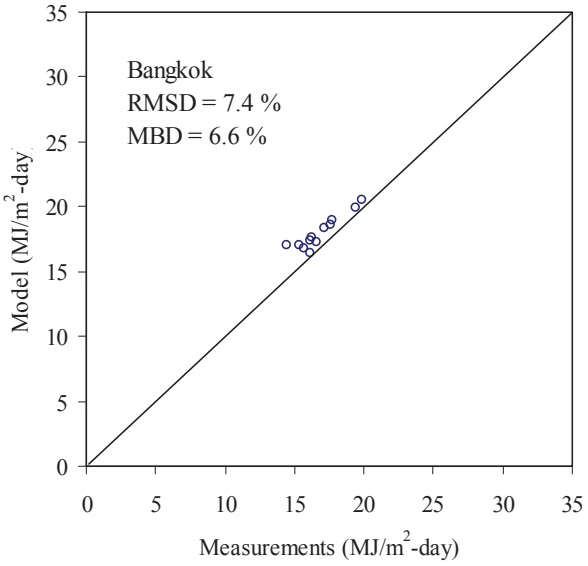

Fig. 2.44 Comparison between the monthly average daily global radiation from the model and from the measurements in Bangkok.

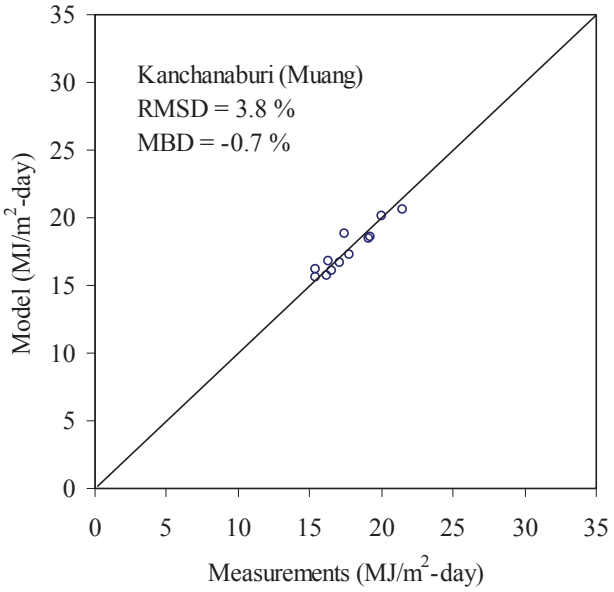

Fig. 2.45 Comparison between the monthly average daily global radiation from the model and from the measurements in Kanchanaburi (Muang).

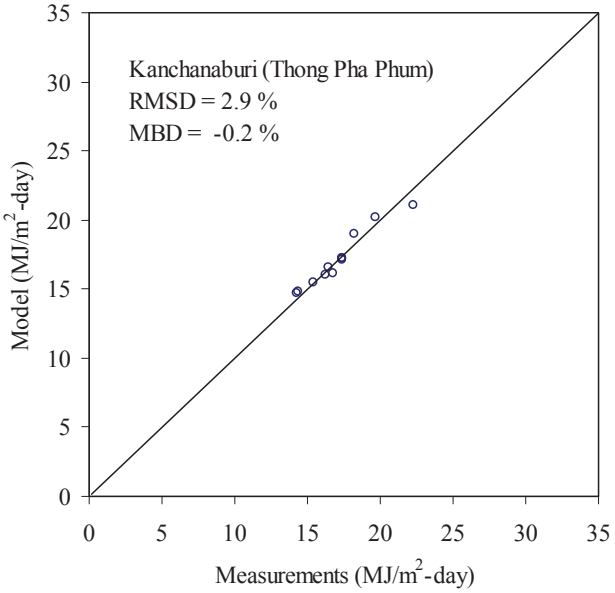

Fig. 2.46 Comparison between the monthly average daily global radiation from the model and from the measurements in Kanchanaburi (Thong Pha Phum).

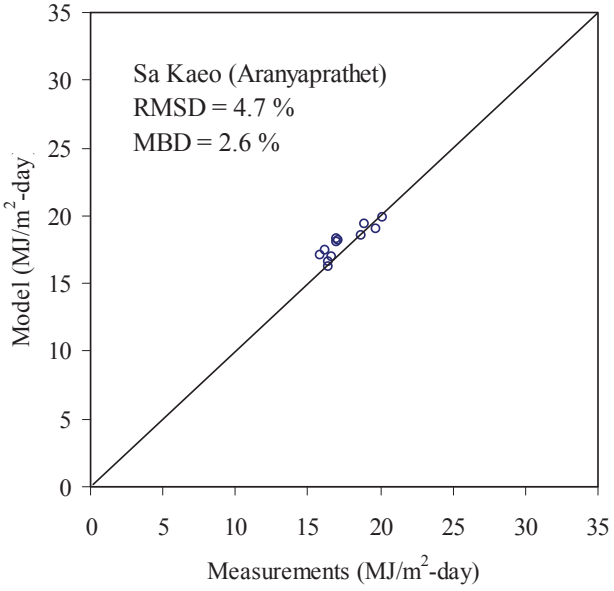

Fig. 2.47 Comparison between the monthly average daily global radiation from the model and from the measurements in Sa Kaeo (Aranyaprathet).

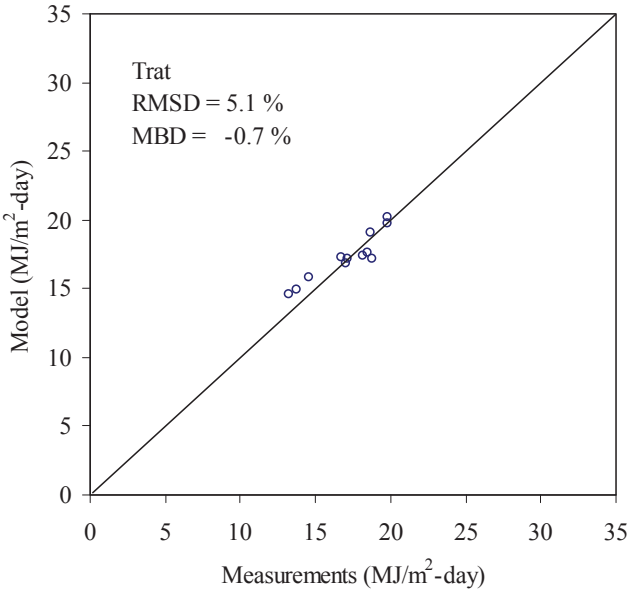

Fig. 2.48 Comparison between the monthly average daily global radiation from the model and from the measurements in Trat.

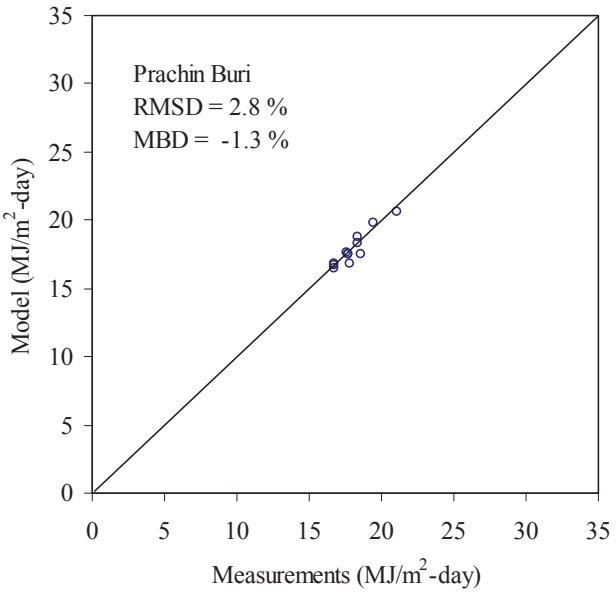

Fig. 2.49 Comparison between the monthly average daily global radiation from the model and from the measurements in Prachin Buri.

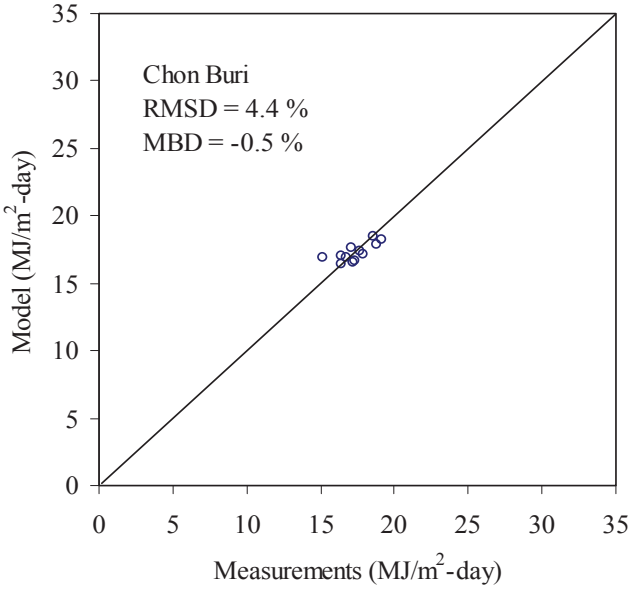

Fig. 2.50 Comparison between the monthly average daily global radiation from the model and from the measurements in Chon Buri.

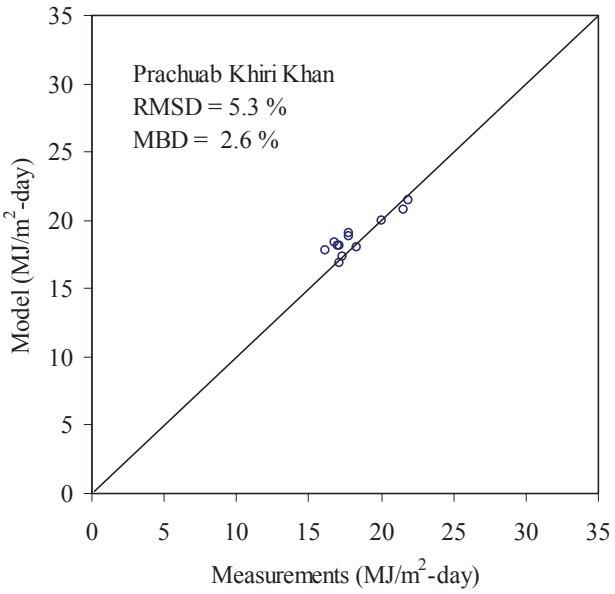

Fig. 2.51 Comparison between the monthly average daily global radiation from the model and from the measurements in Prachuab Khiri Khan.

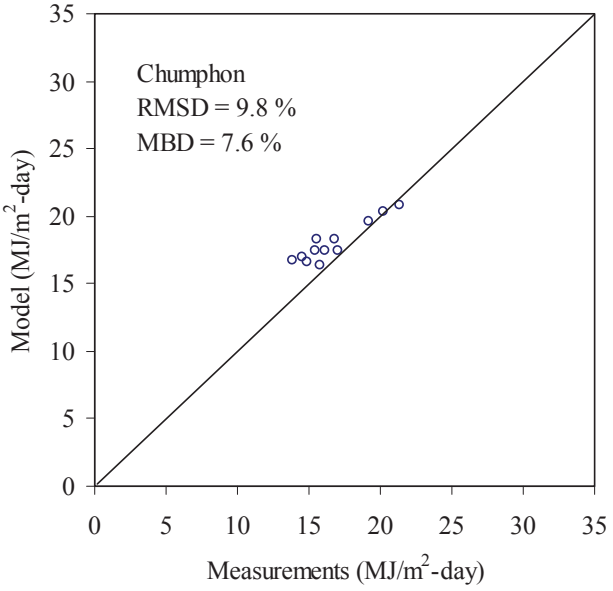

Fig. 2.52 Comparison between the monthly average daily global radiation from the model and from the measurements in Chumphon.

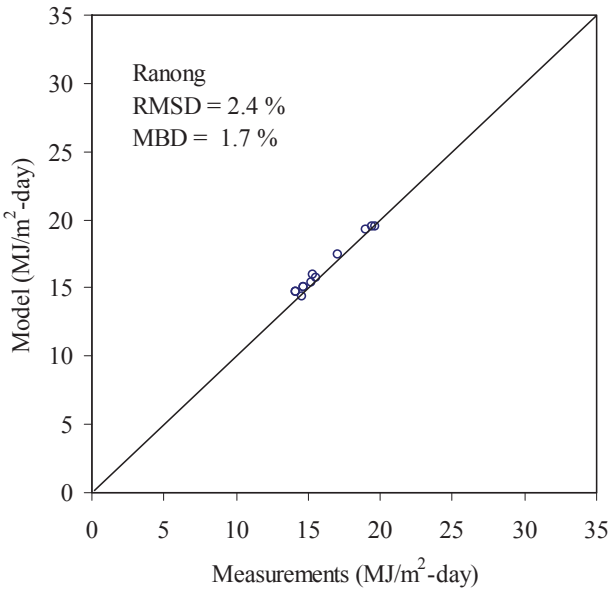

Fig. 2.53 Comparison between the monthly average daily global radiation from the model and from the measurements in Ranong.

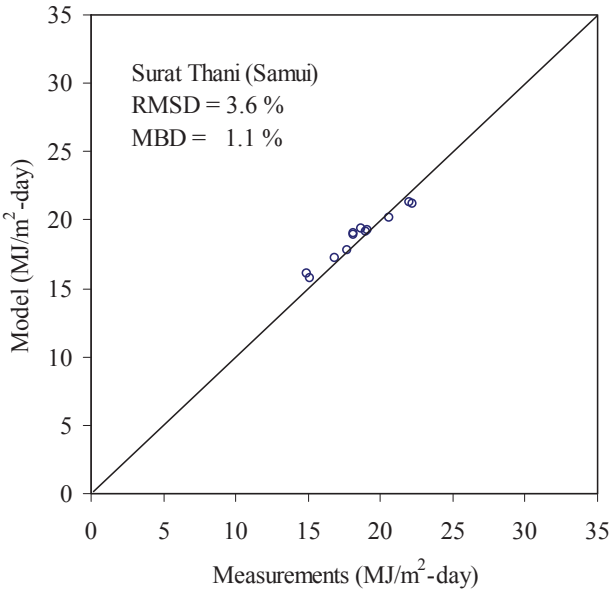

Fig. 2.54 Comparison between the monthly average daily global radiation from the model and from the measurements in Surat Thani (Samui).

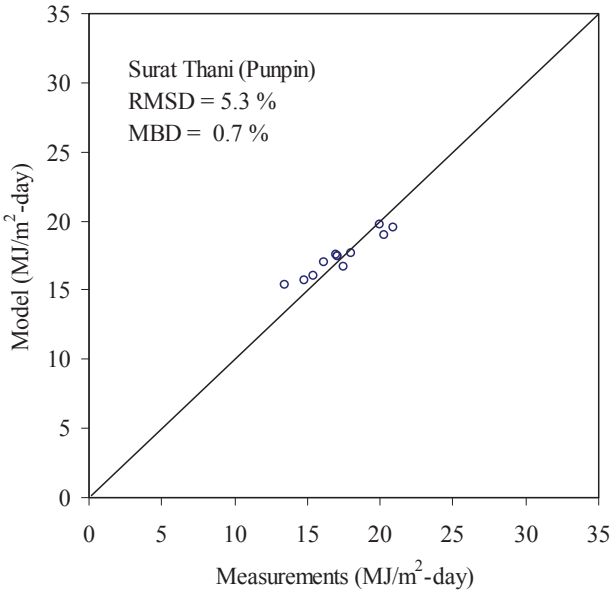

Fig. 2.55 Comparison between the monthly average daily global radiation from the model and from the measurements in Surat Thani (Punpin).

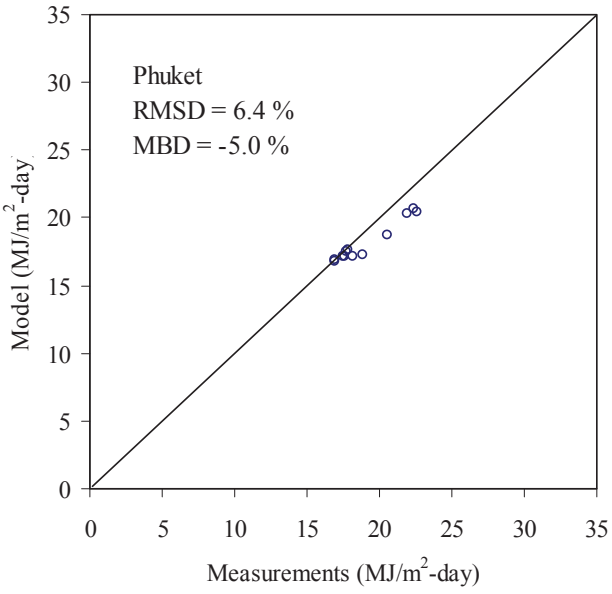

Fig. 2.56 Comparison between the monthly average daily global radiation from the model and from the measurements in Phuket.

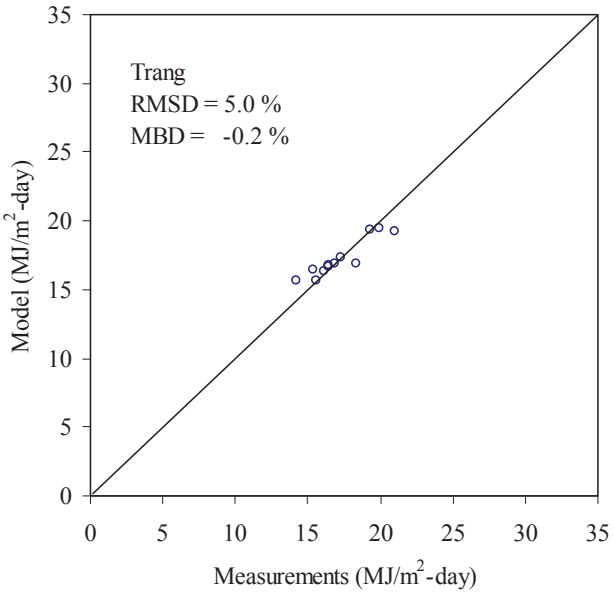

Fig. 2.57 Comparison between the monthly average daily global radiation from the model and from the measurements in Trang.

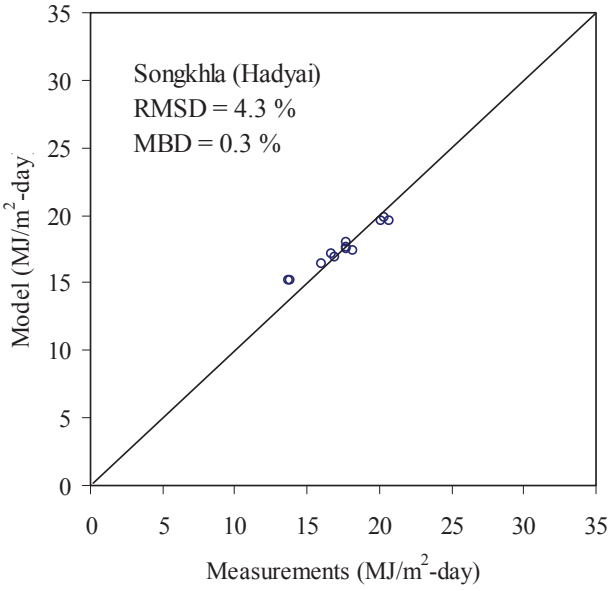

Fig. 2.58 Comparison between the monthly average daily global radiation from the model and from the measurements in Songkhla (Hadyai).

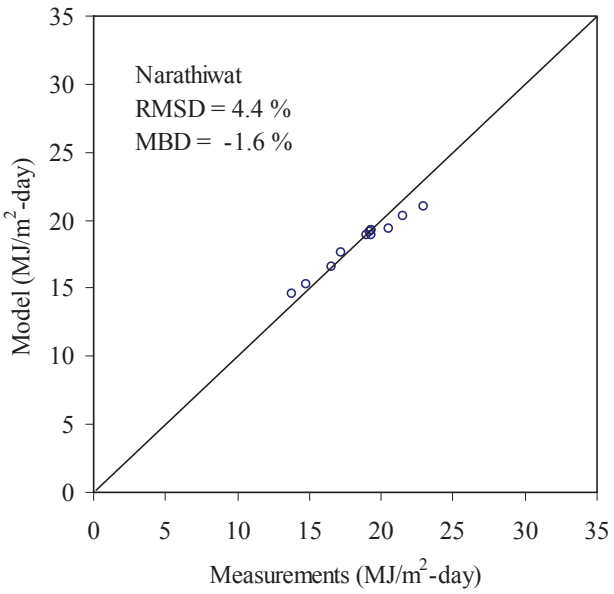

Fig. 2.59 Comparison between the monthly average daily global radiation from the model and from the measurements in Narathiwat.

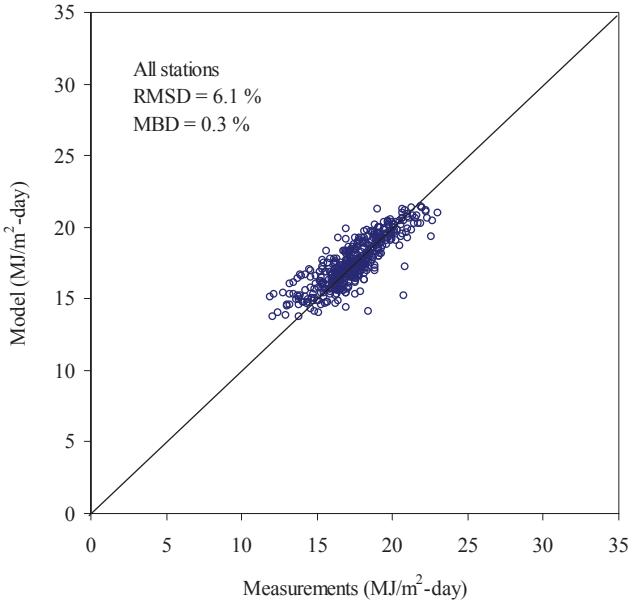

Fig. 2.60 Comparison between the monthly average daily global radiation from the model and from the measurements of all stations.

2.2.5 Generation of solar radiation maps

After the validation, the model was used to generate the solar radiation maps of Thailand. In order to obtain the maps, the satellite-derived atmospheric albedo (ρ'_A) was estimated using the method described in the previous sections. The Eq. (2.28), (2.29), (2.30) and (2.31) were used to convert the satellite-derived atmospheric reflectivity (ρ'_A) into the broadband atmospheric reflectivity (ρ_A). By using Eq. (2.3), the broadband atmospheric transmission (τ) was then calculated, and solar radiation was computed from Eq. (2.4). The calculation was carried out for all arrays of 500×800 pixels covering the entire area of Thailand. The results were averaged to obtain values of long-term monthly and yearly average daily solar radiation. These results are displayed as maps in Fig. 2.61-2.72 and 2.73.

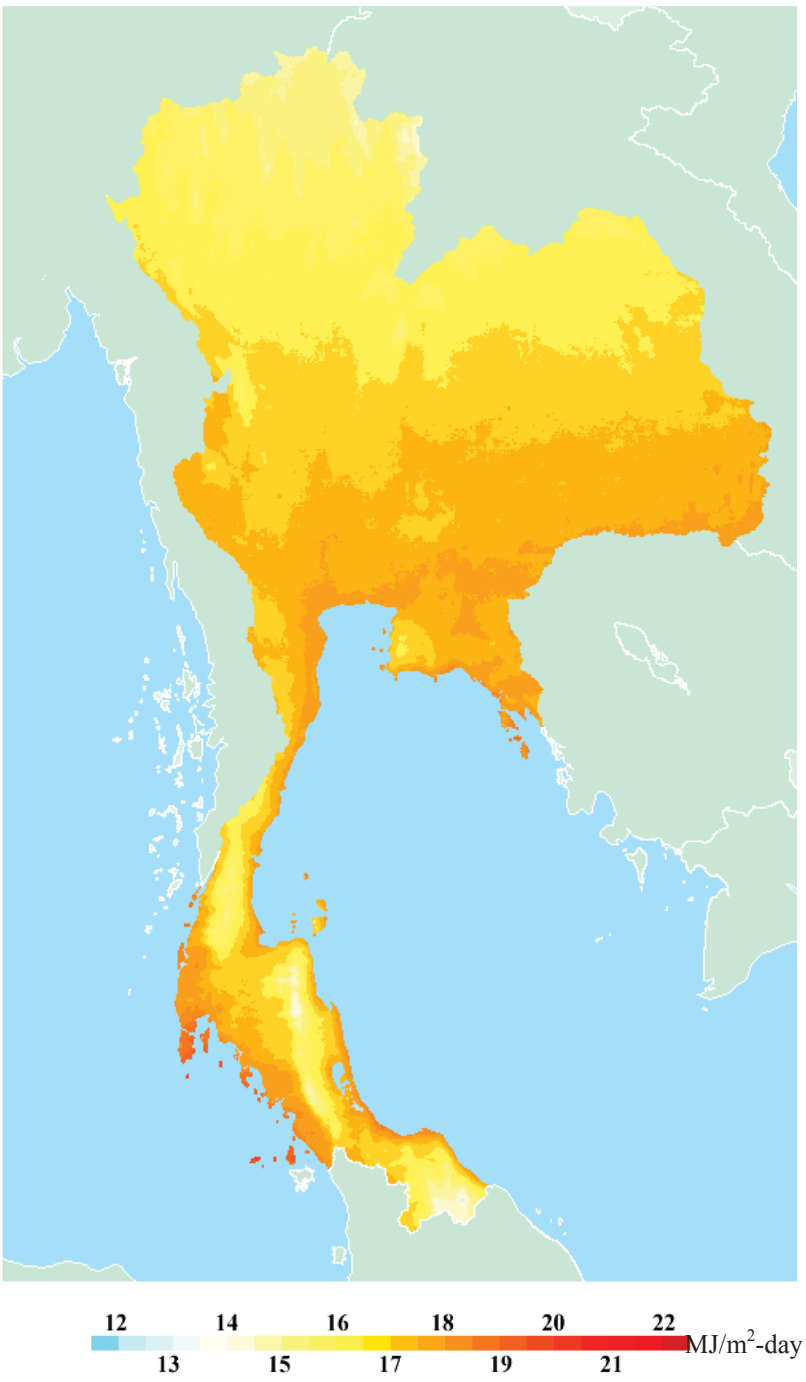

Fig. 2.61 Monthly average of daily global radiation over Thailand. (January)

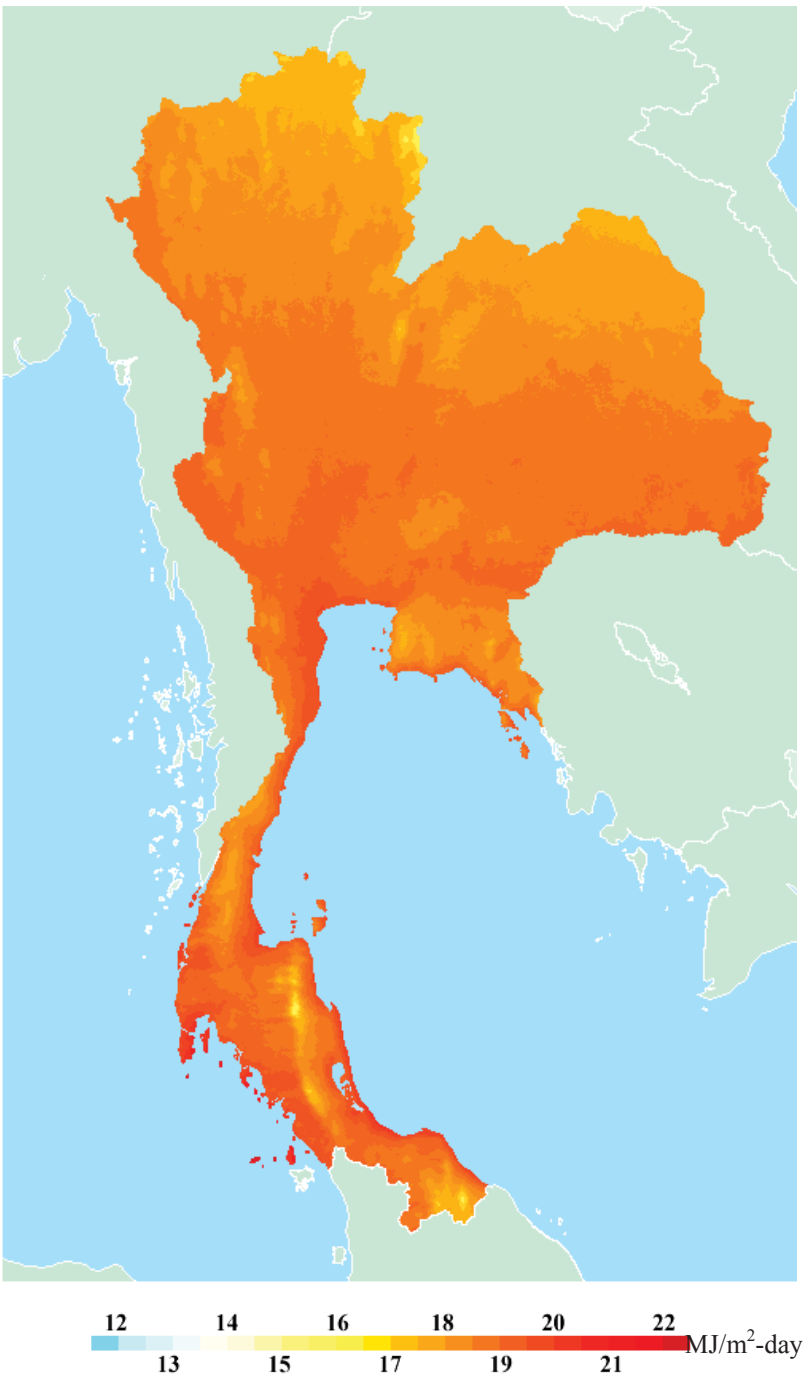

Fig. 2.62 Monthly average of daily global radiation over Thailand. (February)

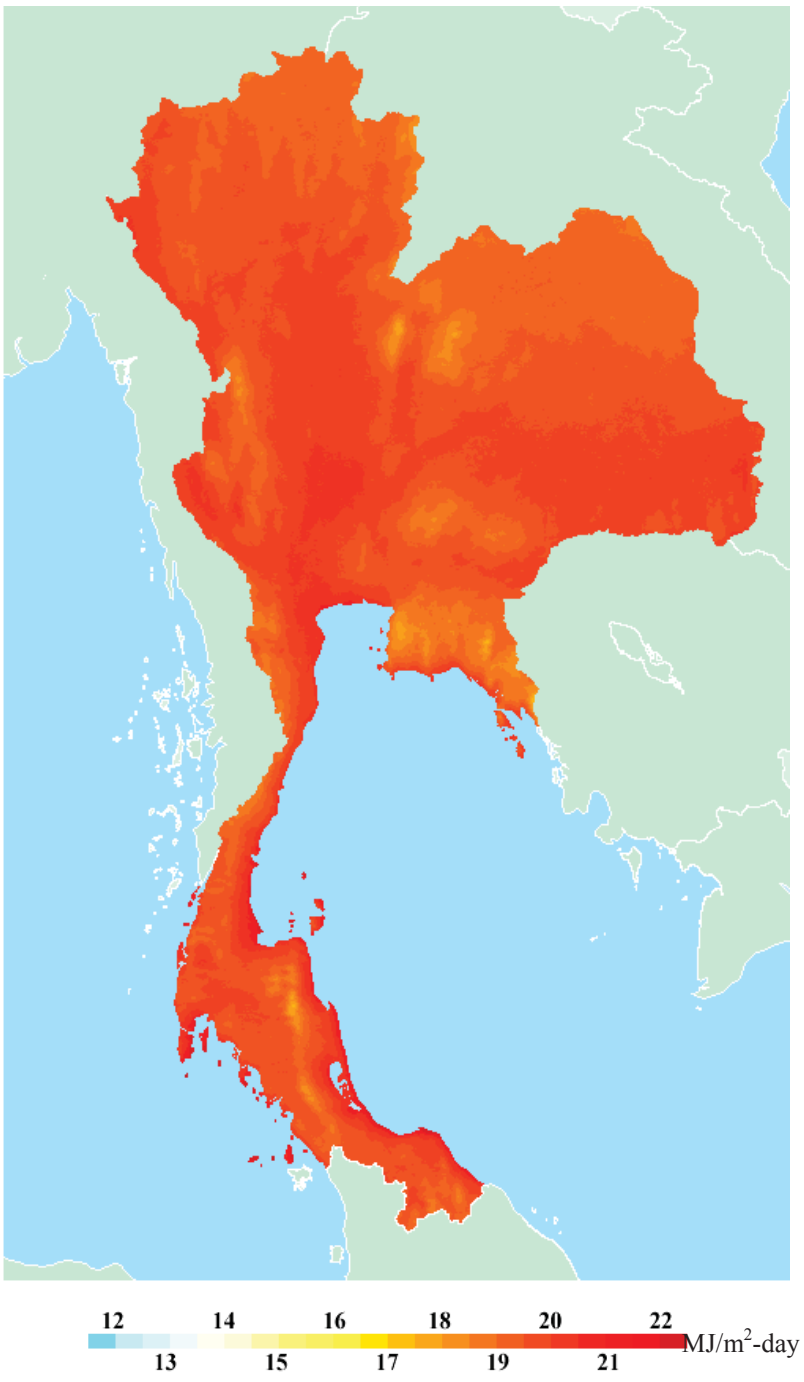

Fig. 2.63 Monthly average of daily global radiation over Thailand. (March)

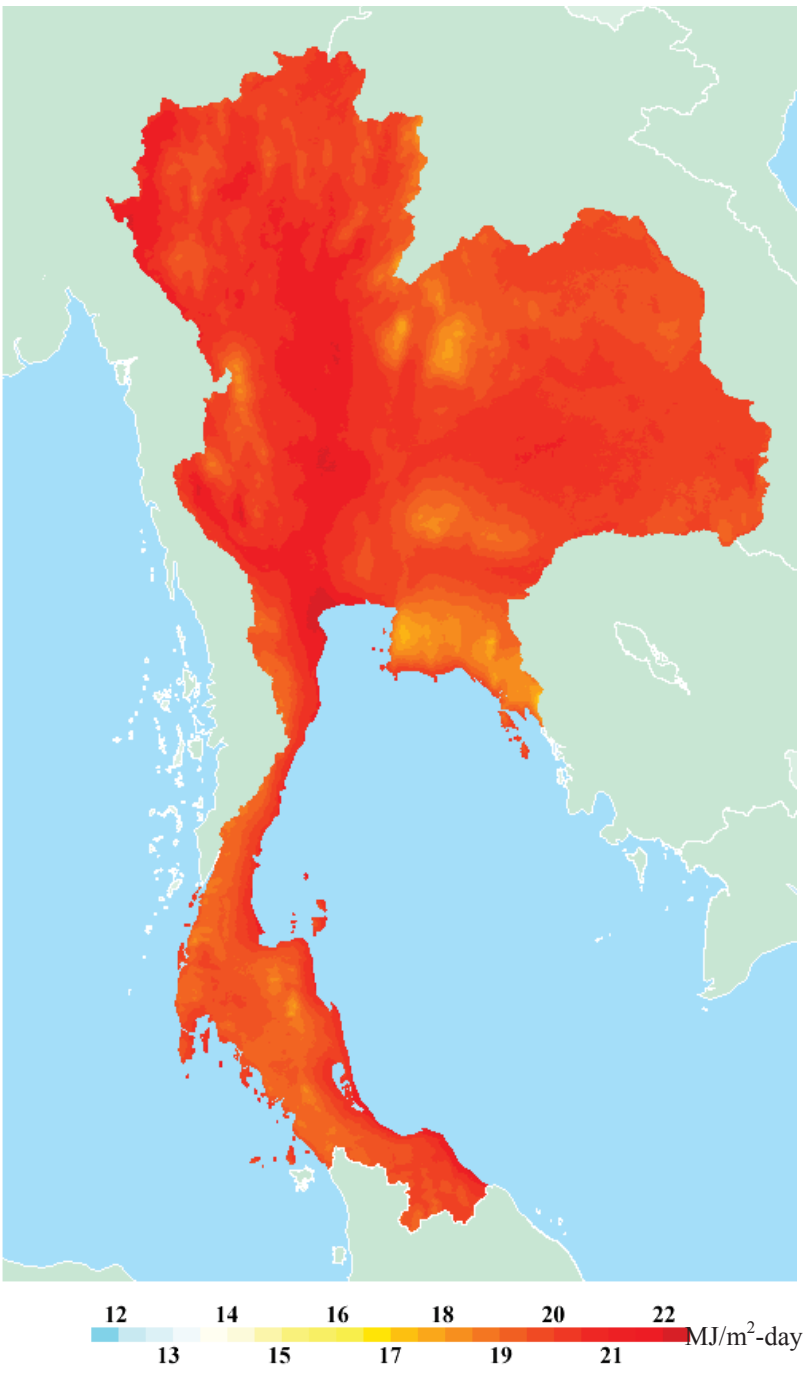

Fig. 2.64 Monthly average of daily global radiation over Thailand. (April)

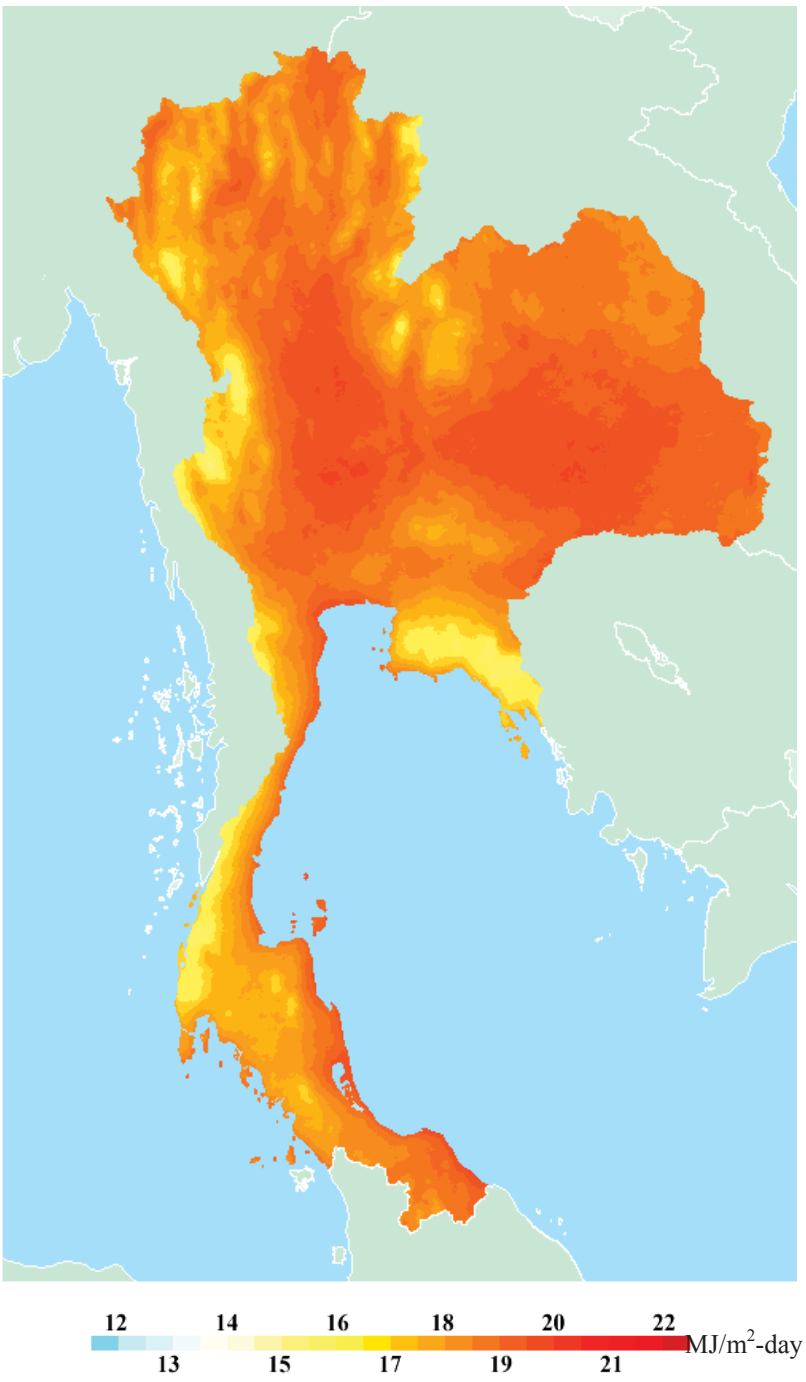

Fig. 2.65 Monthly average of daily global radiation over Thailand. (May)

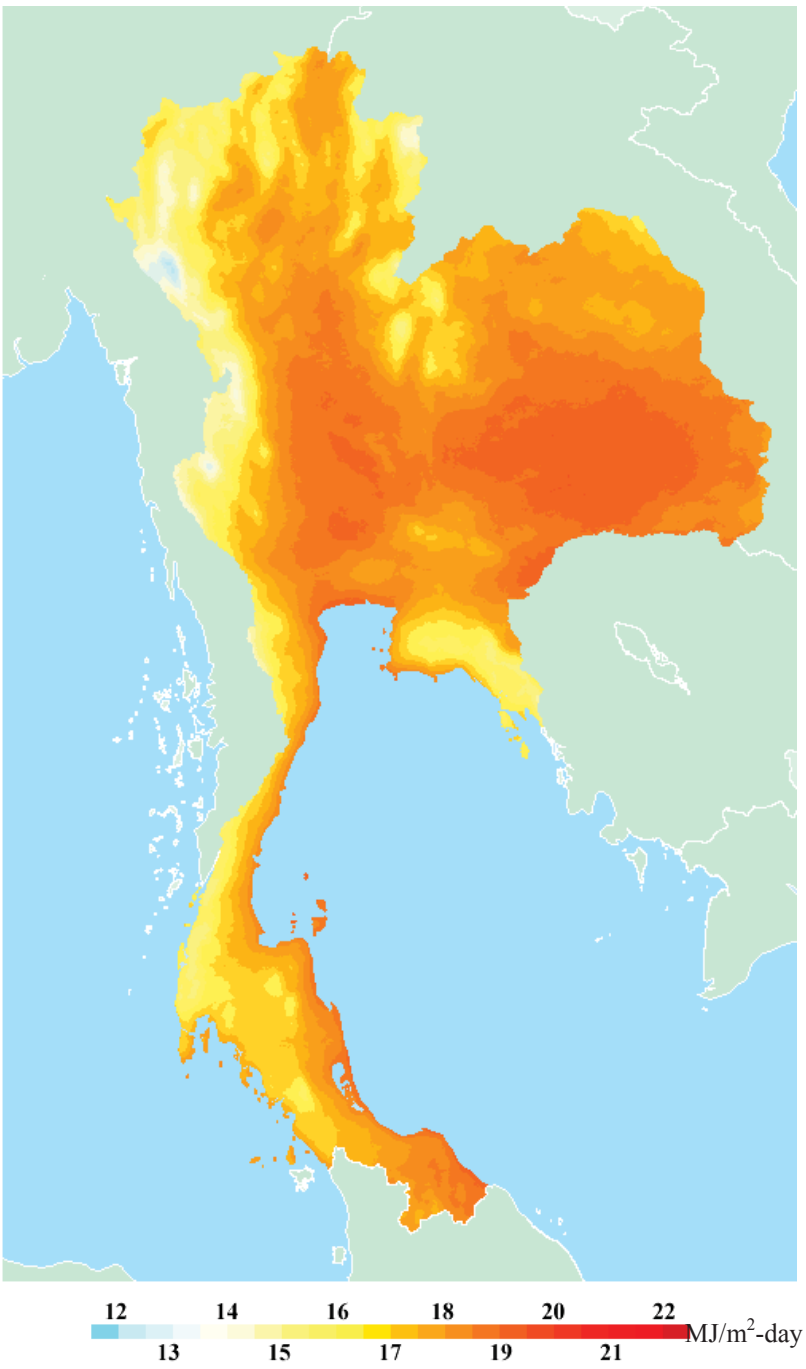

Fig. 2.66 Monthly average of daily global radiation over Thailand. (June)

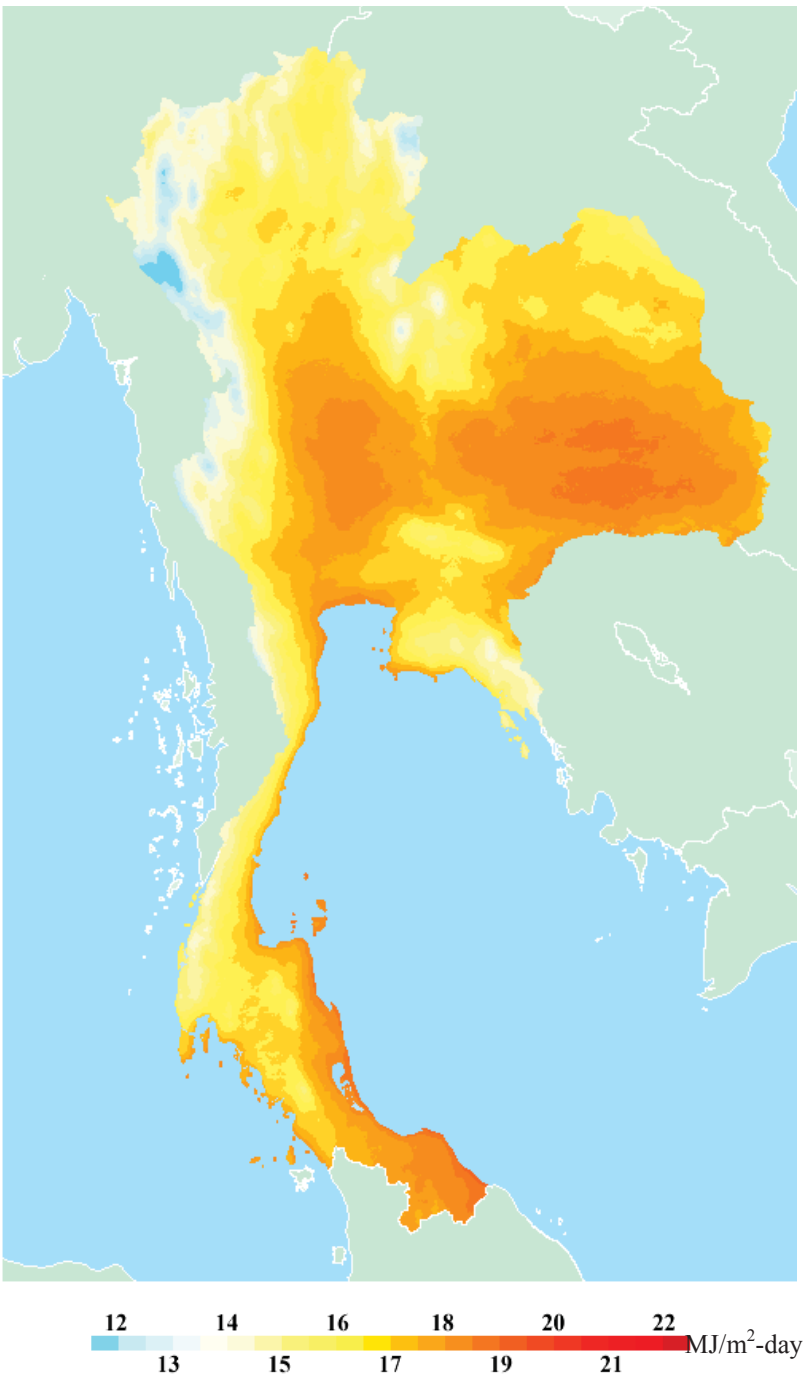

Fig. 2.67 Monthly average of daily global radiation over Thailand. (July)

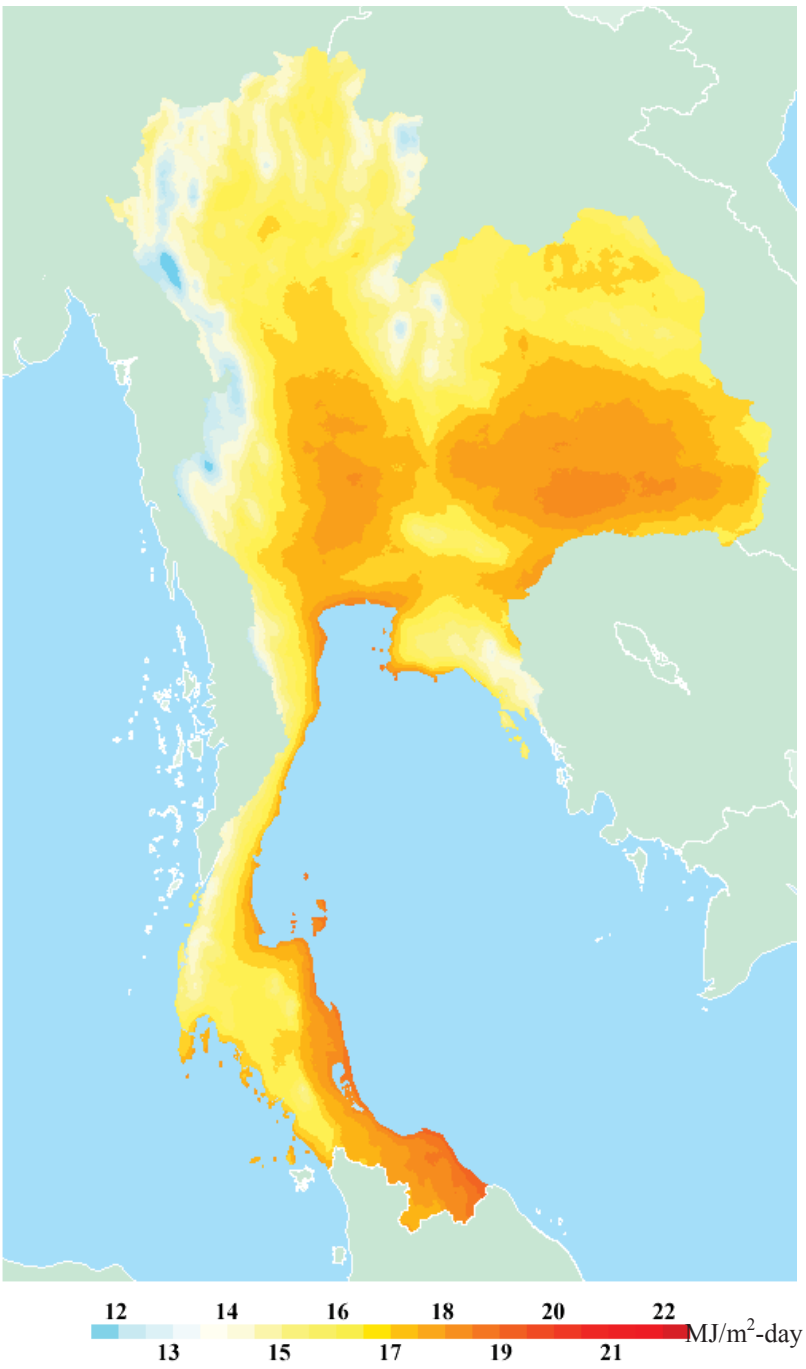

Fig. 2.68 Monthly average of daily global radiation over Thailand. (August)

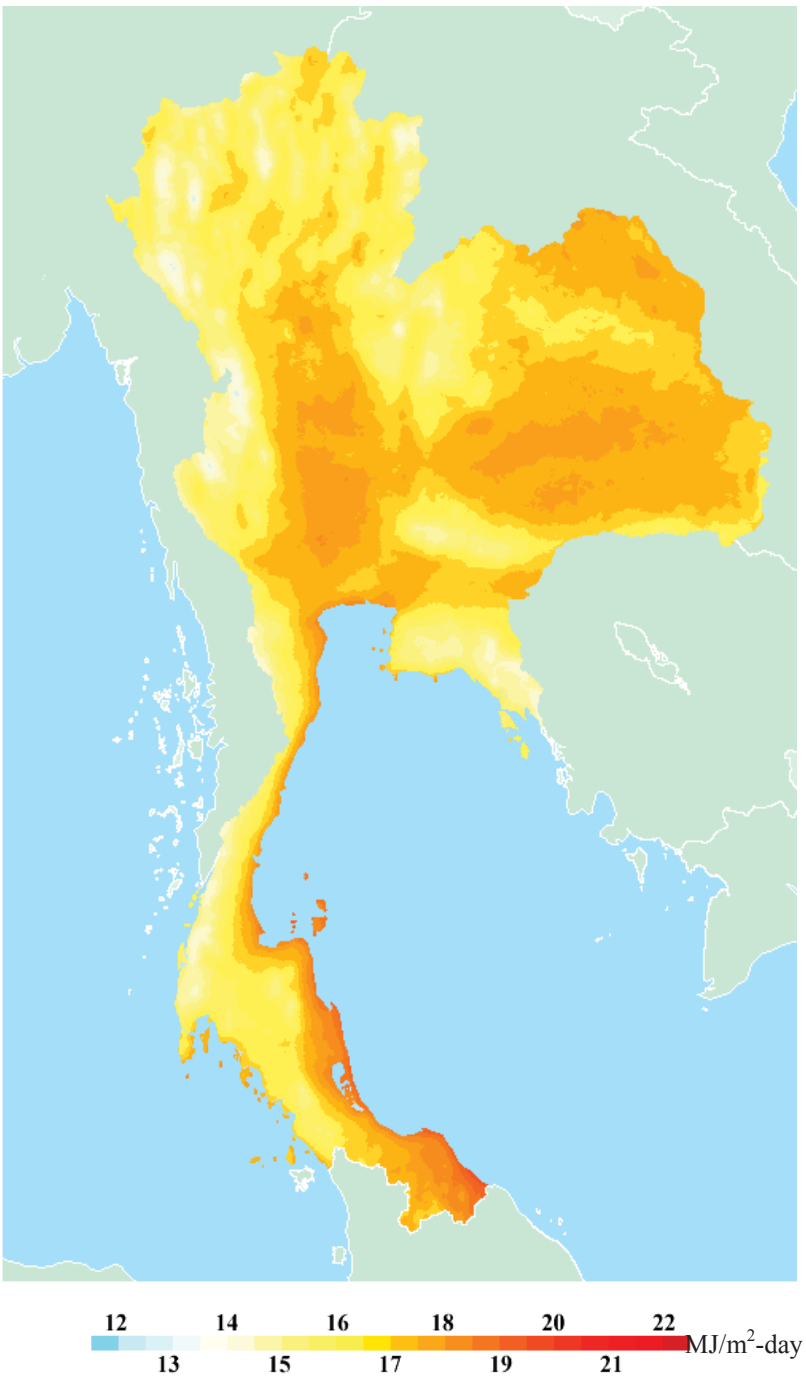

Fig. 2.69 Monthly average of daily global radiation over Thailand. (September)

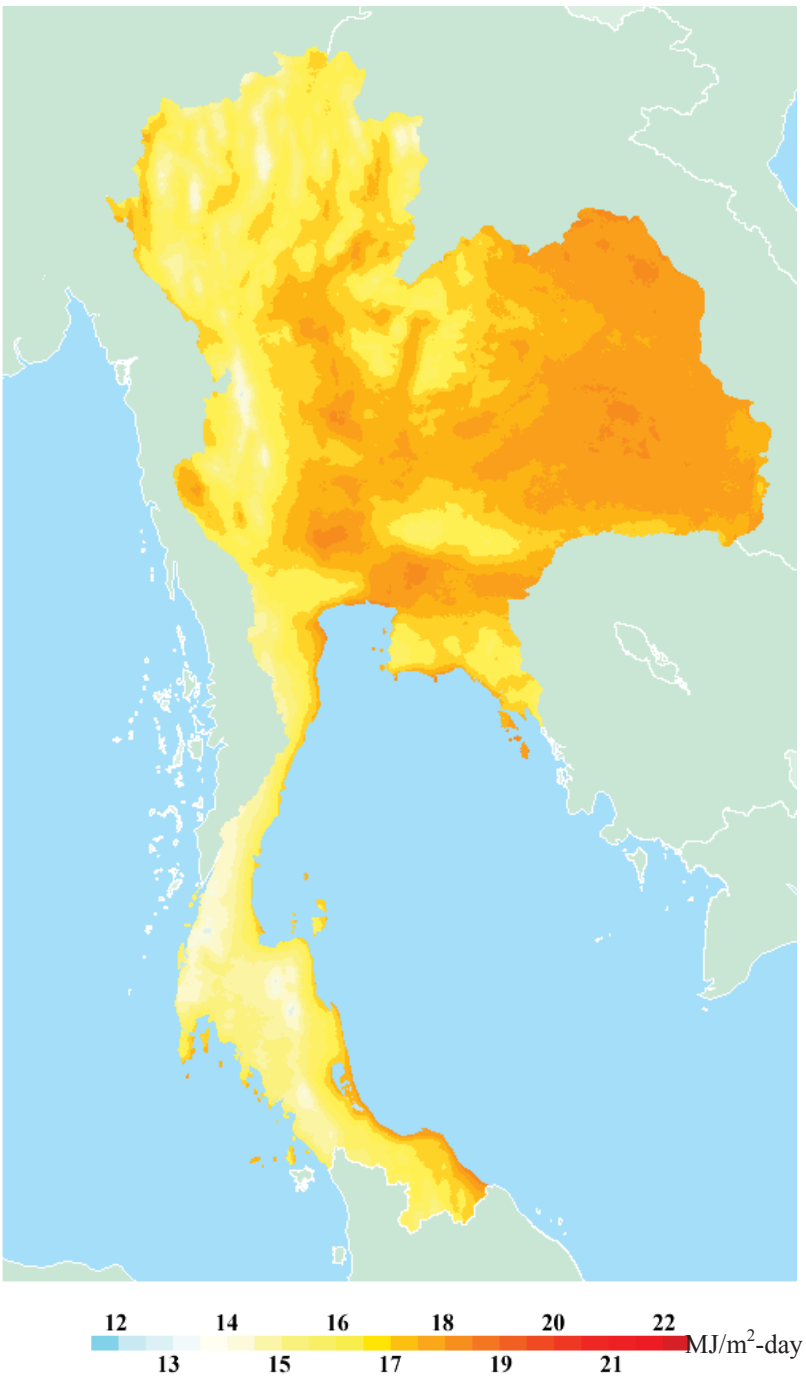

Fig. 2.70 Monthly average of daily global radiation over Thailand. (October)

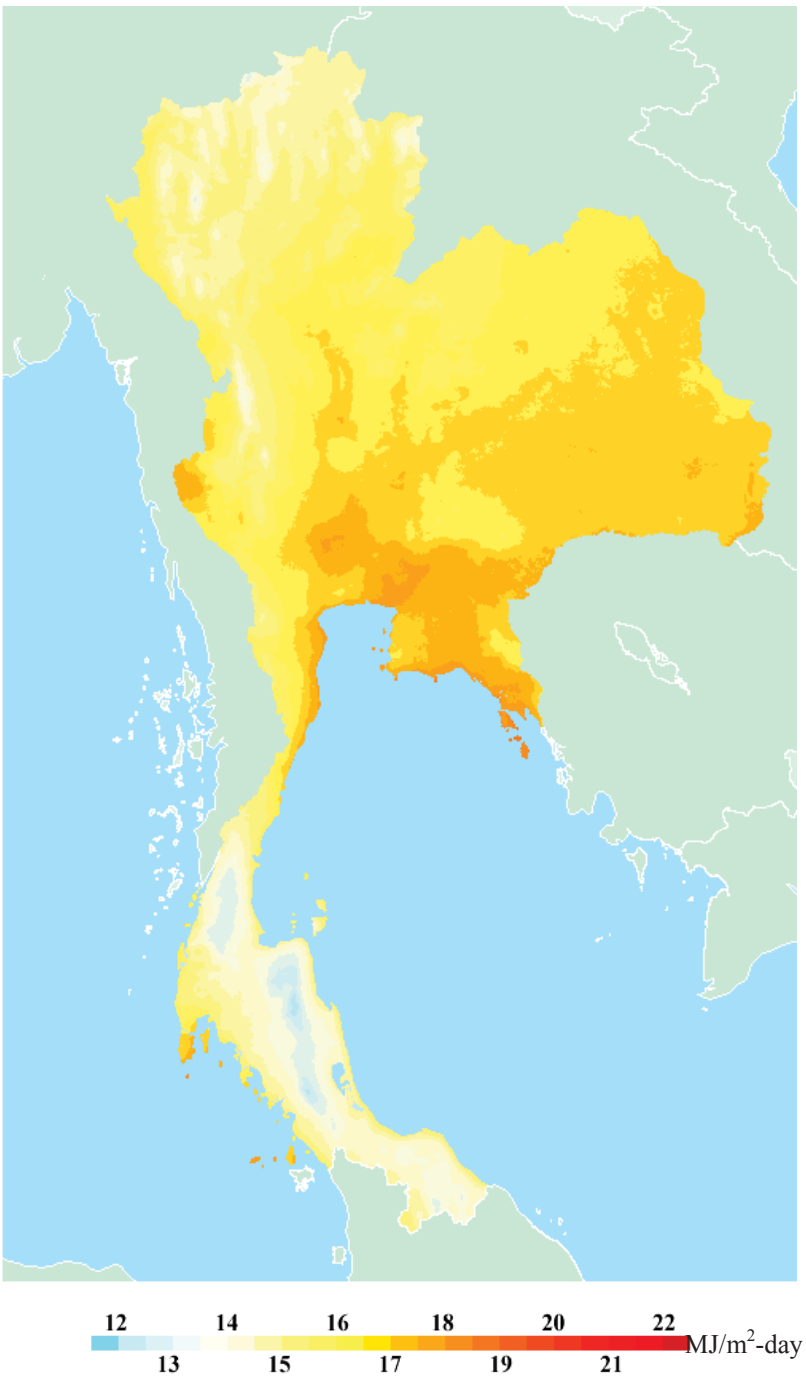

Fig. 2.71 Monthly average of daily global radiation over Thailand. (November)

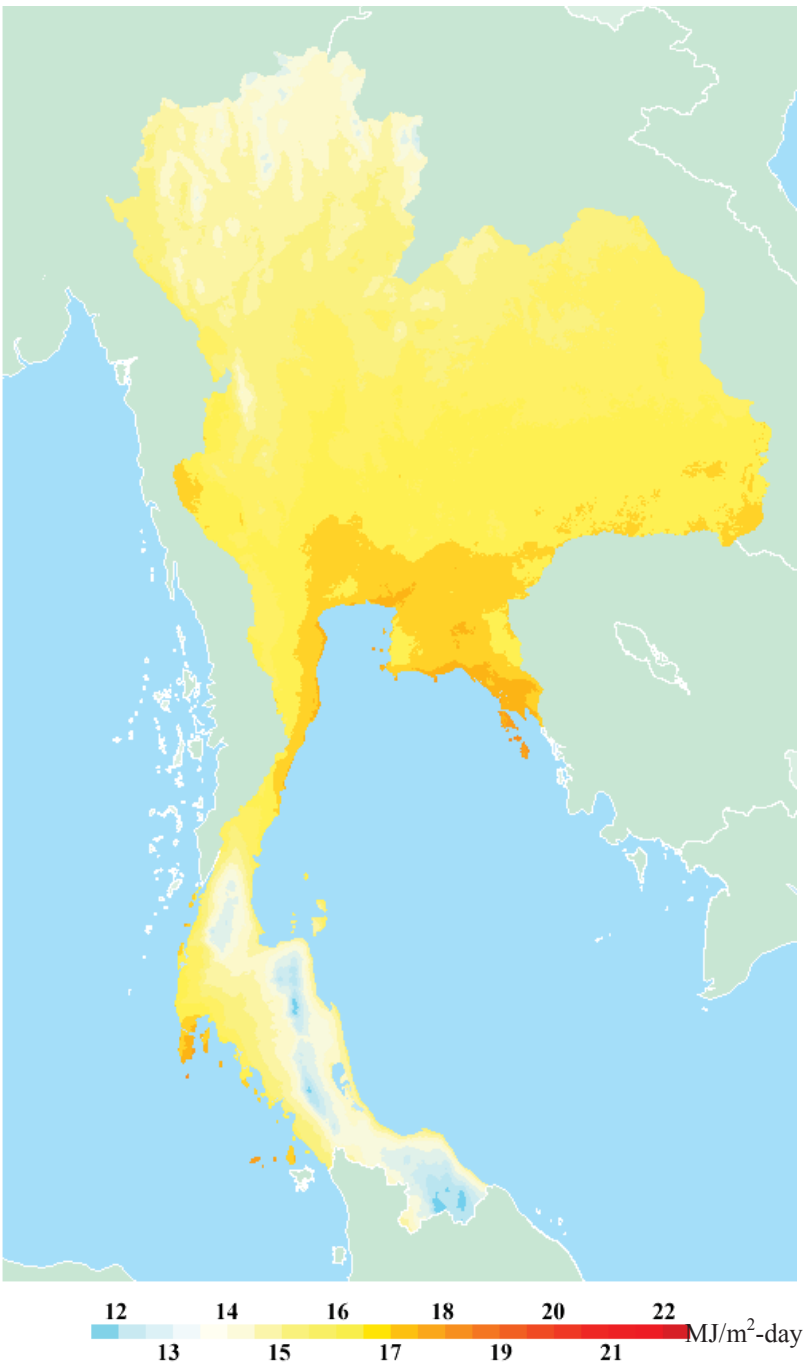

Fig. 2.72 Monthly average of daily global radiation over Thailand. (December)

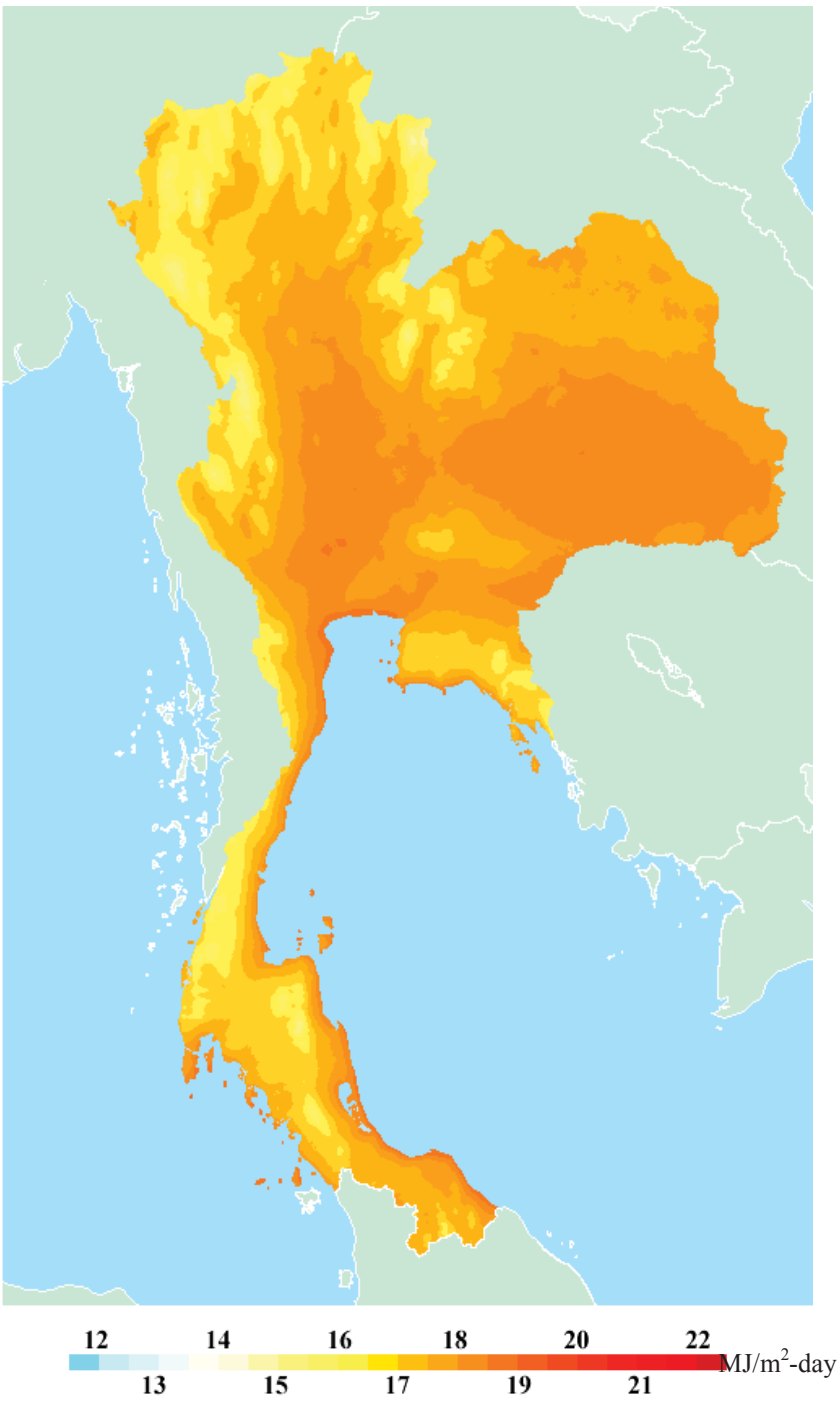

Fig. 2.73 Yearly average of daily global radiation over Thailand.

Considering the maps shown in Fig. 2.62-2.72 and 2.73, distribution of solar radiation in Thailand can be discussed as follows:

In January, low solar radiation of 14-16 MJ/m^2-day is observed in northern Thailand. Although, January is in the winter with many clear days, the sun path is in the south of the celestial equator, causing relatively low solar radiation over the country. The values of low solar radiation of 12-15 MJ/m^2-day is also found in the northernmost regions due to the frequent cloud formation in the mountain ranges. In contrast, high solar radiation is seen over a large part in the east of the country varying between 16-18 MJ/m^2-day.

Solar radiation increases significantly from January to February for most parts of the country. In the north, the values of 16-18 MJ/m^2-day are observed and the values of high solar radiation (18-20 MJ/m^2-day) are noticed in most parts of the country, especially along the coastlines of the southern region.

In March, high solar radiation of over 18 MJ/m^2-day features in most parts of the country. The high solar radiation of more than 20 MJ/m^2-day is observed over a large part of the east and the south of Thailand.

In April, solar radiation at noon time of Thailand is almost perpendicular to the earth's surface, causing high solar radiation of 20-22 MJ/m^2-day observed in most parts of the country. Overall, the pattern of solar radiation of this month shows a similar feature to that of March, but it is slightly higher.

In May, the southwest monsoon, which causes rains and carries moisture from the Andaman Sea, resulting in cloud skies over areas in the south and the east of Thailand. Consequently, low solar radiation (14-17 MJ/m^2-day) is observed in these areas. High solar radiation of 18-20 MJ/m^2-day still remains in the north because these areas receive less effect of the southwest monsoon in this month. The values of 20-22 MJ/m^2-day are observed in the central region and the east.

In June, solar radiation varies from 15-20 MJ/m^2-day for the whole country. Solar radiation is low in the south, the west and the north regions due to a continuation of the southwest monsoon. By contrast, the areas affected by rain shadow, such as the central regions and the east, still receive high solar radiation of 20-22 MJ/m^2-day.

In July, solar radiation of 12-18 MJ/m^2-day is observed for almost the whole country. The lowest range of solar radiation (12-14 MJ/m^2-day) can be found in the north, the west and high mountainous areas. On the other hand, solar radiation of 18-20 MJ/m^2-day prevails in the central region.

In August, the lowest values of 12-16 MJ/m^2-day cover almost the whole country. Under the monsoon condition, low solar radiation (12-14 MJ/m^2-day) is mostly observed in the north which extends from 16°N to 22°N. Along the coastline region, solar radiation exhibits the values of 15-18 MJ/m^2-day, while high solar radiation of 17-18 MJ/m^2-day is observed in the central and the east regions.

In September, solar radiation in Thailand exhibits a marginal increase from the pattern in August. The feature of high solar radiation (16-18 MJ/m^2-day) in the central and eastern regions moves towards the northern part of the country. Overall, the whole country receives solar radiation of about 14-18 MJ/m^2-day.

In October, the northeast monsoon, which brings dry weather condition, is a cause of high solar radiation (17-19 MJ/m^2-day) featured in the most parts of the east. By contrast, a large part of low solar radiation (14-16 MJ/m^2-day) is still observed over most of southern areas.

In November, solar radiation decreases from that observed in October for almost the entire country. Because the noon time solar zenith angles in the north are high as the sun path moves towards the southern sky hemisphere. As a result low solar radiation of 14-16 MJ/m^2-day is observed. In high mountain areas closed to the Thai-Myanmar border, the values of 14-16 MJ/m^2-day are still observed as a result of low humidity and the decreasing evaporation rates.

In December, the values of low solar radiation (14-16 MJ/m^2-day) expand throughout almost all regions of Thailand. In this season, the northeast monsoon is a major cause of dry weather, especially in the northern region. As a result, low solar radiation of 12-16 MJ/m^2-day is also exhibited. Furthermore, in high mountainous areas in the south of Thailand, solar radiation exhibits a much lower values ranging between 12-14 MJ/m^2-day.

On average, daily global solar radiation in Thailand varies from the value of 16 MJ/m^2-day in the north and the west to 20 MJ/m^2-day in the center and the southeast of the country. High solar radiation (>18 MJ/m^2-day) is observed mostly in

the central and northeast regions of the country. In the north, low solar radiation (16 MJ/m^2-day) is observed as a result of clouds and higher solar zenith angle. On the other hand, a pattern of low solar radiation (16-18 MJ/m^2-day) is also seen in the southern region. This is because the monsoon, which brings heavy rains and clouds, plays an important role in depletion of solar radiation in the atmosphere. Overall, it is clearly observed that the monsoons and the rain shadow play an important role in variation of solar radiation in the country. Considering the yearly average (Fig. 2.73), the distribution pattern of solar radiation in Thailand is clearly seen. The year average solar radiation of Thailand is found to be 17.4 MJ/m^2-day, when averaged over the country.

2.3 Conclusions

A satellite-based solar radiation model was modified and used to estimate surface solar radiation over Thailand. The satellite data collected from January 1995 to December 2009 and ground-based meteorological data were used as inputs of the model. The scattering and absorption processes due to clouds, aerosols, water vapour, ozone and other gases were taken into account in the model. The earth-atmospheric reflectivity and ground albedo were estimated by using satellite data collected from GMS4, GMS5, GOES9 and MTSAT-1R during the period from January 1995 to December 2009. Absorption coefficients due to water vapour were computed from precipitable water derived from relative humidity and ambient air temperature. Ozone absorption coefficient was calculated from total column ozone obtained from TOMS/EP and OMI/AURA satellites. The absorption coefficients due to aerosols were estimated from visibility observations. To validate the performance of the satellite-based solar radiation model, the satellite-derived solar radiation calculated from the model was compared to the solar radiation measurements at 38 stations in Thailand. It was found that solar radiation calculated from the model and that obtained from the measurements were in good agreement, with the discrepancy in terms of root mean square difference and mean bias difference of 6.1% and 0.3%, respectively.

After the validation, the model was used to calculate the surface solar radiation over the country and the results were displayed as monthly and yearly solar

radiation maps. It was observed that variations of solar radiation in Thailand were influenced by the tropical monsoons. Solar radiation of more than 19 MJ/m^2-day was found in the summer (March to May) in most parts of the country. High solar radiation (21-22 MJ/m^2-day) areas are in the central and northeast regions. Long-term mean daily solar radiation, when averaged over the country, was found to be 17.4 MJ/m^2-day. These results indicate that Thailand has relatively high solar energy potential.

Chapter 3

An Estimation of Daily Global Solar Radiation using Artificial Neural Networks in Thailand*

3.1 Introduction

In Chapter 2, satellite data were used as main input of a satellite-based radiation model for calculating surface solar radiation in Thailand. In this chapter, we propose to use an artificial neural network model to estimate solar radiation by employing satellite-derived cloud index as a main input of the model.

An artificial neural network (ANN) is an interconnected structure of simple processing units whose function resembles that of the neural system of human brain. In practice, ANN is a computer program which is written in such a way that it can recognize the pattern of a relation between input and output parameters of a system. The recognition is obtained by a training process. A trained ANN can be used to determine the output parameters of the system from the unknown input parameters. The use of ANN allows us to determine the output parameters of a system without using an explicit function relating input and output parameters. It is advantageous to use ANN model for a system which is difficult to find an explicit mathematical relation between the input and output parameters of the system.

For solar radiation calculation, we can consider the earth atmosphere as a system which has extraterrestrial radiation (H_0), cloud (n), water vapour (w), ozone(ℓ), aerosols (AOD) as input parameters and solar radiation (H) at the earth surface as output parameter (Fig 3.1)

*This chapter has been published in Silpakorn University International Conference on Academic Research and Creative Arts : Integration of Art and Science, 25-27 January, 2012

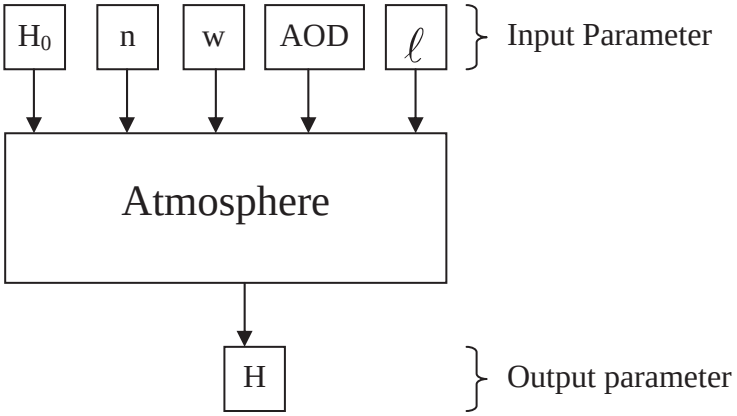

Fig 3.1 Schematic diagram of the earth atmospheric system with parameters effecting solar radiation traveled through it. (H_0 is extraterrestrial radiation, n is cloud index, w is water vapour, ℓ is total ozone column, AOD is an aerosols optical depth at 550 nm and H is solar radiation at the earth surface).

In general, it is difficult to formulate a mathematical function relating these input parameter (H_0, n, w, AOD, ℓ) to the output parameter (H). Therefore in this work, we propose to use ANN to model to relate these input and the output parameters (H).

3.2 Preparation of data for ANN

We will use the input and output parameters of the atmospheric system as shown in Fig 3.1. These parameters are obtained as follows.

3.2.1 The daily global solar radiations

Daily global solar radiations from four measurement stations of four main regions in Thailand for the period of 2003-2010 were prepared. These stations are Chiang Mai (18.78 °N, 98.98 °E), Ubon Ratchatani (15.25 °N, 104.87 °E), Nakhon Pathom (13.82 °N, 100.04 °E) and Songkhla (7.20 °N, 100.60 °E) Fig 3.2. These data were subjected of the quality control. Abnormal data were discarded from the data set.

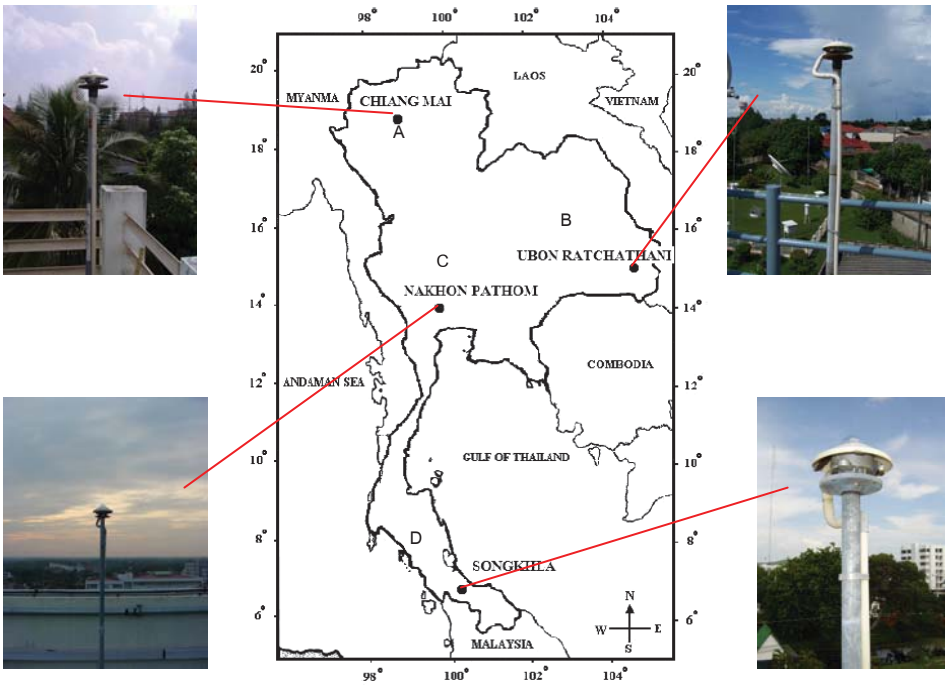

Fig 3.2 Solar radiation measuring station

3.2.2 Cloud index

Cloud is a main factor affecting surface solar radiation. In this work, propose to satellite-derived cloud index to represent the effect of cloud on solar radiation. It is derived from the GMS5 satellite (Jan, 2003 – Apr, 2003), GOES9 satellite (May, 2003 – Oct, 2005) and MTSAT-1R satellite (Nov, 2005 – Dec, 2010). The cloud index is calculated from the following equation.

$$n = \frac{\rho_{ea} - \rho_{min}}{\rho_{max} - \rho_{min}} \qquad (3.1)$$

where n is cloud index

ρ_{ea} is earth-atmospherics reflectivity obtained from satellite data

ρ_{min} is minimum earth-atmospherics reflectivity derived from satellite data

ρ_{max} is maximum earth-atmospherics reflectivity calculated from satellite data

Under the clear sky condition we have $\rho_{ea} = \rho_{min}$ so $n = 0$ and under cloudy sky we have $\rho_{ea} = \rho_{max}$ then $n = 1$. Under partly cloudy condition, cloud index will vary between zero to one, $0 < n < 1$.

3.2.3 Water vapour

Water vapour in terms of precipitable water (cm) was obtained from NCEP/NCAR data base. These data provide precipitable water with a resolution of 1x1 degree. The data were extracted at each station, one value per day. The global view of the data are shown in the Fig. 3.3

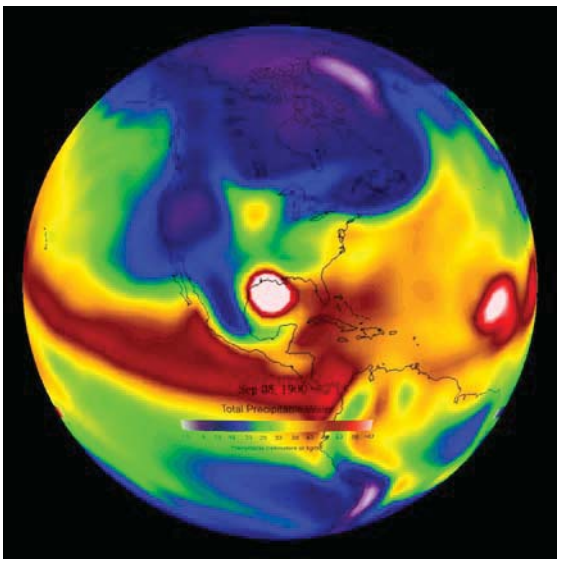

Fig 3.3 Global view of precipitable water

3.2.4 Total ozone column

The total ozone column were retrieved from TOMS/EP (2003-2004) and OMI/AURA (2005-2010).

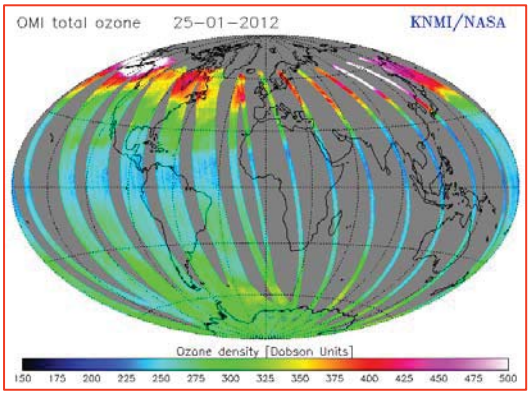

Fig 3.4 Example of Total ozone column from OMI/AURA

3.2.5 Aerosol optical depth

Aerosol data were collected from daily file of TERRA/MODIS satellite which was passed through the country every day at 10 O'clock local time. The aerosol optical depth at 550 nanometer was used in this work.

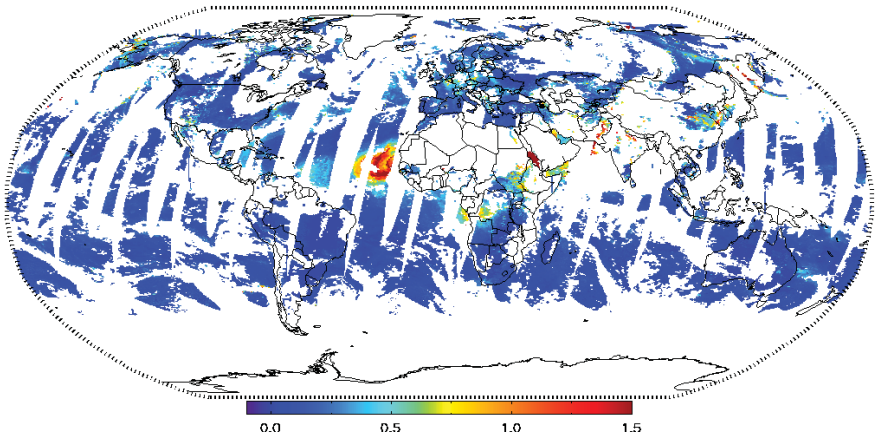

Fig. 3.5 Example of aerosol optical depth from TERRA/MODIS satellite

3.3 ANN modeling of daily global radiation

In this study, we propose to use an independent multi-layer ANN model to predict daily global radiation. The input parameter of ANN model are daily extraterrestrial solar radiation (H_0), cloud index (n), precipitable water (w), total ozone column (ℓ), aerosol optical depth (AOD) and the output parameter is daily

global radiation (H). This ANN model has a multi-layer network with a large number of simple processing elements called neuron. The input layer of the model consists of 5 neurons which correspond to 5 input parameters, whereas the output layer has only one neuron that corresponds to daily global radiation. In general, the number of neurons for each hidden layer can be optionally selected. The more layer number in the system, the more precise is the representation and the greater the training required.

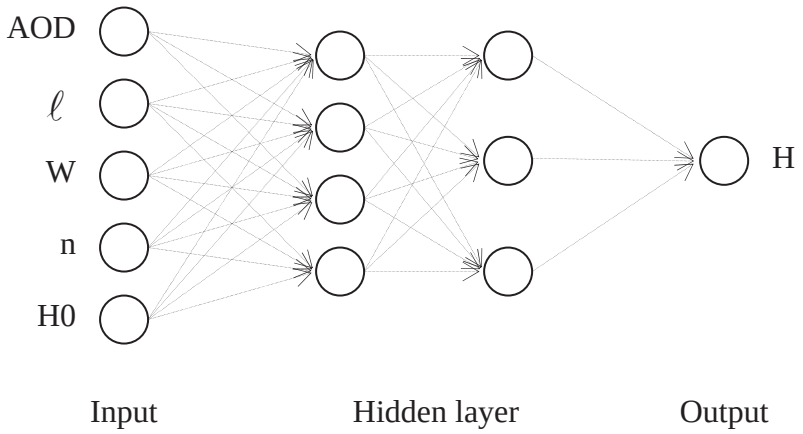

Fig 3.6 Structure of ANN modeling for predicting daily global radiation

The next step is the training of ANN. A number of training algorithms have been developed. In this work, the ANN model was trained by using the back propagation algorithm. The data used for input and output parameters are from Nakhon Pathom for the year 2003-2007. For the test of the performance of the model, we used input data at Nakhon Pathom, Ubon Ratchathani, Chiang Mai and Songkhla for the year 2008-2010.

3.4 Results and Discussion

Daily global radiation predicted by ANN was compared with that obtained from the measurements. The results are shown in Fig. 3.7-3.11.

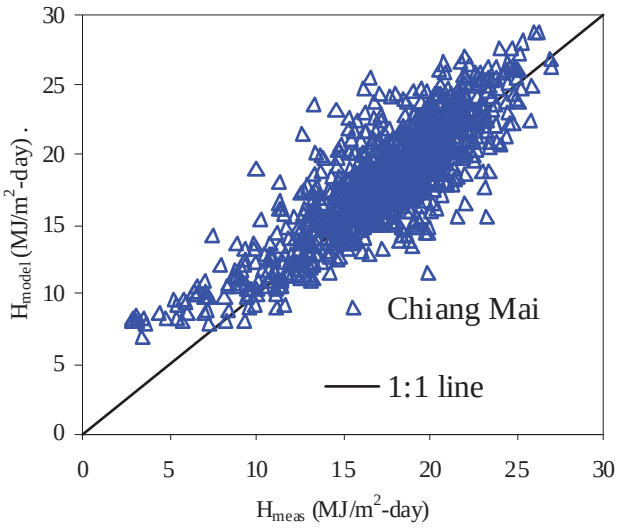

Fig. 3.7 Graphical comparison of daily radiation from ANN (H_{model}) and measurements (H_{meas}) at Chiang Mai

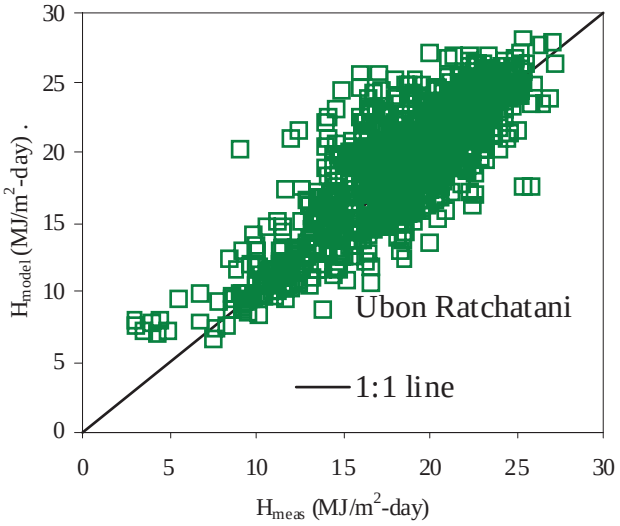

Fig. 3.8 Graphical comparison of daily radiation from ANN (H_{model}) and measurements (H_{meas}) at Ubon Ratchatani

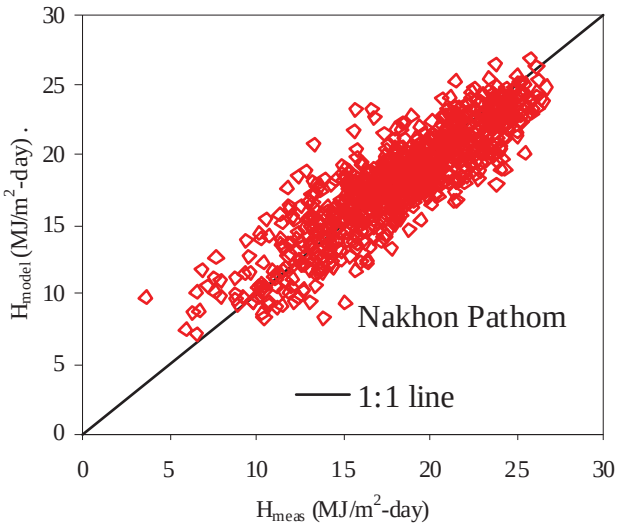

Fig 3.9 Graphical comparison of daily radiation from ANN (H_{model}) and measurements (H_{meas}) at Nakhon Pathom

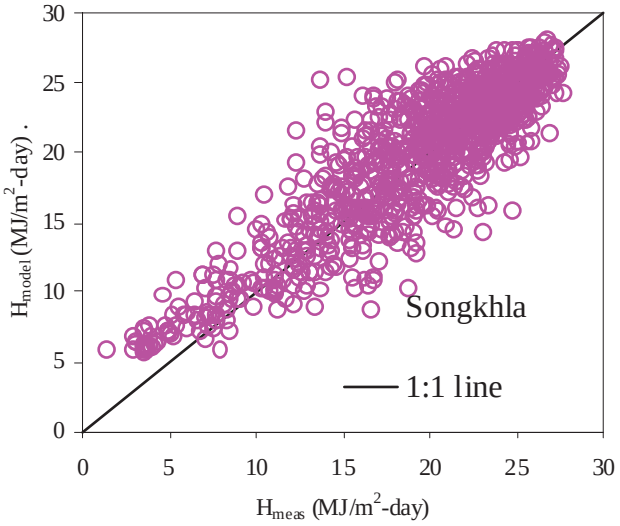

Fig. 3.10 Graphical comparison of daily radiation from ANN (H_{model}) and measurements (H_{meas}) at Songkhla

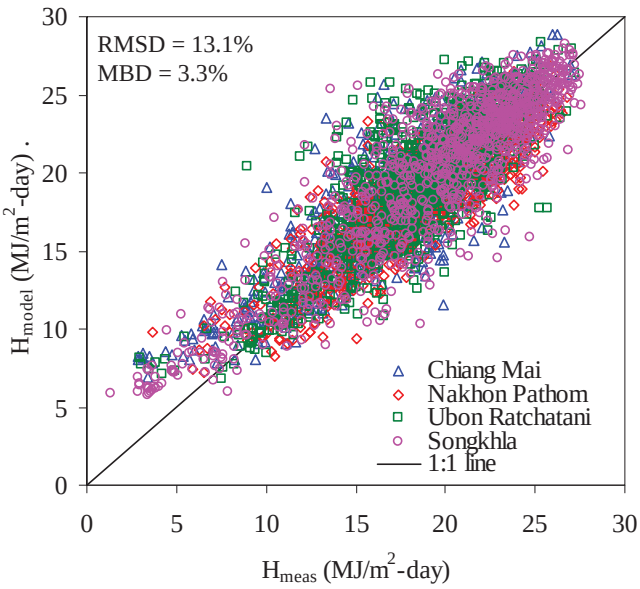

Fig 3.11 Graphical comparison of daily radiation from ANN (H_{model}) and measurements (H_{meas}) at Chiang Mai, Nakhon Pathom, Ubon Ratchatani and Songkhla

Table 3.1 Mean bias difference (MBD) and root mean square difference (RMSD) from the comparison at four stations

Station	MBD (%)	RMSD (%)
Chiang Mai	5.1	13.9
Nakhon Pathom	-0.4	10.0
Ubon Ratchatani	4.9	14.0
Songkhla	3.1	13.4
All stations	3.3	13.1

From Table 3.1 root mean square difference (RMSD) of global solar radiation between measurements and ANN at Chiang Mai, Nakhon Pathom, Ubon Ratchatani and Songkhla are 13.9%, 10.0%, 14.0% and 13.4%, respectively. For the other station except Nakhon Pathom the RMSD value more than that of Nakhon Pathom. This is likely due to the fact that the environments of the other stations are different from those of Nakhon Pathom. However the values of MBD and RMSD for the combined data are 3.3% and 13.1%, respectively which are relatively small.

3.5 Conclusion

In this study, an artificial neural network (ANN) model was developed to estimate daily global solar radiation by using cloud index derived from image data of GMS5, GOES9 and MTSAT-1R satellites, precipitable water from NCEP/NCAR database, ozone data from TOMS/EP and OMI/AURA satellites and aerosol optical depth from TERRA/MODIS satellite. The solar radiation data at Nakhon Pathom (13.82 °N, 100.04 °E) (2003-2007) was used to train ANN by employing the back propagation method. To evaluate its performance, the ANN model which has been trained was used to predict daily solar radiation at Nakhon Pathom (2008-2010). Additionally, the model was also used to estimate the solar radiation at Chiang Mai (18.78 °N, 98.98 °E), Ubon Ratchatani (15.25 °N, 104.87°E) and Songkhla (7.2 °N, 100.6 °E) for the year 2008 to 2010. It was found that the root mean square difference (RMSD) between values of daily solar radiation estimated from the ANN model and those obtained from the measurements at Chiang Mai, Ubon Ratchatani, Nakhon Pathom and Songkhla were in reasonable agreement with the root mean square difference for Chiang Mai, Nakhon Pathom, Ubon Ratchatani and Songkhla of 13.9%, 10.0%, 14.0% and 13.4%, respectively.

Chapter 4

Semi-empirical models for the estimation of clear sky solar global and direct normal irradiances in the tropics*

4.1 Introduction

In some solar energy applications, an estimate of global and direct solar radiation under clear sky conditions is needed. Clear sky global radiation is normally used to predict the maximum performance of solar thermal systems such as solar water heaters and solar crop dryers. Direct normal radiation under clear sky condition is usually required to calculate the maximum temperature of concentrating solar power systems. Satellite-based methods such as HELIOSAT (Cano et al., 1986; Perez et al., 2002; Hammer et al., 2003; Vignolar et al., 2007) also need clear sky solar irradiance for calculating surface solar radiation from satellite data. To respond to this requirement, a number of clear sky solar radiation models have been proposed. These models have different degrees of a complexity, ranging from simple empirical models (Haurwitz, 1945; Haurwitz, 1946; Daneshyar, 1978; Paltridge and Proctor, 1976; Berger, 1979; Adnot et al., 1979; Kasten and Czeplak, 1980; Robledo and Soler, 1769; Ianets and Kudish, 2008; Kondratyev, 1969; Majumdar et al., 1972) to rigorous radiative transfer models (Gueymad, 1995; Tanre et al., 1986; Key and Schweiger, 1998' Ricchiazzi et al. 1998; Berk, 1999; Mayer and Kylling, 2005). Empirical models have an advantage of simplicity, but they usually lack generality. In contrast, radiative transfer models offer more generality and accuracy; however, they are more complex and require more input data which sometimes are not available. Performance of clear sky irradiance models have been tested in many studies (Badescu, 1997; Louche et al., 1988; Ineichen, 2006; Ianetz et al., 2007; Fortin et al., 2008). Published results reveal a wide range of discrepancies between predicted and measured radiation. In addition, most data sets used for model formulation and testing have been obtained from mid latitude countries. There are not many studies that examine the performance of these models in tropical conditions. In general, empirical models have fixed model parameters, thus lacking generality. As solar radiation depends on

*This chapter has been published in Applied Energy 88, 4749–4755 (2011)

physical parameters such as aerosol optical properties and precipitable water, a general model should include these parameters. Recent advances in technology make this information easily available from ground and satellite based measurements (e.g. AERONET and MODIS). Therefore, in this study we propose semi-empirical models which use some of these products for estimating clear sky global and direct normal solar irradiances in the tropics. The performance of these models have been evaluated and compared with other models using data from four sites in Thailand.

4.2 Measurements and data processing

4.2.1 Measurements

Thailand comprises four main regions: the mountainous North, the flat high-land Northeast, the flat low-land Centre and the peninsular South (Fig. 4.5). In each region, our group has solar radiation monitoring stations, namely Chiang Mai (18.78 °N, 98.98 °E) in the North, Ubon Ratchathani (15.25 °N, 104.87 °E) in the Northeast, Nakhon Pathom (13.82 °N, 100.04 °E) in the Centre and Songkhla (7.20 °N, 100.60 °E) in the South. The positions of these stations are shown in Fig. 1 with details in Table 1. Atmospheric conditions and solar radiation are routinely measured, including global and direct normal solar irradiances, aerosol optical properties, precipitable water, and sky imagery. Global irradiance at Chiang Mai, Ubon Ratchathani and Songkhla were measured using Kipp&Zonen pyranometers (model CM21), whereas a Kipp&Zonen pyranometer (model CM11) was employed for measuring global irradiance at Nakhon Pathom. Direct normal irradiance was measured using Kipp&Zonen pyrheliometers (model Ch1) equipped with Kipp&Zonen sun trackers (model 2AP). Voltage signals from these pyranometers and pyrheliometers were recorded by a Yokogawa (model DC100) data logger with a signal capture rate of 1 s. These signals were averaged for the period of 10 minutes and the averaged value was recorded in the data logger memory. The 10-minute average voltage data were sent to our Laboratory in Nakhon Pathom for further processing. At the laboratory, the 10-minute average voltages were divided by the sensitivity factor of each instrument to obtain 10-minute average irradiance, in $W.m^{-2}$. Then the data of the 10-minute average irradiance were used for the model formulation and validation.

The pyranometers at four stations were calibrated yearly using a traveling pyranometer recently calibrated at the Kipp&Zonen factory as a standard. All pyrheliometers were calibrated against an H-F absolute cavity pyrheliometer which participated in the 10th International Pyrheliometer Comparison (IPC-X) at Davos, Switzerland in 2005. At each station, a CIMEL (model CE318) sunphotometer was used to measure the solar spectrum at the wavelengths of 340, 380, 440, 500, 675, 870 and 1,020 nm. The sunphotometers at the four stations belong to our Laboratory, which are members of the Aerosol Robotic Network (AERONET) of NASA (Holben et al., 1998). The spectral data from these sunphotometers were processed by AERONET to obtain aerosol optical properties such as aerosol optical depth, Angstrom wavelength exponent and single scattering albedo. The sunphotometers are regularly calibrated by AERONET. As the sunphotometers have water vapour sensitive channel, precipitable water was also derived from these instruments. The aerosol and precipitable water data obtained from these AERONET sunphotometers in Thailand have the accuracy in the range of 5-10% (Holben, 2010). In order to identify sky conditions, a digital sky camera produced by Prede Co. Ltd (Japan) was installed at each station. The sky camera equipped with a fish-eye lens records a wide-angle digital image of the sky every 10 minutes. Cloud cover and cloud type can be visually identified from the sky image. All instruments were maintained by well-trained officers at the stations. By considering the performance of the measuring instruments, recording devices and calibration procedure, the accuracy of global and direct normal irradiance data were estimated to be 5%.

Fig. 4.1 pyranometer (model CM 11)

Fig. 4.2 Sky camera model PSV-100

Fig. 4.3 Sun tracker model 2AP and Pyrheliometer model CH1

Fig. 4.4 Sunphotometer model CE318

Table 4.1 Position and elevation of the solar radiation monitoring stations

Station	Position		Altitude (m) (Above the mean sea level)
	Latitude	Longitude	
Chiang Mai	18.78 °N	98.98 °E	317
Ubon Ratchathani	15.25 °N	104.87 °E	134
Nakhon Pathom	13.82 °N	100.04 °E	37
Songkhla	7.20 °N	100.60 °E	16

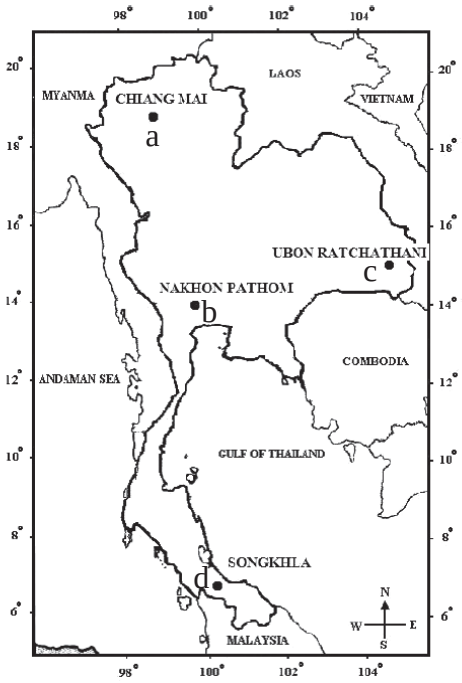

Fig. 4.5 Solar radiation monitoring station a) Chiang Mai b) Nakhon Pathom c) Ubon Ratchathani d) Songkhla

4.2.2 Data preparation

Following the objectives of the study, only global and direct normal irradiances under clear sky conditions were used in this study. At each station, the AERONET sunphotometer was operated side by side with the pyranometer and pyrheliometer. Cloudless sky conditions were identified using the cloud screening procedures of AERONET (Smirnov, 2000). Additionally, sky photographs taken by the digital sky camera at the station were also visually inspected to confirm the cloudless conditions. As the aerosol load and precipitable water are relatively high in Thailand (Jantarach et al., 2009; Janjai et al., 2010), these atmospheric parameters were also used in the models. The Angstrom wavelength exponent (α) and aerosol optical depths (AOD) at each station were obtained from AERONET and the Angstrom turbidity coefficient (β) was derived from using these two variables as reported in Iqbal (Iqbal, 1983). Precipitable water vapour was also used in the model and these data were easily available as they are also one of the products of the

sunphotometer measurement. Finally, ozone data were obtained from OMI /AURA satellite.

The clear sky global irradiance data from the stations in Chiang Mai, Nakhon Pathom and Songkhla for the year 2007 were used to formulate the global irradiance model and the global radiation data from these stations for the year 2008 together with the data from Ubon Ratchathani (15.25 °N, 104.87 °E) were employed to examine the model performance. As aerosol information at Ubon Ratchathani has been available since the end of 2009, only solar radiation data for the year 2010 from this station were used for the validation.

For the clear sky direct normal irradiance, the model formulation was based on the data of the year 2009 from the stations at Chiang Mai, Nakhon Pathom and Songkhla and the data at these stations together with the data from Ubon Ratchathani for the year 2010 were used to evaluate the performance of the model. Details of the periods of these data were summarized in Table 2.

Table 4.2 Schedule for model development and validation. Both model input and validation data consisted in 10-minute average irradiances.

Station	Model Development				Validation			
	Global irradiance		Direct normal irradiance		Global irradiance		Direct normal irradiance	
	Period	Number of data	Period	Number of data	Period	Number of data	Period	Number of data
Chiang Mai	Jan - Dec, 2007	733	Jan - Dec, 2009	1,258	Jan - Dec, 2008	1,674	Jan - Dec, 2010	3,114
Nakhon Pathom	Jan - Dec, 2007	2,569	Jan - Dec, 2009	1,857	Jan - Dec, 2008	1,675	Jan - Dec, 2010	2,432
Songkhla	Jan - Dec, 2007	1,153	Jan - Dec, 2009	1,370	Jan - Dec, 2008	1,306	Jan - Dec, 2010	1,001
Ubon Ratchathani	Not used	-	Not used	-	Jan - Dec, 2010	1,767	Jan - Dec, 2010	1,786

4.3 Model development

4.3.1 Formulation of the models

As empirical models normally lack of generality and physical models are often very complex and impractical, we proposed semi-empirical models as a compromise. In general, aerosols and water vapour play an important role in depletion of the visible and infrared portion of the solar spectrum, while ozone attenuates radiation in the ultraviolet region. To make the model general, these atmospheric effects on the spatial and temporal variability of solar radiation need to be involved in the model. Instead of including these parameters according to the physical laws, they were expressed empirically as follows:

- For global irradiance

$$I_G = A_1 e^{-B_1 m_a} \tag{4.1}$$

$$A_1 = a_1 E_0 I_{sc} (\cos\theta_z)^{b_1} \tag{4.2}$$

$$B_1 = c_1 + d_1\beta + e_1\alpha + f_1 w + g_1 \ell \tag{4.3}$$

- For direct normal irradiance

$$I_{BN} = A_2 e^{-B_2 m_a} \tag{4.4}$$

$$A_2 = a_2 E_0 I_{sc} (\cos\theta_z)^{b_2} \tag{4.5}$$

$$B_2 = c_2 + d_2\beta + e_2\alpha + f_2 w + g_2 \ell \tag{4.6}$$

I_G is clear sky global irradiance ($W.m^{-2}$), I_{BN} is clear sky direct normal irradiance ($W.m^{-2}$), I_{sc} is the solar constant (1366.1 $W.m^{-2}$), m_a is relative optical air mass, θ_z is solar zenith angle (degrees), β is Angstrom turbidity coefficient, α is Angstrom wavelength exponent, w is precipitable water (cm) and ℓ is total column ozone (cm), E_0 is eccentricity correction factor due to variation of sun-earth distance and a_1, a_2, b_1, b_2, c_1, c_2, d_1, d_2, e_1, e_2, f_1, f_2, g_1 and g_2 are empirical constants. Data used in formulation of the models are summarized in Table 3. The eccentricity correction factor was calculated from the following equation (Iqbal, 1983):

$$E_0 = 1.000110 + 0.034221\cos\Gamma + 0.001280\sin\Gamma + 0.000719\cos 2\Gamma + 0.000077\sin 2\Gamma \quad (4.7)$$

where $\Gamma = 2\pi(d_n - 1)/365$ (4.8)

and d_n is the day number of the year. Relative optical air mass (m_a) was calculated from solar zenith angle θ_z (degrees) by using the following Equations (Iqbal, 1983).

$$m_a = m_r(p/p_o) \quad (4.9)$$

where $p/p_o = \exp(-0.0001184h)$ (4.10)

and $m_r = [\cos\theta_z + 0.15(93.885 - \theta_z)^{-1.253}]^{-1}$ (4.11)

p is atmospheric pressure at the measuring station, p_o is the atmospheric pressure at sea level and h is the station altitude in meters above the sea level.

To determine the empirical constants, Eqs. (4.1)-(4.3) and (4.4)-(4.6) were fitted with the corresponding solar irradiance data and the data of β, α, w and λ from Chiang Mai, Ubon Ratchathani and Nakhon Pathom by using a non-linear multi-variable regression technique (Seber and Wild, 1989). The results are: a_1 =0.778227, a_2 =0.71640, b_1 =1.198932, b_2 = 0.35320, c_1 =-0.106634, c_2 = 0.10126, d_1 = 0.337373, d_2= 0.841372, e_1 = 0.009181, e_2 = 0.017649, f_1 = -0.009852, f_2 = 0.004851, g_1 = 0.482012 and g_2 = -0.48286.

4.3.2 Performance of models

To investigate their performance, the models were used to calculate clear sky global and direct normal irradiances at 4 stations: Chiang Mai, Ubon Ratchathani and Nakhon Pathom and Songkhla for the data periods shown in Table 4.2. Values of β, α, w from AERONET and ℓ from OMI/AURA satellite at these stations in the same periods as those of the irradiance data were also used. As these data were not involved in the formulation of the models, they are independent data set. The results for proposed global models are graphically shown in Fig. 4.6 and the other models are shown in Fig. 4.7-4.21. For the result of proposed direct normal models are shown in Fig. 4.22 and other model are shown in Fig. 4.23-4.32.

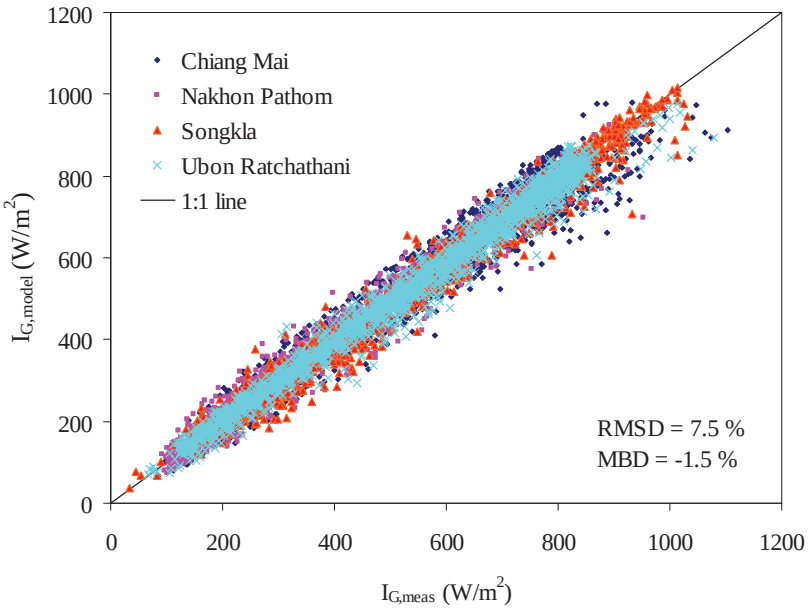

Fig. 4.6 Comparison between clear day global irradiance calculated from the proposed model ($I_{G,model}$) and that obtained from the measurements ($I_{G,meas}$)

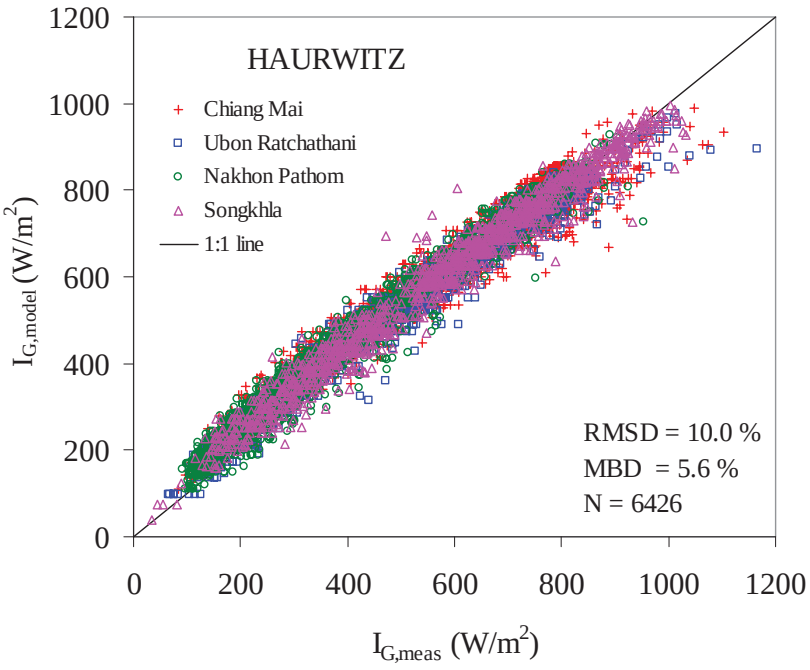

Fig. 4.7 Comparison between clear day global irradiance calculated from HAURWITZ model ($I_{G,model}$) and that obtained from the measurements ($I_{G,meas}$)

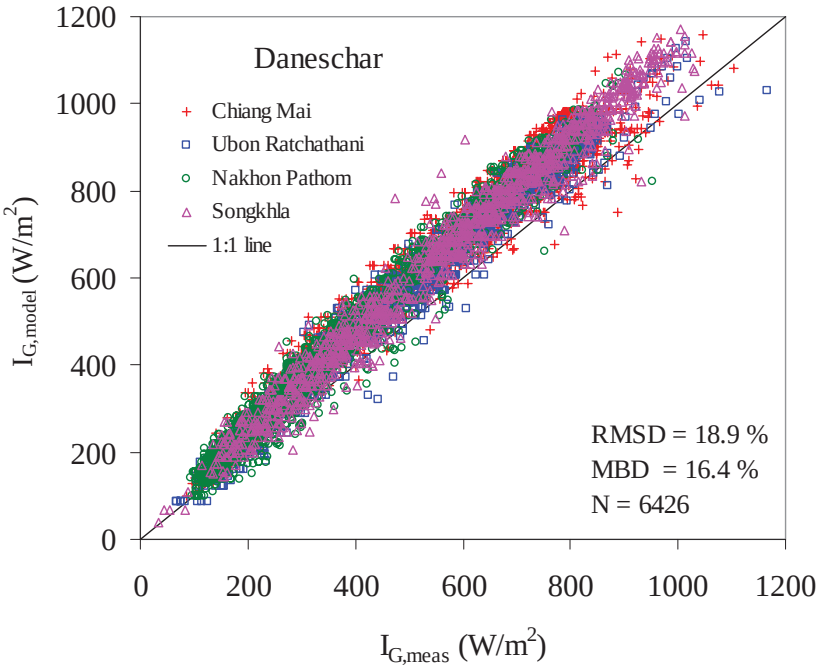

Fig. 4.8 Comparison between clear day global irradiance calculated from Daneschar model ($I_{G,model}$) and that obtained from the measurements ($I_{G,meas}$)

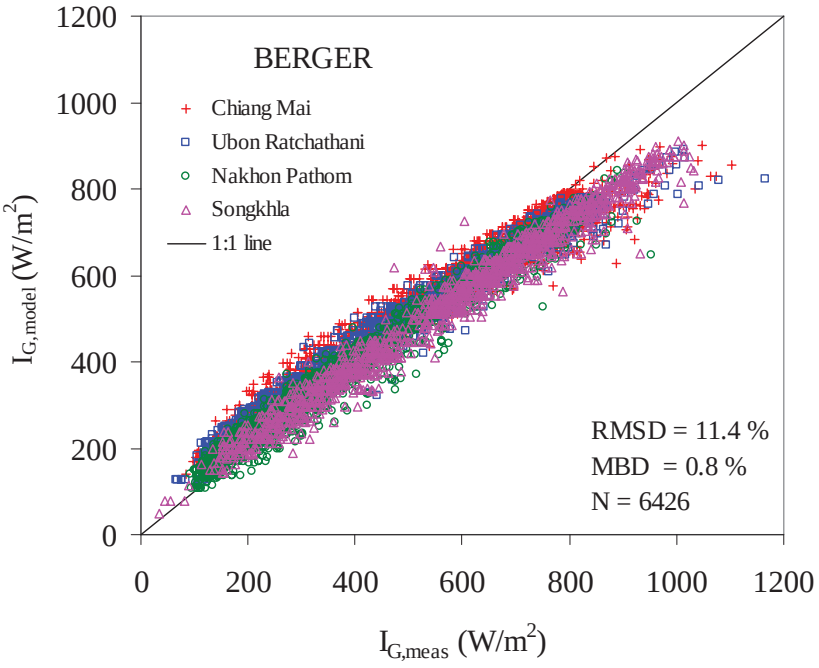

Fig. 4.9 Comparison between clear day global irradiance calculated from BERGER model ($I_{G,model}$) and that obtained from the measurements ($I_{G,meas}$)

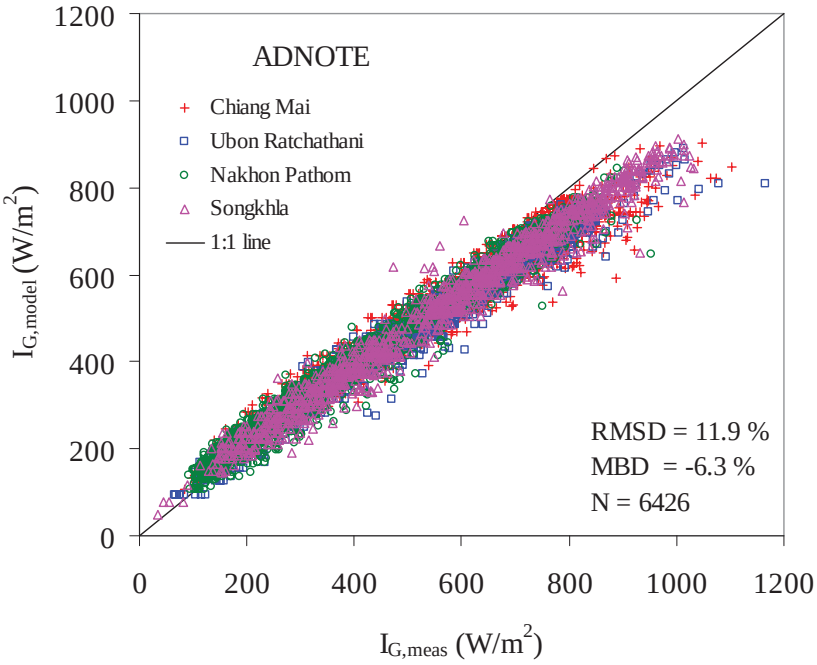

Fig. 4.10 Comparison between clear day global irradiance calculated from ADNOTE model ($I_{G,model}$) and that obtained from the measurements ($I_{G,meas}$)

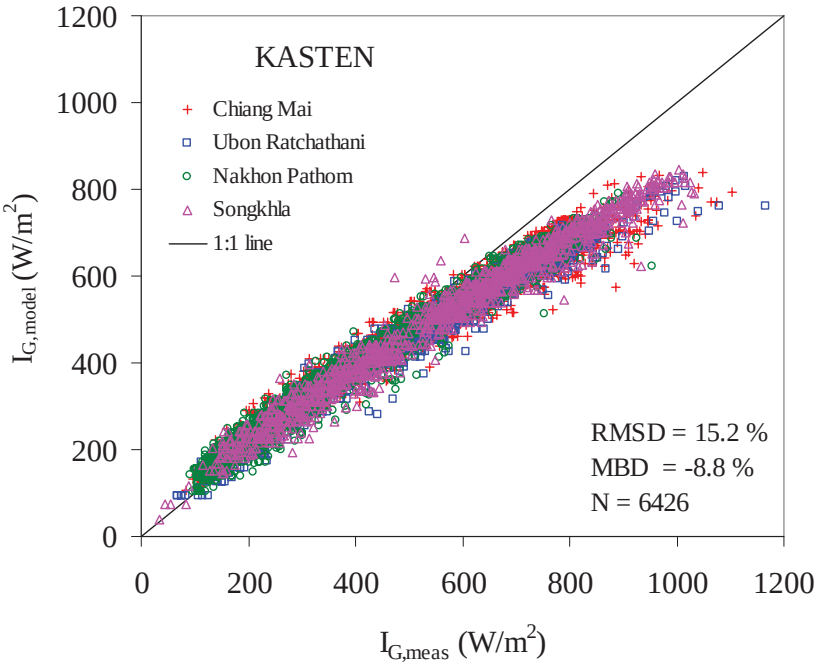

Fig. 4.11 Comparison between clear day global irradiance calculated from KASTEN model ($I_{G,model}$) and that obtained from the measurements ($I_{G,meas}$)

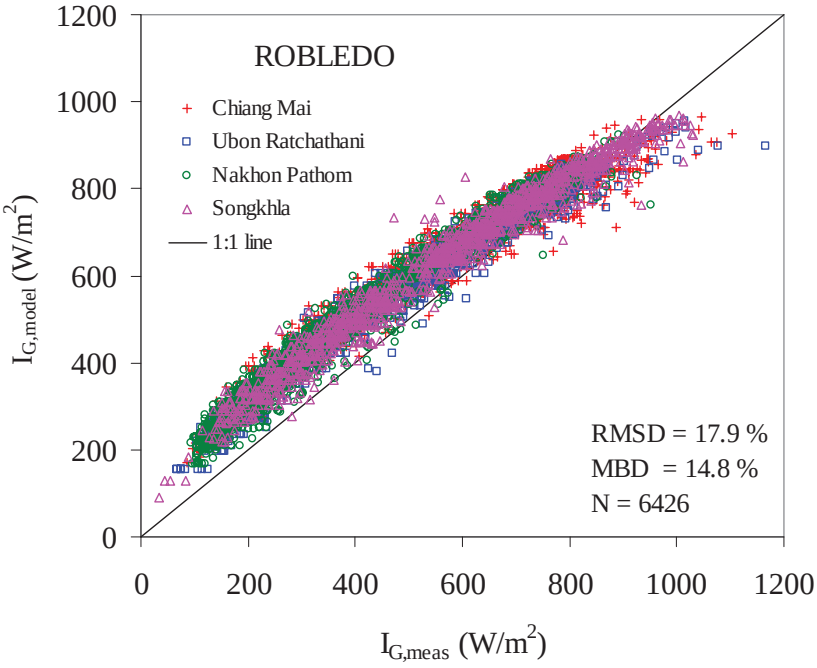

Fig. 4.12 Comparison between clear day global irradiance calculated from ROBLEDO model ($I_{G,model}$) and that obtained from the measurements ($I_{G,meas}$)

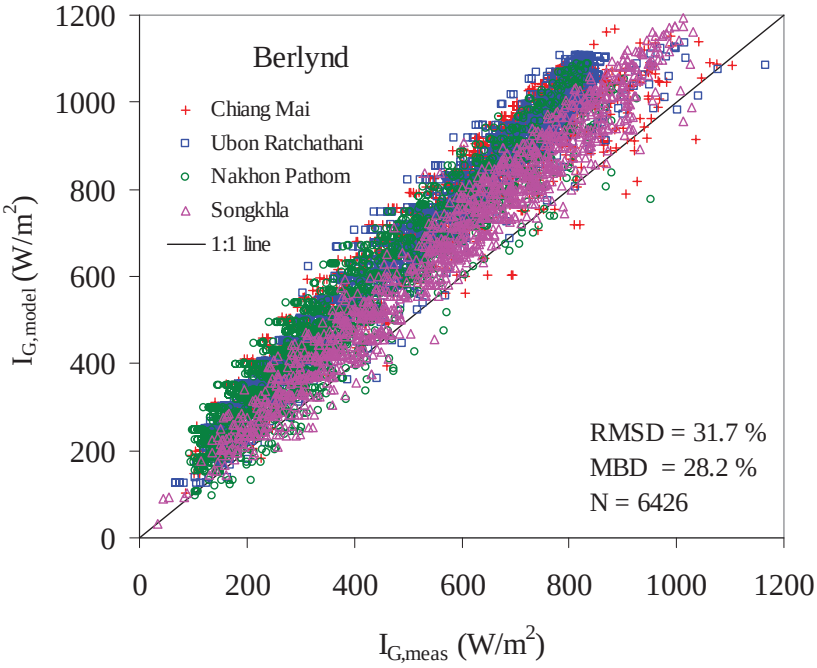

Fig. 4.13 Comparison between clear day global irradiance calculated from Berlynd model ($I_{G,model}$) and that obtained from the measurements ($I_{G,meas}$)

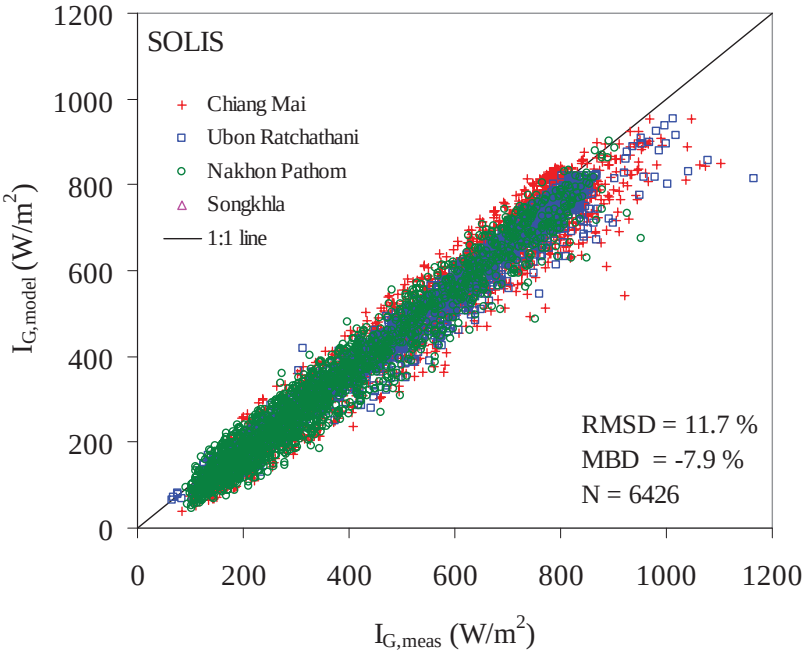

Fig. 4.14 Comparison between clear day global irradiance calculated from SOLIS model ($I_{G,model}$) and that obtained from the measurements ($I_{G,meas}$)

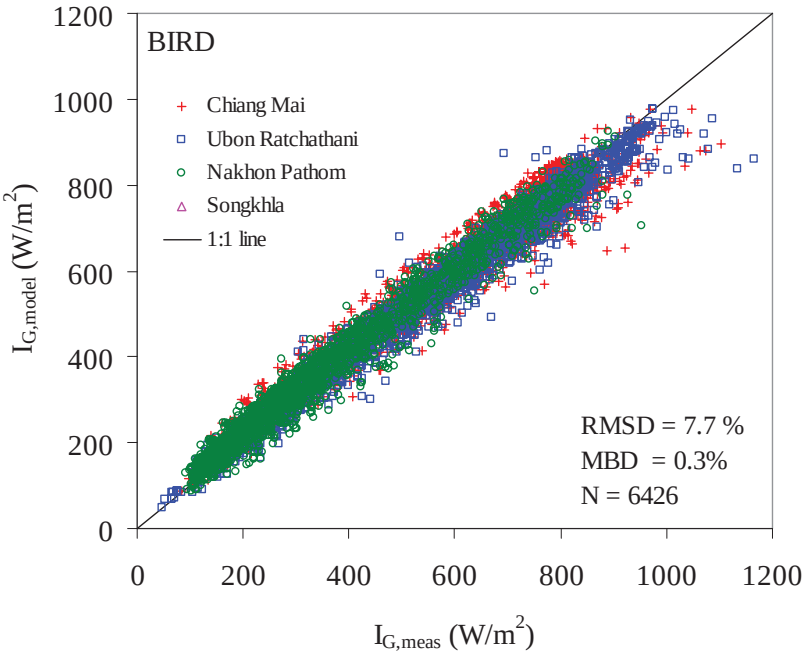

Fig. 4.15 Comparison between clear day global irradiance calculated from BIRD model ($I_{G,model}$) and that obtained from the measurements ($I_{G,meas}$)

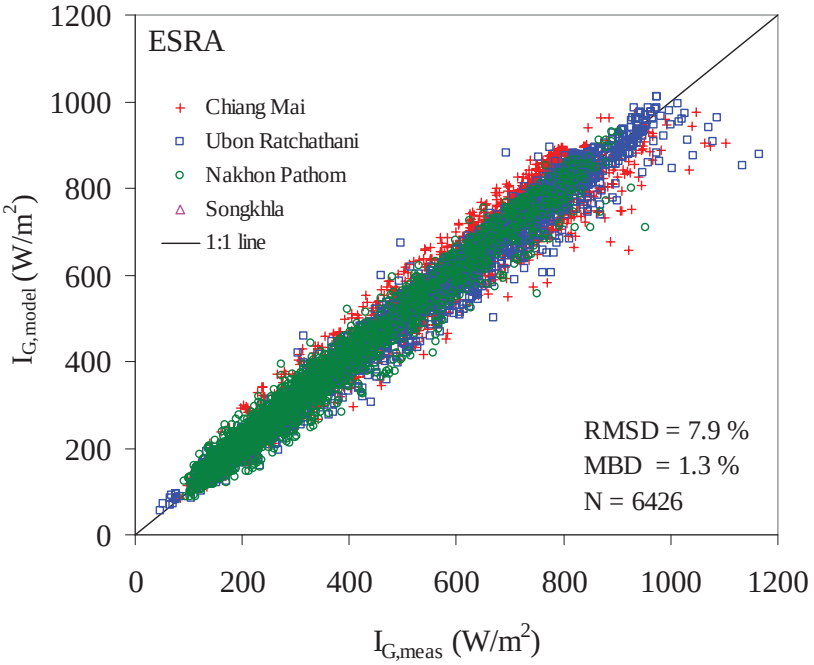

Fig. 4.16 Comparison between clear day global irradiance calculated from ESRA model ($I_{G,model}$) and that obtained from the measurements ($I_{G,meas}$)

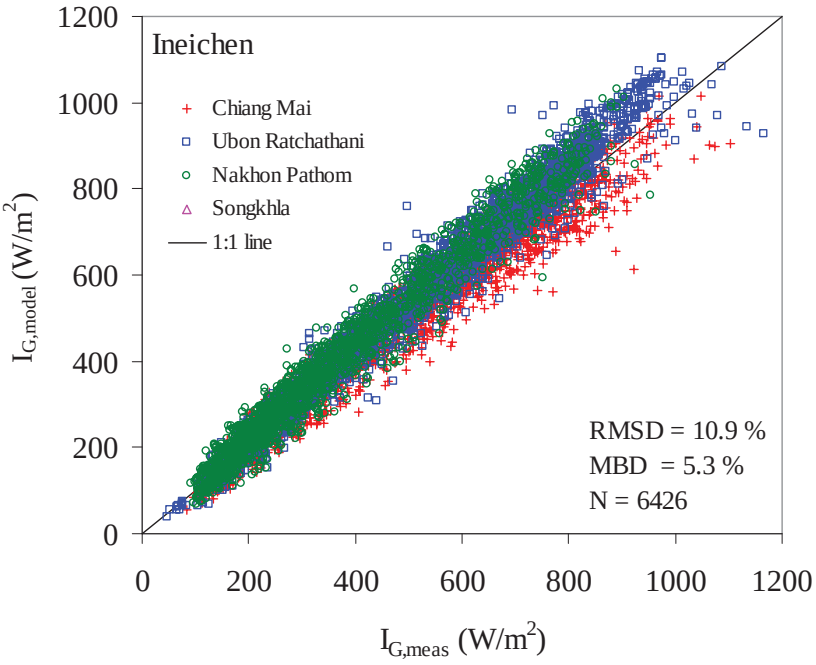

Fig. 4.17 Comparison between clear day global irradiance calculated from Ineichen model ($I_{G,model}$) and that obtained from the measurements ($I_{G,meas}$)

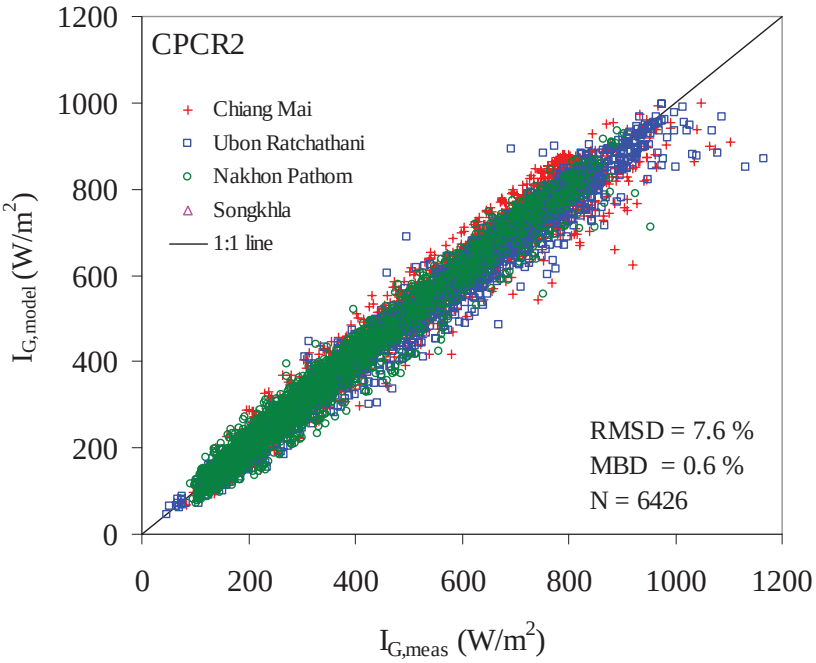

Fig. 4.18 Comparison between clear day global irradiance calculated from CPCR2 model ($I_{G,model}$) and that obtained from the measurements ($I_{G,meas}$)

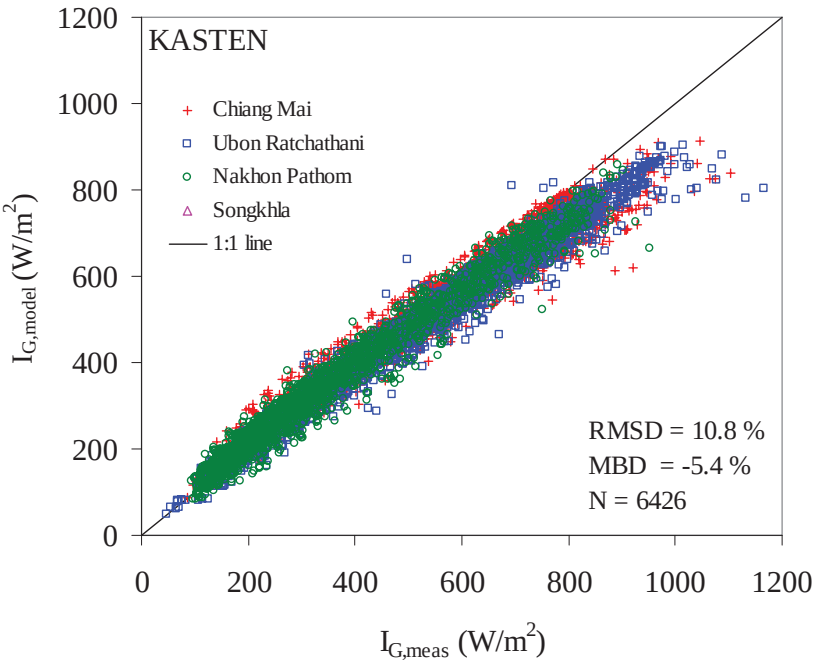

Fig. 4.19 Comparison between clear day global irradiance calculated from KASTEN model ($I_{G,model}$) and that obtained from the measurements ($I_{G,meas}$)

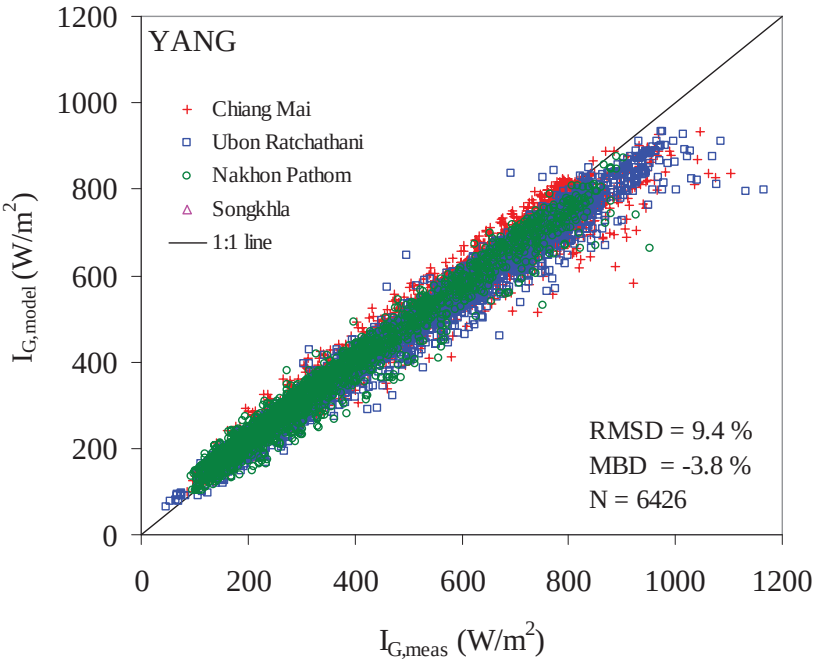

Fig. 4.20 Comparison between clear day global irradiance calculated from YANG model ($I_{G,model}$) and that obtained from the measurements ($I_{G,meas}$)

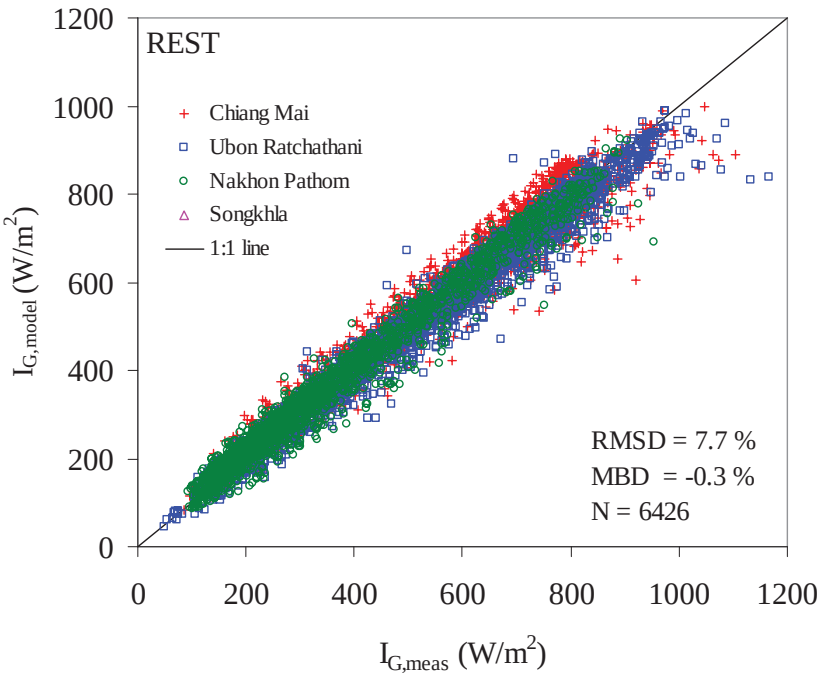

Fig. 4.21 Comparison between clear day global irradiance calculated from REST model ($I_{G,model}$) and that obtained from the measurements ($I_{G,meas}$)

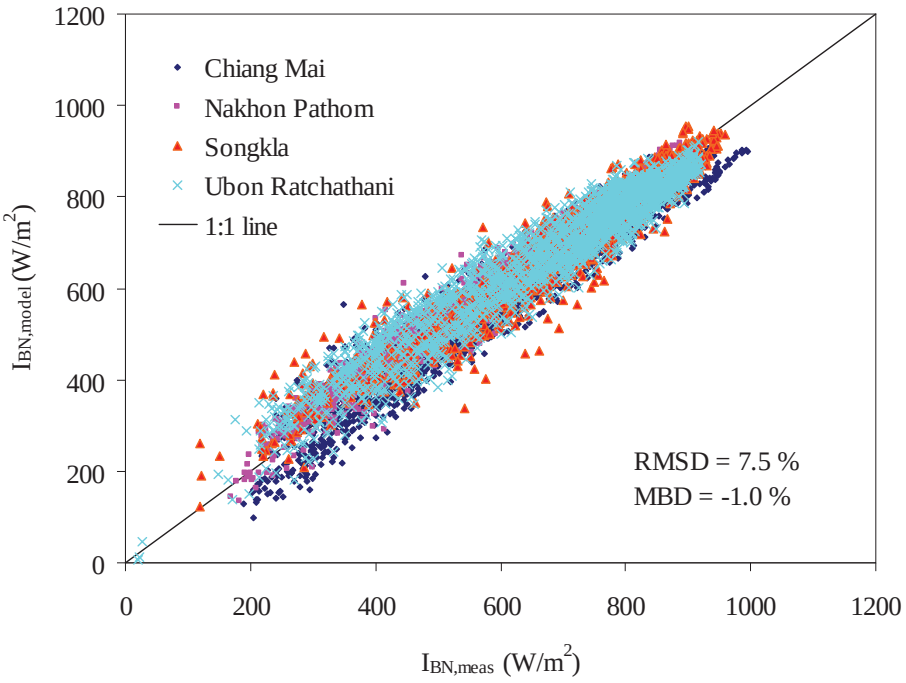

Fig. 4.22 Comparison between clear day direct normal irradiance calculated from the proposed model ($I_{BN,model}$) and that obtained from the measurements ($I_{BN,meas}$)

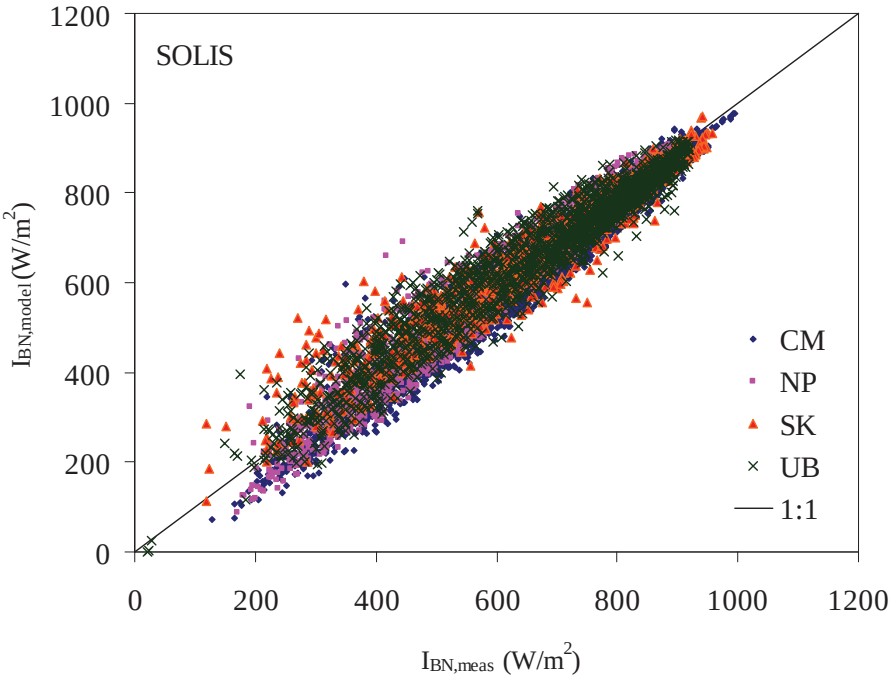

Fig. 4.23 Comparison between clear day direct normal irradiance calculated from SOLIS model ($I_{BN,model}$) and that obtained from the measurements ($I_{BN,meas}$)

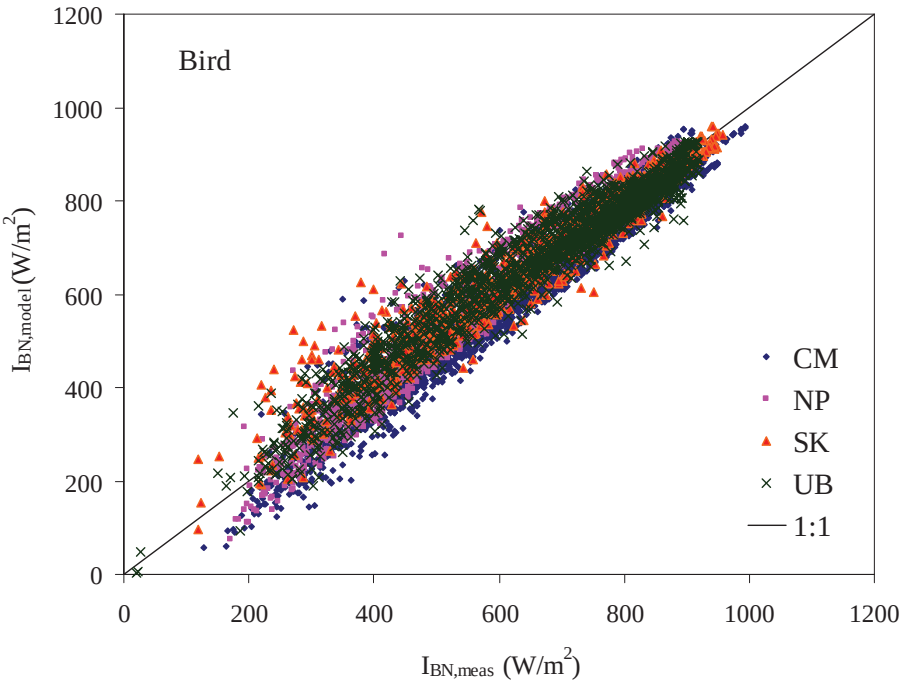

Fig. 4.24 Comparison between clear day direct normal irradiance calculated from Bird model ($I_{BN,model}$) and that obtained from the measurements ($I_{BN,meas}$)

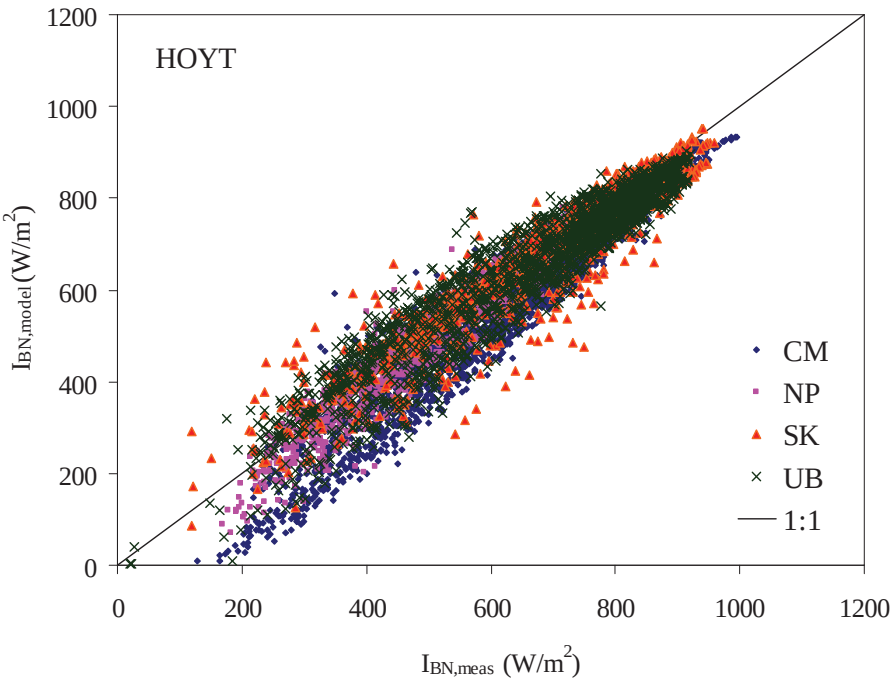

Fig. 4.25 Comparison between clear day direct normal irradiance calculated from HOYT model ($I_{BN,model}$) and that obtained from the measurements ($I_{BN,meas}$)

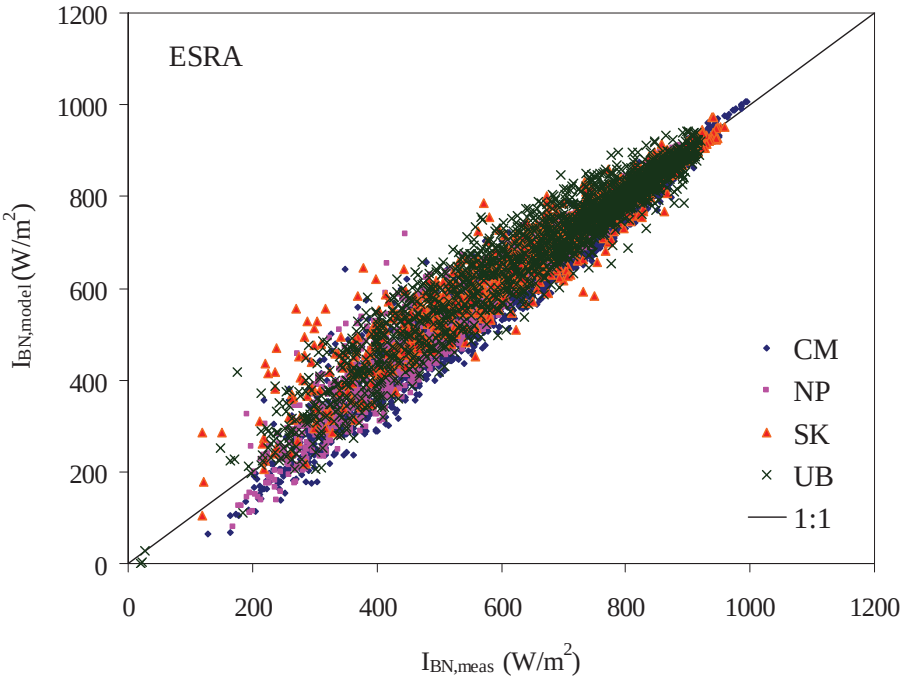

Fig. 4.26 Comparison between clear day direct normal irradiance calculated from ESRA model ($I_{BN,model}$) and that obtained from the measurements ($I_{BN,meas}$)

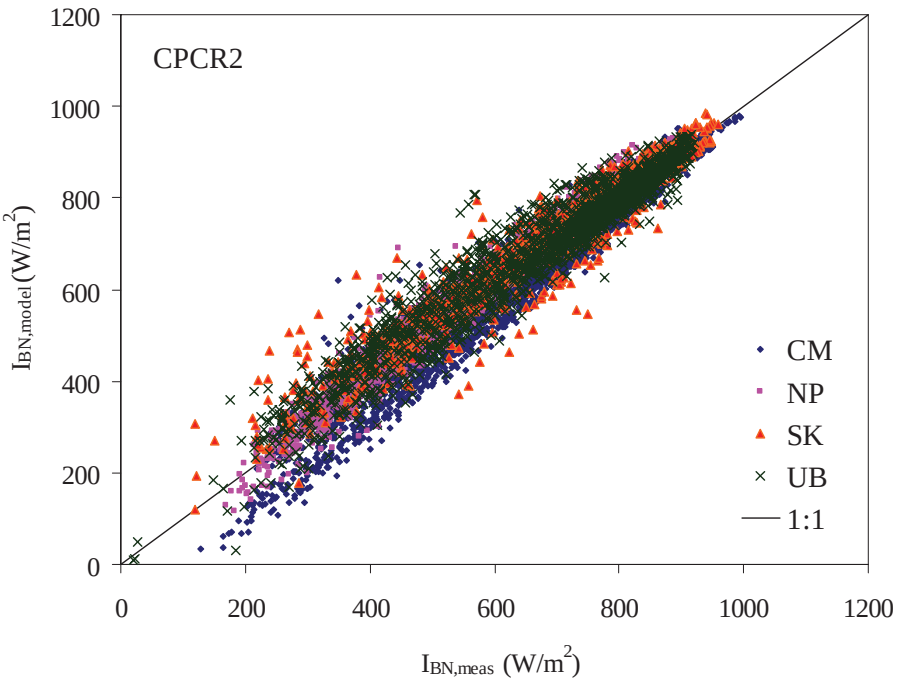

Fig. 4.27 Comparison between clear day direct normal irradiance calculated from CPCR2 model ($I_{BN,model}$) and that obtained from the measurements ($I_{BN,meas}$)

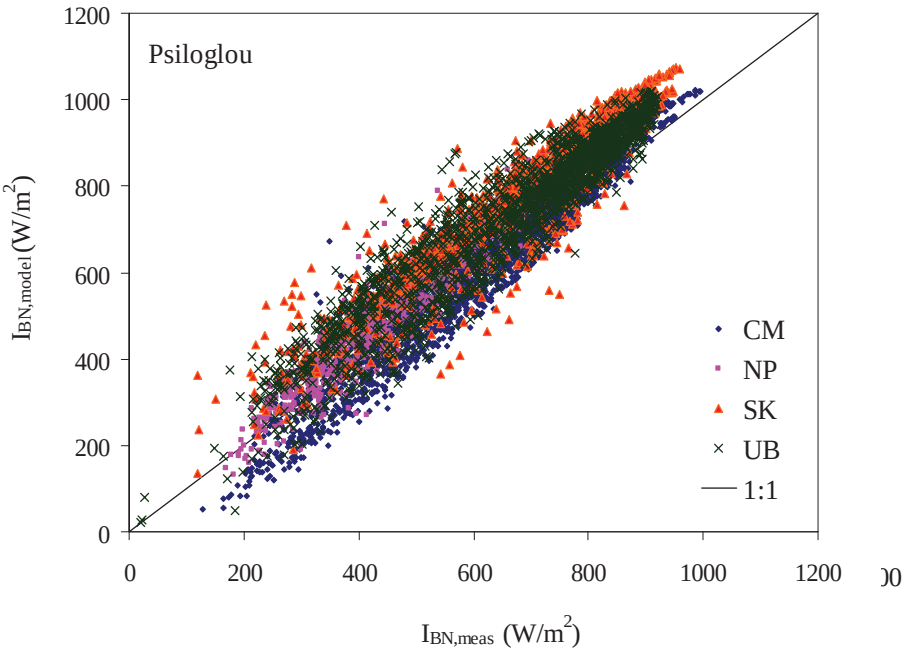

Fig. 4.28 Comparison between clear day direct normal irradiance calculated from Psiloglon model ($I_{BN,model}$) and that obtained from the measurements ($I_{BN,meas}$)

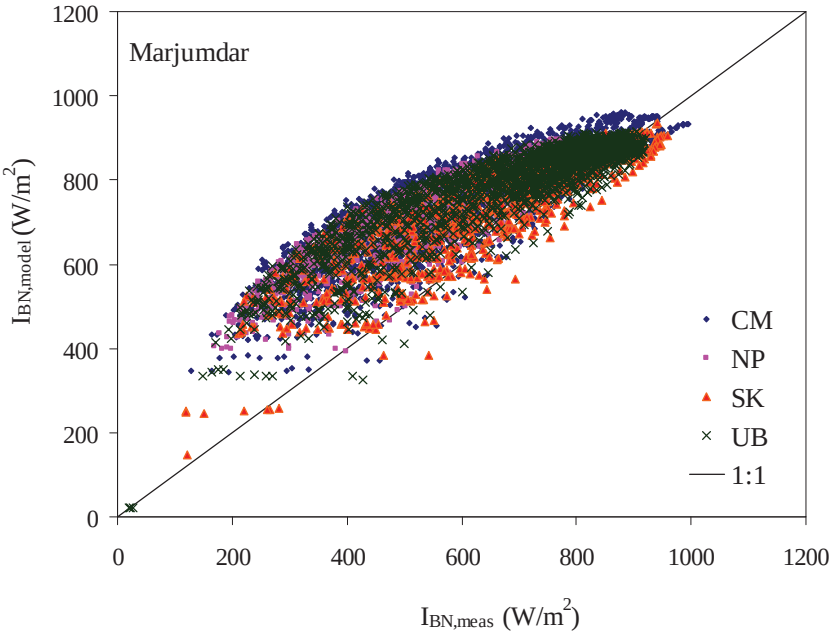

Fig. 4.29 Comparison between clear day direct normal irradiance calculated from Marjumdar model ($I_{BN,model}$) and that obtained from the measurements ($I_{BN,meas}$)

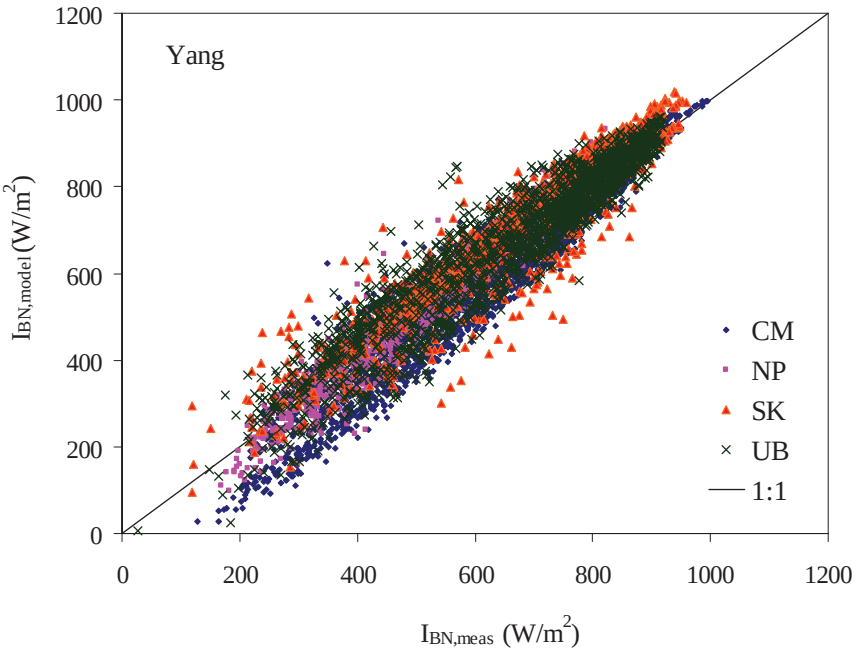

Fig. 4.30 Comparison between clear day direct normal irradiance calculated fromYang model ($I_{BN,model}$) and that obtained from the measurements ($I_{BN,meas}$)

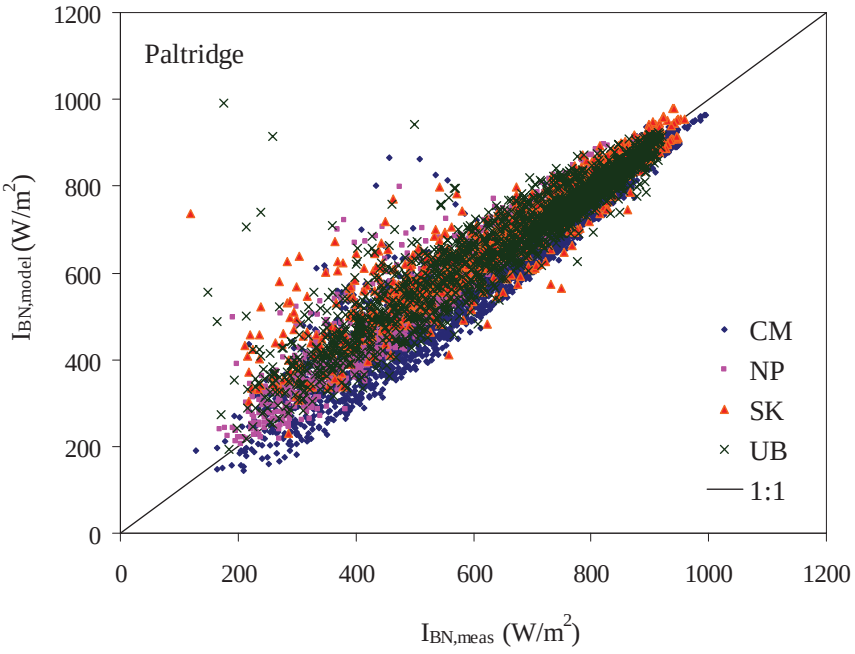

Fig. 4.31 Comparison between clear day direct normal irradiance calculated from Paltridge model ($I_{BN,model}$) and that obtained from the measurements ($I_{BN,meas}$)

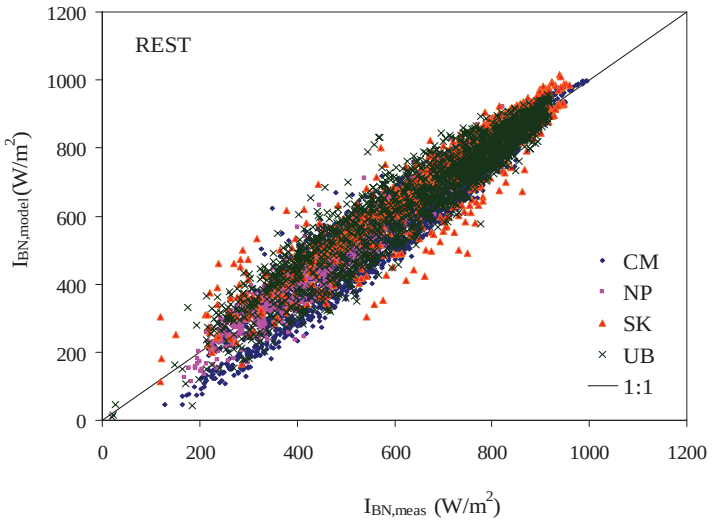

Fig. 4.32 Comparison between clear day direct normal irradiance calculated from REST model ($I_{BN,model}$) and that obtained from the measurements ($I_{BN,meas}$)

Table 4.3 Comparison of the performance of the proposed model for global irradiance and that of other models

Model	Chiang Mai		Nakhon Pathom		Songkhla		Ubon Ratchathani		Combined data from 4 stations	
	MBD (%)	RMSD (%)	MBD (%)	RMSD (%)	MBD (%)	RMSD (%)	MBD (%)	RMSD (%)	MBD (%)	RMSD (%)
Proposed Model	-1.8	8.7	-0.3	8.6	-1.8	6.2	-2.0	6.1	-1.5	7.5
Haurwitz *	5.1	10.1	11.2	14.7	4.2	8.0	3.3	7.7	5.6	10.0
Daneshyar-Paltridge-Proctor *	17.0	19.3	19.6	23.3	15.7	17.8	14.0	16.0	16.4	18.9
Berger – Duffie*[14]	-0.7	11.1	8.7	15.0	-1.3	9.8	-1.5	10.4	0.8	11.4
Adnote-Bourges-Campana-Gicquel *	-6.5	12.0	-1.8	11.3	-7.4	11.1	-8.3	12.3	-6.3	11.9
Kasten-Czeplak*	-9.6	15.2	-3.1	13.7	-10.3	14.8	-10.8	15.7	-8.8	15.2
Robledo - Soler *	12.6	16.1	25.5	27.7	11.9	14.8	12.2	15.0	14.8	17.9
Berlynd*	30.4	32.8	33.0	38.2	16.7	19.5	31.6	33.8	28.2	31.7
SOLIS†	-7.1	11.9	-9.9	15.0	-7.0	9.8	-8.2	10.4	-7.9	11.7
Bird†	0.6	8.5	2.9	9.8	-0.4	6.5	-1.2	6.1	0.3	7.7
ESRA†	2.1	9.3	1.8	9.6	-0.3	6.1	1.4	5.9	1.3	7.9
Ineichen†	-3.2	9.4	-1.2	9.9	-4.9	8.8	-5.3	9.3	5.3	10.9
CPCR2†	-2.0	9.1	-3.3	9.6	-4.6	7.5	-2.9	6.5	0.6	7.6
Kasten†	-5.1	10.8	-2.5	11.0	-6.3	10.2	-7.1	10.7	-5.4	10.8
Yang†	-3.2	9.4	-1.2	9.9	-4.9	8.8	-5.3	9.3	-3.8	9.4
REST†	1.7	8.6	0.8	8.9	-1.7	6.7	-1.8	6.5	-0.3	7.7

Note *empirical model, † physical model

Table 4.4 Comparison of the performance of the proposed model for direct normal irradiance and that of other models

Model	Chiang Mai		Nakhon Pathom		Songkhla		Ubon Ratchathani		Combined data from 4 stations	
	MBD (%)	RMSD (%)	MBD (%)	RMSD (%)	MBD (%)	RMSD (%)	MBD (%)	RMSD (%)	MBD (%)	RMSD (%)
Proposed Model	-3.5	7.5	3.1	6.2	-0.5	8.0	0.2	8.1	-1.0	7.5
SOLIS†	-6.5	9.2	-1.5	8.2	-0.2	7.8	-0.6	7.9	-3.3	8.5
Bird†	-4.9	8.2	2.4	8.5	2.4	7.6	1.5	7.6	-1.0	8.0
Hoyt and Sasamomori†	-8.2	12.0	-1.0	6.5	-0.5	9.3	-2.6	9.6	-4.5	10.3
ESRA†	-2.0	6.6	1.4	7.3	3.9	8.9	3.7	9.0	0.8	7.7
CPCR2†	-3.0	7.7	3.8	6.8	4.5	8.9	2.7	8.1	0.6	7.9
Psiloglou†	2.6	9.5	10.9	13.0	16.3	19.2	10.8	14.6	8.0	13.2
Marjumdar*	21.7	26.0	27.1	30.5	12.3	18.4	18.4	23.8	20.5	25.4
Yang†	-3.5	9.9	3.1	7.6	5.7	11.4	2.1	9.8	0.3	9.7
Paltridge and Platt†	-4.1	9.3	4.6	9.1	5.5	11.6	2.9	10.8	0.5	10.0
REST†	-3.2	9.5	2.4	6.8	4.3	10.6	1.4	9.5	0.0	9.3

Note *empirical model, †physical model

From table 4.3 and 4.4 it was noticed that the proposed models predicted well the clear sky irradiance for all stations. For the global irradiance model, root mean square difference (RMSD) is 7.5% and mean bias difference (MBD) is -1.5%. For the case of direct normal irradiance model, RMSD and MBD are 7.5% and -1.0%, respectively.

For the global irradiance model (Table 4.3), it is observed that RMSD of the proposed model is the lowest, when compared to that of the empirical models of Haurwits (Haurwitx, 1945; Haurwitz 1946), Daneshyar (Danexhyar, 1978; Paltridge, 1976) and Berlynd (Ianets and Kudish, 2008; Kondrayev, 1969), both for the individual station data and combined data. This is due to the fact that the proposed model takes dominant atmospheric parameters such as aerosols and precipitable water into account, resulting in better performance in most cases. When compared to the physical models namely, SOLIS (Ineichen, 2008), Bird (Bird and Hulstrom, 1980), ESRA (Rigollier et al., 2000), Ineichen (Ineichen and Perez, 2002), CPCR2 (Gueymard, 1989), Kasten (Kansten, 1984), Yang (Yang et al., 2001) and REST

(Gueymard, 2003; Alam, 2006), the performance of the proposed model is comparable to that of Bird (Bird and Hulstrom, 1980), CPCR2 (Gueymard, 1989) and REST (Gueymard, 2003; Alam, 2006) models for the combined data set. This is because the proposed model and these physical models use the dominant atmospheric parameter as the model input. However, the proposed model has advantage in terms of simplicity.

For the direct normal irradiance model (Table 3.5), it is clearly seen that the proposed model gives more accurate estimation of direct normal irradiance than that of empirical model (Majumdar et al., 1972). In addition, the performance of the proposed model is comparable to that of ESRA (Rigollier et al., 2000) for the combined data set.

4.4 Conclusion

Semi-empirical models for estimating clear sky global and direct normal irradiances have been developed. The models express global and direct normal irradiances as empirical functions of aerosol parameters, precipitable water, total column ozone, air mass and solar zenith angle. When tested against independent data set, the proposed models give the values of RMSD of 7.5% and MBD of -1.5% for global irradiance and RMSD of 7.5% and MBD of -1.0% for direct normal irradiance. The proposed models, in most cases, provided good estimation of global and direct normal irradiances in the tropical environment of Thailand, with the accuracy comparable to that of some widely used physical models.

Chapter 5

A semi-empirical model for estimating diffuse solar irradiance under a clear sky condition for a tropical environment*

5.1 Introduction

Clear sky diffuse irradiance is an important information as it is usually required for the estimation of clear sky global irradiance (Hammer et al., 2003). It also indirectly indicates a potential applications of concentrating solar power (CSP) technologies.

Existing models for calculating diffuse irradiance on a horizontal surface have various degrees of complexity, ranging from empirical models to rigorous physical models. Empirical models have an advantage in terms of simplicity but they usually lack generality. In contrast to empirical models, physical models or radiative transfer models provide more generality and accuracy but they are more complicated and need more input data which sometime are not available. As a compromise, we proposed a semi-empirical model for estimating diffuse irradiance. The formulation of the model is based on solar radiation and atmospheric parameters measured at 3 stations in the tropical environment of Thailand. The model was validated against an independent data set at 4 stations in this country.

5.2 Measurements and data preparation

Diffuse solar irradiance data used in this work were obtained from our four solar radiation monitoring stations located in different regions of Thailand: Chiang Mai (18.78°N, 98.98°E) in the North, Ubon Ratchatani (15.25°N, 104.87°E) in the Northeast, Nakhon Pathom (13.82°N, 100.04°E) in the Center and Songkhla (7.20°N, 100.60°E) in the South. For each station, diffuse solar irradiance on horizontal surface was measured by using a pyranometer of Kipp&Zonen (model CM11) equipped with a shade ring of Kipp&Zonen (model CM121). The pyranometer was installed on a roof top of a building free from obstructs. A voltage signal from the pyranometer was captured by a data logger of Yokogawa (model DC100) at every second. Afterward,

*This chapter has been published in Procedia Engineering vol.32, page 421-426 (2012)

the signal data were averaged for the period of 10 minutes and the average values were recorded in the data logger. The pyranometers at these stations were calibrated annually using a travelling pyranometer recently calibrated by manufacturer. The accuracy of diffuse irradiance measurements was estimated to be about 8%.

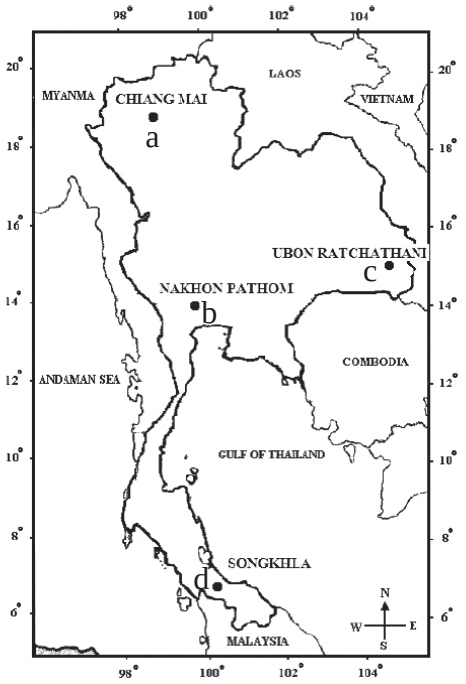

Fig. 5.1 Solar radiation monitoring station a) Chiang Mai b) Nakhon Pathom c) Ubon Ratchathani d) Songkhla

At each station, a Cimel sunphotometer (model CE318) was installed to measure solar spectrum at the wavelength of 340, 380, 440, 500, 675, 870 and 1020 nm. The sunphotometers belong to our laboratory and were operated by our staffs. They are members of the Aerosol Robotic Network (AERONET) of NASA (Holben et al., 1998). The spectrum data from these sunphotometers were processed by AERONET to obtain optical properties of aerosols and precipitable water. The sunphotometers were sent to calibrate regularly at NASA.

As only diffuse irradiance data during clear sky periods were required for the analysis, a sky camera produced by Prede Company, Japan (model PSV-100) was installed at each station. The sky camera was equipped with fish-eye lens capable of

recording digital images of the whole sky. The images of the sky at four stations were taken and recorded every 10 minutes.

The images of the sky were visually inspected to indicate the periods of clear sky. In addition, the spectral data from the sunphotometers were also used to identify the clear sky periods by using the cloud screening procedure of AERONET (Smirnov et al., 2000). The clear sky diffuse irradiance data for the year 2009 from Chiang Mai, Nakhon Pathom and Songkhla were used to formulate a clear sky semi-empirical model. The same type of data for the year 2010 from these stations were employed for the model validation. Due to the lack of aerosol and precipitable data of Ubon Ratchatani in the year 2009, diffuse irradiance data at this station were not used for the model formulation. Diffuse irradiance data for the year 2010 from this station were used for the model validation.

Information of aerosols, precipitable water and atmospheric ozone during the period of 2009-2010 was also prepared. Aerosol optical depth (AOD) derived from the spectrum data obtained from the sunphotometers. Precipitable water was also derived from the spectrum data. The derivations of these parameters were carried out by AERONET. Daily total column ozone was obtained from AURA/OMI satellite.

Fig. 5.2 Diffuse radiation equipments (CM11&CM121) install at a) Chiang Mai b) Nakhon Pathom c) Ubon Ratchathani d) Songkhla

Fig. 5.3 Cimel sunphotometer (CE318) install at a) Chiang Mai b) Nakhon Pathom c) Ubon Ratchathani d) Songkhla

Fig. 5.4 Sky camera (PSV100) install at a) Chiang Mai b) Nakhon Pathom c) Ubon Ratchathani d) Songkhla

5.3 Formulation of the model

As mention earlier, this work aims to develop a semi-empirical model for estimating diffuse irradiance on horizontal surface. The model considers aerosols, water vapour, ozone and solar zenith angle as variables affecting clear sky diffuse irradiance. As diffuse irradiance is normally varies with these variables in a combination form, we proposed to express diffuse irradiation (I_d) as follows:

$$I_d = aI_{sc}E_0(\cos\theta_z)^b(cAOD_{500} + dW + e\ell) \qquad (4.1)$$

where θ_z is solar zenith angle, I_{sc} is solar constant (1366.1 Wm^{-2}), AOD_{500} is aerosol optical depth at 500 nm, w is precipitable water (cm), ℓ is total ozone column (cm), E_0 is eccentricity correction factor due to variation of sun-earth distance and a, b, c, d and e are empirical constants. The eccentricity correction factor was calculated by using the full formula reported in Iqbal (1983).

In order to determine the empirical constants, the model was used to fit the data of Id, AOD500, w and ℓ collected at Chiang Mai, Nakhon Pathom and Songkhla during a clear period of the year 2009 by using the non-linear regression technique (Seber and Wild, 1989). The constants a, b, c, d and e are shown in Table 1.

Table 5.1 Values of the empirical constants for the diffuse horizontal irradiance model.

Constants	Value
a	0.300000
b	0.734235
c	0.347038
d	0.034209
e	1.144026

5.4 Model validation

Although the model was formulated by using the high quality data from three stations, it is necessary to test the performance of the model. To evaluate its performance, the model was used to compute clear sky diffuse irradiance at Chiang Mai, Nakhon Pathom and Songkhla for the year 2010. Additionally, the data from Ubon Ratchatani for the year 2010 were also use to validate the model. The diffuse irradiance and all input data of the year 2010 from there stations are considered to be an independent dataset as they were not involved in the model formulation. Values of diffuse irradiance calculated from the model were compared with those obtained from the measurements. The values of root mean square difference (RMSD) and mean bias difference (MBD) for each station are shown in Table 2.

Table 2 the model shows a prediction of diffuse irradiance at Chiang Mai, Nakhon Pathom, Ubon Ratchatani and Songkhla with the RMSD of 18.6%, 13.7%, 16.9% and 25.3%, respectively. It is observed that RMSD of Songkhla is higher than that of other stations. This may be due to the fact that Songkhla is only the station which is situated near the sea and the aerosols at this station are mainly sea salt particles which are different from aerosols of the other stations. The difference in light scattering property of aerosols in Songkhla, as compared to the other stations, is likely to cause the higher error of the estimation. However, the discrepancy between the calculated and measured diffuse irradiances from the combined data of four stations in terms of MBD and RMSD are 3.6% and 18.0%, respectively. It is noted that the accuracy of the proposed model for estimating diffuse irradiance is lower than that of the models for calculating global and direct normal irradiances developed in our previous work (Janjai et al., 2011). This may be explained as follows.

Diffuse irradiance is caused by molecular and aerosol scattering. The portion of diffuse irradiance scattered by aerosols depends strongly on their scattering properties. The treatment of the effect of aerosols in the proposed model by using only aerosol optical depth may not be sufficient to represent the aerosol effect. For the case of global and direct normal irradiance models, their accuracy is less dependent on aerosol scattering as compared to that of the diffuse model. Additionally, due to the shade ring, the accuracy of diffuse irradiance measurements is less than that of global and direct normal irradiance measurements.

Apart from the model validation, the performance of the proposed model was also compared with other physical models. These are Bird's model (Bird and Hulstrom, 1980&1981), CPCR2 model (Gueymard, 1989), ESRA model (Rigollier, 2000), REST model (Gueymard, 2003) and SOLIS model (Ineichen, 2008). These models were used to calculate diffuse irradiance at four stations for the year 2010. The formulations of these physical models are shown in table 3. All input data required by these models were evaluated at the positions of these stations. Values of RMSD and MBD are also shown in Table 5.2.

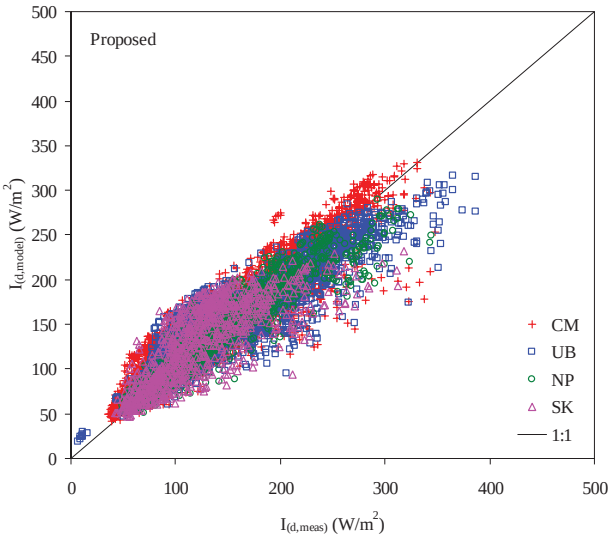

Fig. 5.5 Comparison between clear sky diffuse irradiance calculated from Proposed model ($I_{d,model)}$ and that obtained from the measurements ($I_{d,meas}$) for a) Chiang Mai b) Ubon Ratchathani c) Nakhon Pathom and d) Songkhla

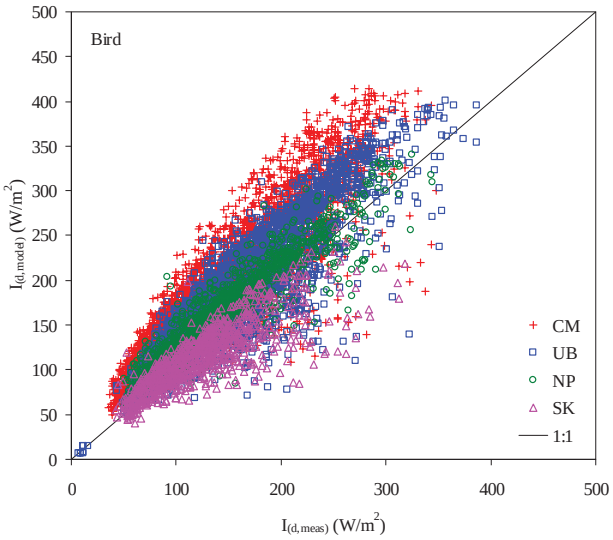

Fig. 5.6 Comparison between clear sky diffuse irradiance calculated from Bird model ($I_{d,model}$) and that obtained from the measurements ($I_{d,meas}$) for a) Chiang Mai b) Ubon Ratchathani c) Nakhon Pathom and d) Songkhla

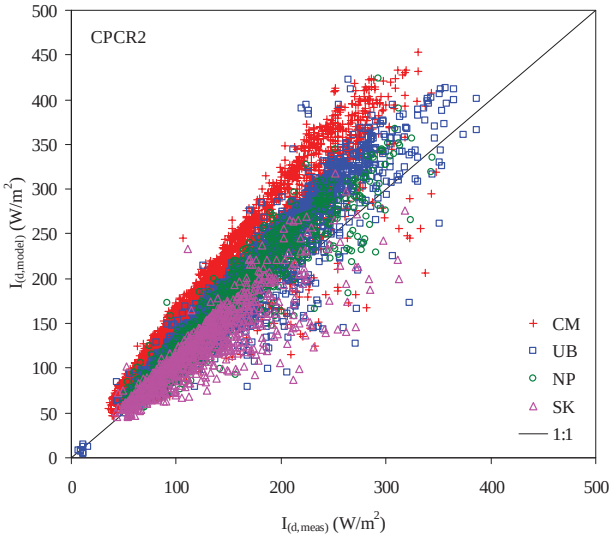

Fig. 5.7 Comparison between clear sky diffuse irradiance calculated from CPCR2 model ($I_{d,model}$) and that obtained from the measurements ($I_{d,meas}$) for a) Chiang Mai b) Ubon Ratchathani c) Nakhon Pathom and d) Songkhla

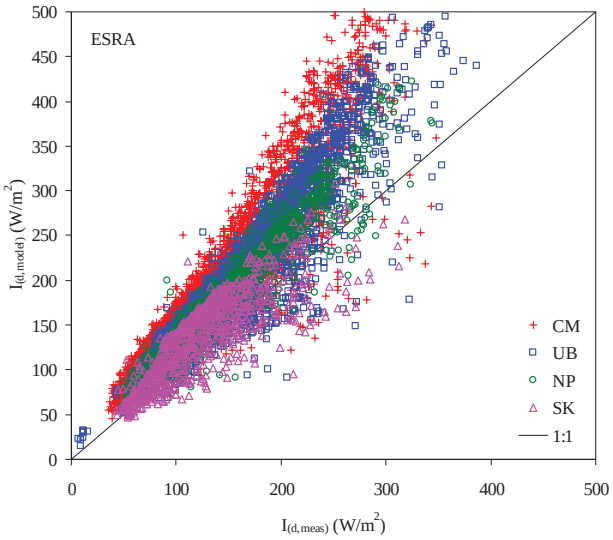

Fig. 5.8 Comparison between clear sky diffuse irradiance calculated from ESRA model ($I_{d,model}$) and that obtained from the measurements ($I_{d,meas}$) for a) Chiang Mai b) Ubon Ratchathani c) Nakhon Pathom and d) Songkhla

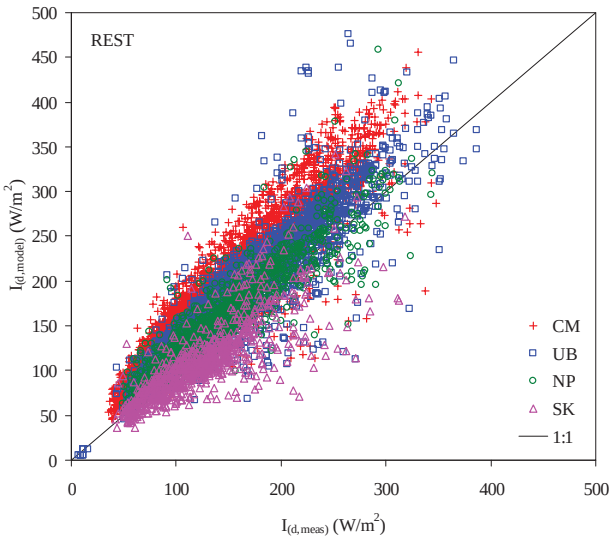

Fig. 5.9 Comparison between clear sky diffuse irradiance calculated from REST model ($I_{d,model}$) and that obtained from the measurements ($I_{d,meas}$) for a) Chiang Mai b) Ubon Ratchathani c) Nakhon Pathom and d) Songkhla

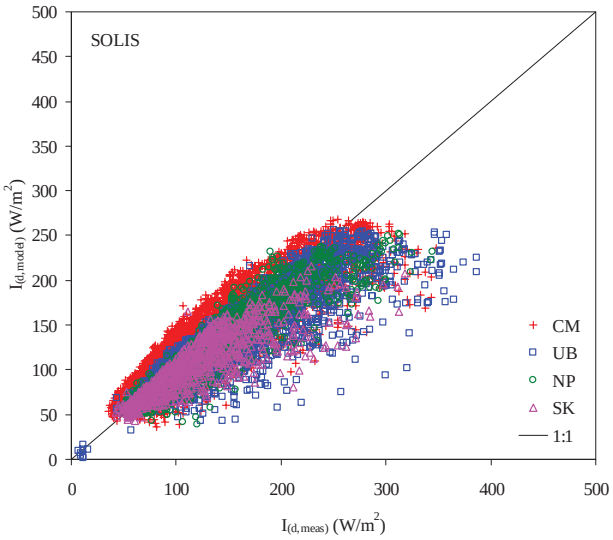

Fig. 5.10 Comparison between clear sky diffuse irradiance calculated from SOLIS model ($I_{d,model}$) and that obtained from the measurements ($I_{d,meas}$) for a) Chiang Mai b) Ubon Ratchathani c) Nakhon Pathom and d) Songkhla

Table 5.2. RMSD and MBD between the calculated and measured diffuse horizontal irradiance.

Model	Chiang Mai		Nakhon Pathom		Ubon Ratchathani		Songkhla		Combined data from four stations	
	MBD (%)	RMSD (%)	MBD (%)	RMSD (%)	MBD (%)	RMSD (%)	MBD (%)	RMSD (%)	MBD (%)	RMSD (%)
Proposed model	7.9	18.6	-2.7	13.7	-0.1	16.9	4.9	25.3	3.6	18.0
Bird and Hulstrom	31.2	39.7	13.8	19.6	15.1	25.7	-8.0	23.9	20.4	31.8
CPCR2	33.2	40.1	13.3	19.4	16.6	23.0	-1.1	20.1	22.3	31.1
ESRA	41.1	51.8	22.6	27.2	27.7	36.4	9.7	23.7	31.7	42.2
REST	32.7	38.2	10.4	18.9	14.5	23.1	4.9	25.3	20.1	30.4
SOLIS	1.4	20.8	-10.4	18.5	-11.4	23.4	-8.0	23.9	-5.6	21.9

It can be seen that, the proposed model gives better accuracy than that of the other models. This is because of the proposed model is tuned to fit the local conditions. The higher errors obtain from the other models may be caused by the aerosol treatment in these models, which is not match to the local aerosol properties.

5.5 Conclusion

A semi-empirical model to calculate diffuse irradiance for a tropical environment has been proposed. The model expresses diffuse irradiance as an empirical function of the aerosol optical depth, precipitable water, total column ozone and solar zenith angle. The non-linear regression technique was used to compute the coefficients of the model. Then the performance of the proposed model was evaluated by using an independent dataset. The comparison between the diffuse irradiance obtained from the model and ground-based measurements showed reasonable agreement with MBD and RMSD of 3.6% and 18.0%, respectively. The model compared favourably with the other models.

Chapter 6
Conclusions

In this work solar radiation in Thailand has been investigated. A satellite-based solar radiation model was modified and used to estimate monthly average of daily global radiation over the country. The satellite data collected from January 1995 to December 2009 were used as main input of the model. The results were displayed as monthly and yearly solar radiation maps. Based on these maps, it was observed that variations of solar radiation in Thailand were strongly influenced by the northeast and southeast monsoons. Solar radiation more than 19 MJ/m^2-day was found in the summer (March-May) in most part of the country. High solar radiation (21-22 MJ/m^2-day) areas are in the Central and Northeast regions. Long-term average daily solar radiation, when averaged over the country, was found to be 17.4 MJ/m^2-day.

An artificial neural network (ANN) model has also been developed to estimate daily global solar radiation by using four input parameters, namely satellite-derived cloud index, precipitable water, total column ozone and aerosol optical depth the values of the solar radiation and the input parameters measured at Nakhon Pathom (13.82 °N, 100.04 °E) were used to train ANN by employing the back propagation algorithm. The ANN model which has been trained was used to calculate daily global radiation measured at other solar radiation monitoring stations situated in the main regions of the country. It was found that the values of calculated and measured daily global solar radiation are in reasonable agreement.

Finally, semi-empirical models for estimating clear sky global, direct and diffuse irradiances were also proposed in this work. The models express global, direct and diffuse irradiances as empirical function of aerosol parameters, precipitable water, total column ozone, air mass and solar zenith angle. The proposed models, in most cases, provided good estimation of global, direct and diffuse irradiances.

As the number of solar radiation monitoring stations in Thailand is still limited, it is recommended that the number of these stations should be increased in order to provide more data for improving the performance of the models developed in this work.

References

Adnot J, Bourges B, Campana D, Gicquel R. Utilisation des courbes de frequence cumulees pour le calcul des installation solaires. In: Lestienne R, editor. Analise Statistique des Processus Meteorologiques Appliquee a l'Energie Solaire. Paris: CNRS; 1979. p. 9-40.

Alam S. Prediction of direct and global solar irradiance using broadband models: Validation of REST model, Renewable Energy 2006;31:1253-63.

Badescu V. Verification of some very simple clear and cloudy sky models to evaluate global solar irradiance. Solar Energy 1997;61:251-64.

Berger X. Etude du Climat en Region Nicoise en vue d'Applications a l'Habitat Solaire. Paris: CNRS; 1979.

Berk A. MODTRAN4 User's Manual. Air Force Research Lab: Hanscomb MA;1999.

Bird RE, Hulstrom RL. Direct isolation models. SERI/TR-335-344, Solar Energy Research Institute (SERI/NREL) 1980.

Bird RE, Hulstrom RL. A Simplified Clear Sky Model for Direct and Diffuse Insolation on Horizontal Surfaces. SERI/TR-642-761, Solar Energy Research Institute (SERI/NREL) 1981.

Cano D, Monget JM, Albuisson M, Gurnard H, Regas N, Wald LA, A method for the determination of the global solar radiation from meteorological satellite data, Solar Energy 1986;37:31-9.

Daneshyar M. Solar radiation statistics for Iran. Solar Energy 1978;21:345–9.

Fortin JG, Anctil F, Parent LE, Bolinder MA. Comparison of empirical daily surface incoming solar radiation model. Agricultural and Forest Meteorology 2008; 148: 1332-40.

Gautier C, Diak G, Masse S. A simple physical model to estimate incident solar radiation at the surface from GOES satellite data. Journal Applied Meteorology 1980;36:1005-1012.

Gueymard C. A two-band model for the calculation of clear sky solar irradiance, illuminance and photosynthetically active radiation at the earth surface, Solar Energy 1989;43:252-65.

Gueymard C. Direct solar transmittance and irradiance predictions with broadband models Part I: detailed theoretical performance assessment, Solar Energy 2003;74:355-79

Gueymard C. SMARTS2, Simple model of the atmospheric radiative transfer of sunshine: algorithms and performance assessment. Report FSEC-PF-270-95, Florida Solar Energy Center, Cocoa, FL;1995.

Hammer A, Heinemann D, Hoyer C, Kuhlemann R, Lorenz E, Muller R, Beyer HG. Solar energy assessment using remote sensing technologies. Remote Sensing of Environment 2003;86:423-32.

Haurwitz B. Insolation in relation to cloudiness and cloud density. Journal of Meteorology 1945;2:154-66.

Haurwitz B. Insolation in relation to cloud type. Journal of Meteorology 1946;3:123-4.

Holben BN, Eck TF, Slutsker I, Tanre D, Buis JP, Setzer A, Vermote E, Reagan JA, Kaufman YJ, Nakajima T, Lavenu F, Jankowiak I, Simirnov A. AERONET-A federated instrument network and data archive for aerosol characterization. Remote Sensing of Environment 1998;66:1-16.

Ianets A, Kudish A. A method for determining the solar global and defining the diffuse and beam irradiation on a clear day, In: Badescu V, editor. Modeling Solar Radiation at the Earth's Surface. Berlin: Springer; 2008. p. 93-113.

Ianetz A, Lyubansky V, Setter I, Kriheli B, Evseev EG, Kudish AI. Inter-comparison of different models for estimating clear sky solar global radiation for the Negev region of Israel. Energy Conversion and Management 2007;48:259-68.

Ineichen P. A broadband simplified version of Solis clear sky model, Solar Energy 2008;82:758-62.

Ineichen P. Comparison of eight clear sky broadband models against 16 independent data banks. Solar Energy 2006;80:468-478.

Ineichen P, Perez R. A new air mass independent formulation for the Linke turbidity coefficient, Solar Energy 2002;73:151-57.

Iqbal M. An Introduction to Solar Radiation. New York: Academic Press; 1983.

Janjai S, Wanvong W, Laksanaboonsong J. The determination of surface albedo of Thailand using satellite data, In Proceeding of the 2nd Joint International Conference on Sustainable Energy and Environment (SEE2006) Bangkok, Thailand, 2006, 156-161.

Janjai S, Laksanaboonsong J, Nunez M, Thongsathitya A. Development of a method generating operational solar radiation maps from satellite data for a tropical environment, Solar Energy 2005; 78, 739-751.

Janjai S., Sricharoen K., Pattarapanitchai S. Semi-empirical models for the estimation of clear sky solar global and direct normal irradiances in the tropics, Applied Energy 2011;88:4749-55.

Janjai S, Rospirom R. Geographical distribution of the precipitable water over Thailand. In: Proceeding of 3rd Silpakorn University Research Fair, 28-29 January 2010, Nakhon Pathom, Thailand; 2010. p. 92-98.

Jantarach T, Janjai S, Nunez M. A study of aerosol optical properties in Thailand for investigation of climate change. Proceedings of the International Conference on Power a Greener Future: Nanomaterial for Solar Energy Conversion, Luxor, Egypt, 2009; 82-83.

Kasten F, Czeplak G. Solar and terrestrial radiation dependent on the amount and type of clouds. Solar Energy 1980; 24:177-89.

Kasten F, Parametriesierung der Globalstrahlung durch Bedekungsgrad und Trubungsfaktor. Annalen der Meteorologie Neue Folge 1984; 20:49-50

Key JR, Schweiger AJ. Tool for atmospheric radiative transfer: streamer and fluxnet. Computers & Geosciences 1998;24:443-51.

Kondratyev KY. Radiation in the Atmosphere. New York: Academic Press; 1969. p.463.

Louche A, Simonnot G, Iqbal M. Experimental verification of some clear-sky insolation models. Solar Energy 1988;41(3):273-79.

Majumdar NC, Mathur BL, Kaushik SB. Prediction of direct solar radiation for low atmospheric turbidity, Solar Energy 1972;13:383-94.

Mayer B, Kylling, A. The libRadtran solfware package for radiative transfer calculation description and examples of use. Atmospheric Chemistry and Physical Discussions 2005;5:1319-381.

Nunez M. The development of a satellite-based insolation model for the tropical western Pacific ocean, Int. J. Climatol., 1993;13:607-627.

Paltridge GW, Proctor D. Monthly mean solar radiation statistics for Australia. Solar Energy 1976;18:234–43.

Perez R, Ineichen P, Moore K, Kmiecik M, Chain C, George R, Vignola F. A new operational model for satellite-derived irradiances: Description and validation. Solar Energy 2002;73(5):307-17.

Robledo L, Soler A. Luminous efficacy of global solar radiation for clear skies. Energy Conversion and Management 2000;41:1769-79.

Ricchiazzi P, Yang S, Gautier C, Sowle D. SBDART: A research and teaching software tool for plane-parallel radiative transfer in the Earth's atmosphere. Bulletin of the American Meteorological Society 1998;79:2101-14.

Rigollier C, Bauer O, Wald L. On the clear sky model of the ESRA-EUROPEAN solar radiation Atlas-with respect to the Heliosat method, Solar Energy 2000;68:33-48.

Seber GAF, Wild CJ, Nonlinear Regression. New York: John Wiley&Sons; 1989.

Smirnov A, Holben BN, Eck TF, Dubovik O, Slutsker I. Cloud-Screening and Quality Control Algorithms for the AERONET Database. Remote Sensing of Environment 2000;73:337-49.

Tanre′ D, Deroo C, Duhaut P, Herman N, Morcrette JJ, Perbos J, Deschamps PY, Simulation of the Satellite Signal in the Solar Spectrum, Technical Report, Laboratoire d′ Optique Atmospherique, Universite′ des Science et Technique de Lille, 59655 Villeneuve d′ Ascq Cedex, France ; 1986.

Tarpley, J.D. Estimating incident solar radiation at the surface from geostationary satellite data. Journal of Applied Meteorology 1979;18:1172-1181.

Vignola F, Harlan P, Perez R, Kmiecik M. Analysis of satellite derived beam and global solar radiation data. Solar Energy 2007;81:768-72.

Yang K, Huang GW, Tamai N. A hybrid model for estimating global solar radiation, Solar Energy 2001;70:13-22.

Appendix 1

Parts of this thesis have been published in international journals and conference proceeding as follows:

1. Janjai, S., Masiri, I., Pattarapanitchai, S., Laksanaboonsong J. (2012). An Improved Model for the Estimation of Solar Radiation from Satellite Data for Thailand. Journal of the Institute of Engineering, 8, 130–139.
2. Janjai, S., Sricharoen, K., Pattarapanitchai, S. (2011). Semi-empirical models for the estimation of clear sky solar global and direct normal irradiances in the tropics. Applied Energy, 88, 4749-4755. (impact factor = 3.915)
3. Pattarapanitchai, S.; Janjai, S. (2012). A semi-empirical model for estimating diffuse solar irradiance under a clear sky condition for a tropical environment. Procedia Engineering 32, 421-426.
4. Pattarapanitchai,S., Janjai, S. An Estimation of Daily Global Solar Radiation using Artificial Neural Networks in Thailand. Proceedings of the 5th Silpakorn University International Conference on Academic Research and Creative Arts : Integration of Art and Science, 25-27 January, 2012, Silpakorn University, Snamchandra Palace Campus, Nakhon Phathom, Thailand.

Autobiography

Name:	Somjet Pattarapanitchai
Sex:	Male
Date of birth:	31 August 1983
Address:	63 M.5 Hnongsarai sub-district, Donchedi district, Suphanburi province, 73000

Education

2005	Bachelor of Science (Physics) Silpakorn University, Nakhon Pathom, Thailand
2008	Master of Science (Physics) Silpakorn University, Graduate School
2009	Doctor of Philosophy (Physics) Silpakorn University, Graduate School